Institute of Nuclear Physics
Kraków, Poland
www.ifj.edu.pl/reports/2001.html

Report No 1879/PH
July 2001

Are Centauros exotic signals of the QGP?

Ewa Gładysz-Dziaduś

Institute of Nuclear Physics, Cracow, Poland

Abstract

The exotic cosmic ray events are revieved with special emphasis on the connection between their hadron rich composition and their strong penetrability in matter. Theoretical attempts to explain the Centauro-like phenomena are summarized. Results of accelerator experiments looking for Centauro-related objects are described and discussed. The discussion is completed with an overview of the future collider (RHIC and LHC) experiments which are expected to produce and detect such exotic objects in the laboratory. In particular the CASTOR detector, a subsystem of the ALICE experiment dedicated to Centauro and strange objects research in heavy ion collisions at LHC energies is presented in detail. Simulations of the passage of Centauros and strangelets through the deep CASTOR calorimeter are shown.

Contents

1 Introduction **4**
- 1.1 Quark-gluon plasma and its signatures . . . 5
- 1.2 Highlights from accelerator experiments . . . 9
- 1.3 Experimental hints from unusual cosmic ray events . . . 12

2 Centauro related phenomena in Chacaltaya and Pamir chambers **15**
- 2.1 Centauros of original type . . . 18
  - 2.1.1 "Classical" Chacaltaya Centauros . . . 18
  - 2.1.2 Other Centauro and Centauro-like events . . . 24
- 2.2 Mini-Centauros . . . 33
- 2.3 Chirons . . . 37
- 2.4 Penetrating clusters and Halo . . . 47
- 2.5 Anomalous transition curves . . . 51

3 Centauro species statistics **55**
- 3.1 Mts. Chacaltaya and Pamir experiments . . . 55
- 3.2 Mts. Kanbala and Fuji experiments. . . . 59
- 3.3 JACEE Experiment. . . . 59
- 3.4 Summary of the Centauro species statistics . . . 60

4 Centauro explanations **62**
- 4.1 Exotic extraterrestrial glob of matter . . . 63
- 4.2 Diffractive fireballs . . . 65
- 4.3 DCC . . . 66
  - 4.3.1 Centauros as DCC manifestation . . . 66
  - 4.3.2 DCC search in γ-hadron families . . . 69
- 4.4 Strange Quark Matter . . . 71
  - 4.4.1 Extraterrestrial strangelets . . . 74
  - 4.4.2 Strangelets formed in the Centauro fireball . . . 76

5 Search for Centauros in accelerator experiments **93**
- 5.1 Past experiments at CERN SPS collider . . . 93
- 5.2 Current experiments at Tevatron and CERN SPS . . . 94
- 5.3 Future experiments at RHIC and LHC . . . 97

6 CASTOR: a detector for Centauro And STrange Object Research 101
6.1 The design of the CASTOR calorimeter 102
6.2 Probes and observables of LHC Centauros and Strangelets 103
6.2.1 Rate of Centauros in CASTOR 104
6.2.2 Average characteristics estimates 105
6.2.3 Expected signatures 107

7 Centauro and/or Strangelet Simulations 111
7.1 Generator for Centauros 111
7.2 Simulations of Centauro events 112
7.3 Exotic objects in deep calorimeters 113
7.3.1 Strangelets in the CASTOR calorimeter 117
7.3.2 "Mixed" events in the CASTOR calorimeter 128

8 Summary 135

List of Figures

1.1 Schematic phase diagram of nuclear matter [1]. 6
1.2 Average pseudorapidity distribution of particle multiplicities and energy flow. 50 central Pb+Pb collisions at energy $\sqrt{s} = 5.5$ A TeV were generated by HIJING. CASTOR geometrical acceptance is indicated [11]. 14
1.3 Baryon number distribution for central Pb+Pb collisions at energy $\sqrt{s} =$ 5.5 A TeV generated by HIJING and VENUS. 14

2.1 Schemes of typical emulsion chambers [20]. 16
2.2 Illustration of Centauro I [23]. 19
2.3 Strongly penetrating cascades from Centauro VII [31]. 26
2.4 Transition curve in terms of optical density D_{290} of high energy cascade detected in family Elena [35]. Black dots are experimental points without methodical corrections, crosses are corrected experimental points. Calculated curves for γ–quanta are also shown. 27
2.5 Diagram of the number of hadrons and hadronic energy fraction: Chacaltaya events with the total visible energy greater than 100 TeV [38]: ($\circ$) Centauro, ($\times$) Mini-Centauro, ($\bullet$) others; ($\star$) C-K [36]. 28
2.6 Transition curves in X-ray film darkness D (measured in three diaphragms of a radius R = 48, 84 and 140 μ) for cascade no. 197.08. Energy (in TeV units) liberated into the soft component is indicated at each hump (averaged over three estimated values) [36]. 29
2.7 Penetrating black core in the family "Tatyana". The curve presents the darkness of the core with halo on the X-ray films with the depth in radiation units in the chamber [38]. 32
2.8 Transition curves of high energy showers in Chiron I [20]. The curves expected for electromagnetic cascades are also shown by dotted and dashed lines. 39
2.9 Examples of transition curves in the family Ch18-B154S-B133I [56]: a) single-core shower, b) multi-core shower. 41
2.10 Transition curves of high energy showers in the family C22-113S-84I [31]. Simulated electromagnetic cascade curve is shown by dotted line. 42
2.11 Examples of transition curves from Chiron type families. 43
2.12 Average transition curves of high energy showers of $\Sigma E_{vis} \geq 10$ TeV from Chiron type families [20]. 45
2.13 Distribution of shower starting positions of high energy showers, measured by λ_{geo} [20]. 46

2.14 Transition curves of the three highest energy showers from the event C22-178S139I [31]. Dotted curves are simulated electromagnetic cascades. 48
2.15 Examples of anomalous transition curves registered in Chacaltaya two–storey chambers [20]. 51
2.16 Examples of anomalous transition curves registered in thick lead chambers [20]. 52
2.17 Distribution of widths of simulated and observed cascades [7]. 53

3.1 $N_h - Q_h$ diagram of families ($\Sigma E_\gamma \geq 100$ TeV) observed at Mt. Chacaltaya (Ch.15 - Ch.21). Centauros are shown by marks (I-V and 1). Contours give the normalized density of the simulated events [8]. 57
3.2 (a) $N_h - Q_h$ diagram of families detected in Pamir, Chacaltaya and Pamir-Joint chambers, (b) The same for the simulated families. Different marks signify the different primary cosmic-ray nuclei: (•) proton, (○) α, (◇) CNO, (×) heavy, (+) Fe, [53]. Plots on the right side are for the families selected under the criterion that the average of the lateral spread after decascading is smaller than 300 GeV·m. 58

4.1 Centauro fireball evolution scheme [136]. 78
4.2 Location of the Centauro point (T, μ_q) on the phase diagram for two temperatures: $T(\mu_q = 0)$= 250 and 210 MeV (dashed curves). Solid curve is for $\mu_s = 0$ in the hadron gas. The plot at the right side shows entropy per baryon versus quarkchemical potential, for two phase curves [139]. 81
4.3 Stability curves plotted as T versus R for fixed μ_q = 300, 500, 700 MeV for a strangelet with A=75. 84
4.4 Example of simulated transition curve produced by an unstable strangelet decaying into a bundle of 7 neutrons, recorded in the thick lead chamber. Neutron energy $E_n \simeq E_{str}/A_{str} \simeq 200$ TeV). Numbers of electrons N_e are counted within the radius of 50 μm. 87
4.5 Similarity between the experimental data taken from [54] and simulated cascades produced by a bundle of 7 neutrons (full histogram): (a) distribution of mutual distance between the consecutive maxima; (b) distribution of ratios of the energy contained in the particular maxima to the average energy of the humps. 88
4.6 Example of simulated transition curve obtained under the assumption of the successive evaporation of neutrons from a metastable strangelet passing through the lead chamber ($A_{str} = 15, E_{str} = 200$ A TeV, $\tau \sim 10^{-15}$ s). . . . 90
4.7 Example of simulated transition curve recorded in the lead chamber produced by successive interaction of a long-lived strangelet with lead nuclei ($A_{str} = 15$, $\mu_q = 600$ MeV). 91

5.1 Kinematical range of rapidity for the Tevatron and cosmic-ray experiments [76]. Particle density vs. rapidity is shown in (a) for the Tevatron collider, with the range of sensitivity of the Fermilab Collider Detector. In (b) the same rapidity space for cosmic ray experiments is shown with energy flow, $d(E_N \cdot N)/dy$, vs. rapidity. 95

6.1 Scheme of the CASTOR detector. 102
6.2 The view of the CASTOR calorimeter. 103

7.1 Average multiplicities of particles produced in "usual" (HIJING) event and by Centauro mechanism. Only particles within CASTOR acceptance are shown. 114
7.2 Transverse momentum distributions of (a) strangelets and (b) hadrons from Centauro decay. 115
7.3 Probability of a strangelet (full line) and other particles (dashed line) production from the decay of Centauro fireball as a function of pseudorapidity. The region of the geometrical CASTOR acceptance is indicated with dotted lines. 116
7.4 Transition curves produced by bundles of 7 (dotted-dashed curve) and 10 (dotted curve) neutrons of energy $E_n \approx 1.2$ TeV and 20 (dashed curve) neutrons of energy $E_n \approx 1$ TeV evaporated by a short-lived strangelet of $A_{str} = 40$. Full line histogram shows the HIJING estimated background. Energy deposit (MeV) in the calorimeter layers, in the octant containing a strangelet, is shown. 119
7.5 Transition curves of stable strangelets with energy $E_{str} = 40$ TeV, baryon number $A_{str} = 40$, quark chemical potential $\mu_q = 600$ MeV (dashed curve) and $\mu_q = 1000$ MeV (dotted curve). Energy deposit (MeV) in the calorimeter layers, in the octant containing a strangelet, is shown. Full line histograms in Figs. 7.5–7.10 show the HIJING estimated background. 120
7.6 Transition curves of stable strangelets with $E_{str} = 20$ TeV, $A_{str} = 20$, $\mu_q = 600$ MeV (two simulations: dashed and dotted curves) and $\mu_q = 1000$ MeV (dotted-dashed curve). Energy deposit (MeV) in the calorimeter layers, in the octant containing a strangelet, is shown. 121
7.7 Transition curves of stable strangelets with $E_{str} = 14$-15 TeV. Dashed curve: $A_{str} = 20$, $E_{str} \approx 700$ A GeV, $\mu_q = 600$ MeV; Dotted curve: $A_{str} = 20$, $E_{str} \approx 700$ A GeV, $\mu_q = 1000$ MeV; Dashed-dotted: $A_{str} = 15$, $E_{str} \approx 1000$ A GeV, $\mu_q = 600$ MeV. Energy deposit (MeV) in the calorimeter layers, in the octant containing a strangelet, is shown. 123
7.8 Transition curves of stable strangelets with $E_{str} \approx 10$ TeV. Dashed curve: $A_{str} = 20$, $E_{str} \approx 500$ A GeV, $\mu_q = 600$ MeV; Dotted curve: $A_{str} = 20$, $E_{str} \approx 500$ A GeV, $\mu_q = 1000$ MeV; Dashed-dotted curve: $A_{str} = 15$, $E_{str} \approx 700$ A GeV, $\mu_q = 600$ MeV. Energy deposit (MeV) in the calorimeter layers, in the octant containing a strangelet, is shown. 124
7.9 Transition curves of stable strangelets with $E_{str} \approx 8$ TeV. Dashed curve: $A_{str} = 20$, $E_{str} \approx 400$ A GeV, $\mu_q = 1000$ MeV; Dotted curve: $A_{str} = 15$, $E_{str} \approx 500$ A GeV, $\mu_q = 600$ MeV. Energy deposit (MeV) in the calorimeter layers, in the octant containing a strangelet, is shown. 125
7.10 Unstable strangelet ($A_{str} = 22$, $E_{str} \approx 22$ TeV) transformed into a stable one after evaporation of 7 neutrons. Energy deposit (MeV) in the calorimeter layers, in the octant containing a strangelet, is shown. 127

7.11 a) Transition curves produced by a stable strangelet (A_{str}= 20, E_{str} = 20 TeV, μ_q = 600 MeV) and by the HIJING background separately; b) Summed signal in the "strangelet" sector in comparison with the average of other sectors assuming readings of every layer, i.e. every 5 mm in electromagnetic and 10 mm in hadronic sectors; c) same as (b), but readings of the summed signal from consecutive groups of 4 layers. 129
7.12 Transition curves produced by Centauro event "C"(T = 250 MeV, μ_q = 1000 MeV) with an ustable strangelet "STR"(A_{str} = 14, E_{str} = 14 TeV), in comparison with HIJING "H". Energy deposit (MeV) in the calorimeter layers, in the octant containing a strangelet, is shown. 131
7.13 Transition curves produced by Centauro event "C" (T = 250 MeV, μ_q = 1000 MeV) with a stable strangelet "STR"(A_{str} = 20, E_{str} = 20 TeV), in comparison with HIJING "H". Energy deposit (MeV) in the calorimeter layers, in the octant containing a strangelet, is shown. 132
7.14 Examples of resulting transition curves being the sum of Centauro, strangelet and background contributions, and in comparison the HIJING event. Energy deposit (MeV) in the calorimeter layers, in the octant containing a strangelet, is shown. 133

List of Tables

2.1 Family statistics. . . . 18
2.2 Characteristics of Chacaltaya Centauros. . . . 21
2.3 Centauro species with geometry measurement. . . . 22
2.4 Average characteristics of 5 Chacaltaya Centauros assuming nucleon-nucleon or nucleus-nucleus collisions. . . . 23
2.5 Unusual cascades in Centauro-like event C-K. . . . 29
2.6 Centauro-like events. . . . 34
2.7 Hadron-rich events. . . . 35
2.8 Hadron-rich events, continuation. . . . 36
2.9 Mini-Centauros in Pamir-joint chambers, examples. . . . 37
2.10 Chiron I (family 198S-154I). . . . 40
2.11 Chiron–type events, examples. . . . 44
2.12 Giant-mini-clusters, examples. . . . 49

3.1 Clean Centauros from two-storey Chacaltaya chambers. . . . 56
3.2 Centauro statistics 61

4.1 Summary of observed and estimated thermodynamic and kinematical quantities characteristic of the cosmic–ray Centauro events [17, 18]. . . . 80

5.1 Centauro search in accelerators. . . . 99
5.2 Centauro search in accelerators, continuation. . . . 100

6.1 CASTOR calorimeter specifications 104
6.2 Multiplicities of LHC Centauro fireball decay products 107
6.3 Average characteristics of Centauro events and Strangelets produced in cosmic rays and at the LHC [11]. . . . 108

Chapter 1

Introduction

The main purpose of this work is to indicate and discuss some *unconventional signatures of the quark-gluon plasma*. The idea arised from the analysis of super-high energy cosmic ray events detected in emulsion chambers exposed at the mountain altitudes. These data reveal many unexpected features which could be understood by means of the quark-gluon plasma picture and hence they could be the new and unexplored so far field of the signs of that new state of matter. The new accelerator experiments should not neglect the chance of enriching the studied signals by incorporating the unusual phenomena observed in cosmic ray experiments to the investigated ones, despite of many uncertainties and even their mysterious aspects.

The title of this work is rather symbolic. Centauro is a creature being in one half of a man and in the other half of a horse, both parts don't fit one to the other. It is strange and mysterious, we are not sure if and how could it match to the real word. Morever, we are not sure if it exists at all. But we tell and think about it. Centauro is a good symbol of our current knowledge about the cosmic ray exotic events.

In this paper the experimental situation concerning the Centauro events and other related phenomena is reviewed, with intention to emphasized a weakly known relation between Centauro species and the so–called strongly penetrating component. The work bases as well as on the quite recent publications and also on the very old ones, sometimes forgotten preprints or conference proceedings. The volume of available information regarding to this subject is extremely large, so I am sorry if something essential was omitted.

The first purpose of this work was to answer the following question: were the Centauro related phenomena really observed or is it some kind of photomorgana? Each reader should answer by himself. My personal opinion is that despite of many experimental uncertainties, some mess in the data and difficulties in their interpretation, we really observe something new, what is outside of the extrapolation of our present knowledge. The future accelerator experiments (RHIC, LHC) should take advantage of using these hints in their investigations.

The second question adressed was: where and how to look for these phenomena? The compositness of the answer arises from the fact that many different aspects, such as: the naked experimental characteristics obtained from cosmic ray experiments, the so far negative results of accelerator searches and also the theoretical speculations, all of them should be taken into account. In connection with it, the past, present and future accelerator Centauro searches are presented and several different models are described.

Among the numerous attemts to explain Centauros, some models which could be tested in accelerator experiments and in particular these based on the quark-gluon plasma idea were chosen to this review.

Most attention is given to the proposed by us scenario of the Centauro strange quark matter fireball. Its production in nucleus-nucleus collisions and a subsequent evolution could possibly result in the strangelet(s) formation, in the strangeness distillation process. The passage of strangelets through a deep emulsion chamber (calorimeter) should give the specific energy deposition pattern which could be a very spectacular quark-gluon plasma signature. This signal is independent of the strangelet charge (it allows to detect also strangelets with Z=0) and promises to detect as well as long and short-lived strangelets, in contrary to other experimentally used signatures, based mainly on Z/A ratio and sensitive only to stable strangelets.

Both experimental Centauro characteristics and model predictions indicate the forward rapidity region as the most favourable place for production and detection of such anomalous phenomena. This is very essential statement in the context of the current and future experiments, mostly concentrated on the exploration of the midrapidity region. This point is also strongly forced in the paper, claiming the CASTOR detector (proposed as the ALICE experiment subsystem) as the good tool for the new physics studies.

1.1 Quark-gluon plasma and its signatures

The important purpose of the elementary particle physics is to gain an understanding of the equation of state of nuclear, hadronic and partonic matter, commonly referred to as nuclear matter. This endeavor is of cross-disciplinary interest to nuclear physics, astrophysics, cosmology and particle physics. It is also the main motivation for studying relativistic heavy ion collisions which are primarily searching for the so–called quark-gluon plasma (QGP). A quark-gluon plasma is a state in which quarks and gluons, the fundamental constituents of matter, are no longer confined within the dimensions of the nucleon, but free to move around over a volume in which a high enough temperature and/or density prevails. The plasma exhibits the so–called " chiral symmetry " which in normal nuclear matter is spontaneously broken, resulting in effective quark masses which are much larger than the actual masses. A quark-hadron phase transition is believed to have occured at about ten micro-seconds after the Big Bang when the Universe was at a temperature of approximately 150 to 200 MeV. The QGP may also exist in the cores of dense stars at high baryon densities. The critical energy density for the quark-gluon plasma formation is predicted to be $\sim$1 GeV/fm^3, or seven times the energy density of normal nuclear matter. The compilation of heavy-ion studies, looking for the quark-gluon plasma state, can be found for example in [1, 2]. More detailed reviews of theoretical and experimental topics of the quark-matter are presented in [3, 4, 5].

Displayed in Figure 1.1 is a schematic phase diagram of nuclear matter, showing the behaviour of nuclear matter as a function of temperature and density (or pressure).

Conventional nuclear physics concerns low temperatures and near to normal nuclear matter density. This region is presently accessible in heavy ion studies at the SPS accelerator facility at CERN and at the AGS accelerator at Brookhaven National Laboratory. Some part of these collisions may traverse the transition region into the quark-gluon plasma

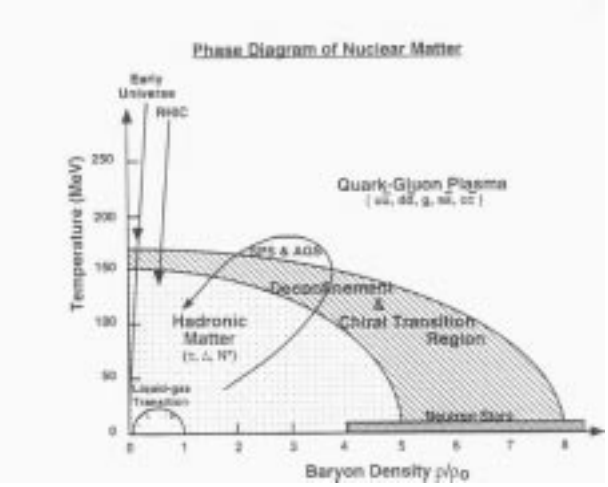

Figure 1.1: Schematic phase diagram of nuclear matter [1].

regime. The Relativistic Heavy Ion Collider (RHIC) at Brookhaven has just started, and the LHC at CERN scheduled for 2006 should reach temperatures and densities close to that of the early Universe.

In collisions of relativistic heavy ions one expects to investigate the perturbative vacuum of Quantum Chromo-Dynamics (QCD), and understand better a symmetry breaking mechanism and the origin of particle masses. The QCD vacuum is predicted to have a complex internal structure, made up of a quark-antiquark condensate sea, while isolated quarks are not expected. This sea possesses energy and mass, and can undergo fluctuations about its zero point. The remarkable feature of QCD is that at large distances or small momentum transfer, the strong coupling constant (α_s) is large, thus at low energy densities, quarks and gluons are confined in colorless hadrons and the vacuum acts as a color dielectric. At short distances or large momentum transfer, the coupling constant is small and this is the regime of an asymptotic freedom. At the high energy densities (high temperature and/or baryon density) the quark-gluon plasma phase is expected to be formed. Then the quark-antiquark condensate vacuum is expected to melt, hadrons dissolve into freely propagating quarks and gluons, and the vacuum becomes a color conductor, or the true perturbative QCD vacuum. A phase transition from a confined phase (hadronic matter) to a deconfined phase (quark-gluon plasma) is predicted to occur at a temperature of approximately 150 MeV.

Another phase transition, which is predicted to accompany the QGP transition, is the *restoration of chiral symmetry*. The mass of a quark depends upon the distance over which it is probed by a second quark or antiquark. *Constituent* quarks are dressed in virtual cloud of quark-antiquark pairs and gluons. The quarks obtain large effective masses ($m_u \sim m_d \sim 300$ MeV, $m_s \sim 500$ MeV) by interactions among themselves and with the surrounding vacuum. The shorter the distance between quarks, the smaller the mass, since the interaction weakens at short distance. *Current quarks*, which are in the regime of asymptotic freedom, are nearly bare (i.e. have near zero mass). At energy densities

sufficiently high, a phase transition should occur where partons become deconfined and their masses decrease ($m_u \sim m_d \sim 0$, $m_s \sim 150$ MeV) and chiral symmetry is partially restored.

As the QGP phase is rather complicated transient state, many interesting or even unexpected phenomena could be observed during its formation, expansion, cooling, and hadronization. There are many predictions for possible signatures of QGP formation and of partial restoration of chiral symmetry, grouped into several classes. The following topics have been proposed to investigate:

- *Thermodynamic Variables*
  This class includes a determination of energy density ε, pressure P, and entropy density s of the interacting system as a function of the temperature T and the baryochemical potential μ_b. If a phase transition to QGP occurs, a rapid rise in the effective number of degrees of freedom (expressed by ε/T^4 or s/T^3) should be observed over a small range of T. The variables T, s and ε can be identified with the average transverse momentum $\langle p_T \rangle$, the hadron rapidity density dN/dy, and the transverse energy density dE_T/dy, respectively. Measurements of the cross sections for the production of various types of particles as a function of transverse momentum and rapidity can test thermalization and space-time evolution of the system. Rapidity distributions of the more abundantly-produced light particles, such as pions and kaons should provide important information on the dynamics of the collision process.

- *Fluctuations*
  Thermodynamical instabilities during the phase transition could lead to large fluctuations. Critical fluctuations, appearing in energy density, entropy density, multiplicity, particle ratios etc., should be looked for in individual events, as a function of p_T, rapidity, azimuthal angles etc.

- *Electromagnetic signals*
  The only way to see the quarks directly is to detect the electromagnetic radiation which they emit. Real and virtual photons in the form of lepton pairs are an ideal probe of the early stages of the interaction, since they escape the interaction region without subsequent interaction or modification due to the final state of the interaction. They can probe the interior of the quark-gluon plasma during its hottest and earliest phase. If an extremely hot QGP is formed, initially photons in the transverse momentum range 2-5 GeV/c should be emitted. Lower momentum photons are expected to be primarily emitted from the mixed phase. Unfortunately there are also many other processes which can produce photons, which are primarily electromagnetic decays of hadrons and resonances and direct hard photons from QCD Compton scattering or lepton pairs from Drell-Yan process. Thus the main problem is, how to separate the yields for electromagnetic probes, which are rather small relative to background processes. Lepton pairs from QGP are expected to be identifiable in the 1-1.5 GeV invariant mass range. At lower invariant masses betwen 0.5 and 1 GeV, lepton pairs from hadronic sources are expected to dominate and provide information on the possible medium modifications of hadrons at high density. The light vector mesons (ρ, ω, ϕ) with lifetimes of the order of the expansion time scale

will partially decay during the evolution of the system. Like J/ψ they can decay into lepton pairs (e^+e^- or $\mu^+\mu^-$) and their characteristic quantities (mass, width, branching ratios) observable in the leptonic decay, should change in the dense matter. In particular, the ϕ mass, width and production rate is expected to be extremely sensitive to changes in the quark masses due to a possible chiral phase transition at high energy densities. Especially a drop of vector meson masses preceeding chiral symmetry restoration, and a change in the K-meson mass would affect the width of the ϕ meson ($\phi \rightarrow K^+K^-$ in 49.1%).

- *Quarkonium suppression*
  J/ψ are made of c and $\overline{c}$ quarks. They are rare because charm quarks are very heavy and can only be produced at the very first stages immediately after the collision, while the constituents of the two nuclei still have their full energy. The suppression of J/ψ production in a quark-gluon plasma occurs because a $c\overline{c}$ pair formed by the fusion of two gluons cannot bind inside the quark-gluon phase. The confining strong force, which would normally bind the newly created charm quarks within a small, but finite time (formation time) into a J/ψ, is screened in the QGP by deconfined quarks and gluons. If the screening radius (Debye radius), which is inversely proportional to the density of colour charges and therefore to the energy density, is smaller then the size of the J/ψ ($\simeq$ 0.5 fm), a bound state cannot be formed. The charm quarks dissolve and separate in space to later appear after hadronization as two mesons with open charm. High-p_T, "fast" charm pairs can escape the QGP unaffected. The problem is that the final-state rescattering of the J/ψ (absorption) complicates the interpretation.

  Less tightly bound excited states of the $c\overline{c}$ system, such as $\psi^{'}$ and χ_c, are more easily dissociated and will be suppressed even more than the J/ψ. Similar arguments can be made also for the heavier $\Upsilon, \Upsilon^{'}, \Upsilon^{''}(b\overline{b}$ systems).

- *Strangeness (heavy flavour) enhancement*
  An enhancement in the production of strange particles resulting from chemical equilibrium of a system of quarks and gluons was one of the first predictions for a signature of QGP formation. In "chemical" equilibrium, the abundances of particle species (hadrons/quarks) are governed by Bolzmann factors, i.e. essentially by temperature, respective masses and chemical potential. Compared with hadronic processes, the production of strange quarks is favoured in a QGP because there the mass of the strange quark is reduced from $\sim$ 500 MeV to $\sim$ 150 MeV (chiral symmetry restoration), i.e. a value comparable with the critical temperature. In addition, in a baryon-rich region the creation of light u and d quarks is hindered by the large number of valence quarks already present in the colliding nuclei (Pauli blocking), leading to a large chemical potential for these quarks in favour of s and $\overline{s}$ production.

  There are two major aspects of the so–called "strangeness signal". The more conventional aspect of strangeness as a QGP signature is an enhanced production of strange hadrons in heavy-ion collisions when compared to nucleon-nucleon or nucleon-nucleus collisions at the same energy. However, the interpretation of the strangeness content depends on our understanding of the hadronization scenario and on the time scales

and relaxation times for equilibration in the various phases. In a QGP scenario the production of strange hadrons is expected to be saturated by $s\overline{s}$ pair production in gluon-gluon reactions, thus especially multi-strange baryons and anti-baryons are predicted to be strongly enhanced. The more speculative aspect is connected with the possible existence of exotic matter, i.e. the droplets of strange quark-matter.

Also an enhancement of charm can be expected.

- *Disoriented Chiral Condensate*
  DCC is a coherent excitation of the pion field corresponding to a local misalignment of the chiral order parameter. According to this speculative hypothesis the pieces of strong interacting vacuum with a rotated chiral order parameter might be produced in high energy particle collisions. The temporary restoration of chiral symmetry during a relativistic heavy ion collisions could result in the formation of domains of a disoriented chiral condensate (DCC). Such domains would decay into neutral and charged pions, favouring pion ratios N_{π^0}/N_{π} substantially different from 1/3. Thus, abnormal ratios of neutral to charged-particle energy and multiplicity can be the excellent signature of the QGP.

- *High p_T probes of QCD*
  The colour structure of QCD matter can be probed by its effects on the propagation of a fast parton. The characteristics of the fragmentation products of hard scattering can provide information on the matter through which the hard scattered parton propagates. The stopping power of a quark-gluon plasma is predicted to be higher than that of hadronic matter. As a result the spectra of high p_T particles and jets will be modified due to attenuation in the medium (shadowing and quenching effects). A quark or gluon jet propagating through a dense medium will not only lose energy but will also be deflected. This effect can destroy the coplanarity of the two jets from a hard parton-parton scattering with the incident beam axis.

1.2 Highlights from accelerator experiments

The experimental programmes in relativistic heavy ions using the BNL-AGS and CERN-SPS started in 1986. At BNL ion beams of silicon and gold, accelerated to momenta of 14 and 11 GeV/c per nucleon respectively, have been utilised in approximately 10 fixed-target experiments. About 15 heavy ion experiments at CERN studied heavy ion interactions, utilizing beams of oxygen at 60 and 200 GeV/c per nucleon, sulphur at 200 GeV/c per nucleon and Pb at 160 GeV/c per nucleon. The experiments were all optimised for measuring different signals which might indicate if and how a quark-gluon plasma was formed. Some of them optimised their detectors for one rare signal, while others developed multipurpose detectors which were sensitive to multiple signals. Many interesting effects, concerning mainly the equilibration of hadronic matter, chiral symmetry restoration and deconfinement, which generally support the QGP hypothesis, have been observed in the AGS and SPS experiments.

- First of all, it seems that the conditions required for the QGP formation have been reached. For instance, a large degree of stopping, resulting in the transfer of a

large amount of energy from the relative motion into other degrees of freedom, was observed in central collisions of the heaviest systems at the AGS and SPS (e.g. NA49, NA44, E866, E877 experiments). At SPS, this creates the high energy densities ($\varepsilon \sim 1.5 - 2.0$ GeV/fm^3) beyond those predicted for production of a quark-gluon plasma. The early, very dense state (fireball) has an energy density of $\sim$ 3-4 GeV/fm^3 what corresponds a temperature of about 240 MeV.

- The data do not contradict the picture in which the created quark-gluon plasma cools down and becomes more dilute. At an energy density of $\sim$ 1 GeV/fm^3 (and a temperature of $\sim$ 170-180 MeV) the quarks and gluons condensate into hadrons, and the final abundancies of the different types of particles are fixed. At an energy density of around 50 MeV/fm^3 (and a temperature of $\sim$ 100-200 MeV) the hadrons stop interacting completely and the fireball freezes out. At this point it is expanding at over half the speed of light. Thermal and chemical equilibrium models are generally able to reproduce the particle abundances and particle spectra measured in central collisions, once the strong influence of the collective nuclear flow is taken into account. As a result, the parameters which best fit the particle ratios and particle spectra were found: the temperature at chemical equilibrium T = 160 - 175 (120 -140) MeV, the baryochemical potential μ_b = 200 - 270 (540), and the strangeness saturation factor γ_s = 0.6 - 1.0 for SPS (AGS) energies. Thus, there is evidence for chemical and thermal equilibrium from the accelerator experiments results, although the issue of strangeness saturation (i.e. if $\gamma_s = 1$), which is required for deconfinement is still to be settled (NA44 and NA49 experiments find only partial chemical equilibrium for strange particles).

- An imporant aspect of "chemical equilibrium" is the observed enhancement of strange particles. We can ask how many strange quarks and antiquarks are formed relative to the newly produced up and down quarks and antiquarks. For proton-proton and electron-positron collisions, the fraction of extra strange quarks made is $\sim$ 0.2. But for the nucleus-nucleus the fraction is twice as high, i.e. it is seen "global strangeness enhancement by a factor of two" (NA49). Most of these extra strange quarks must have been created before the hadrons were made, i.e. in a stage of interacting quark gluon matter. These extra strange quarks are apparently seen in an increased production of the very rare particles that contain two or three strange quarks. Such multi-strange hadrons are enhanced more strongly (WA97, NA49, NA50) up to a factor 15 for the Ω hyperon and its antiparticle (WA97). This effect was found not only in Pb+Pb collisions, but even in central S+S collisions (NA35, WA85, WA94).

- An increase in the pion to baryon ratio from approximately 1 to about 7, when going from the AGS to the SPS energies indicates the rise in entropy density.

- Measurements of charmonium production exhibit a suppression of the yield of both the J/ψ and the $\psi^{'}$ relative to Drell-Yan pair production for central collisions of Pb+Pb at the SPS (NA50, NA38 Collaborations). The yield of the $\psi^{'}$ relative to Drell-Yan is also observed to be suppressed for central collisions of the lighter S+Pb system, whereas the J/ψ is not. These results follow the expected pattern that the Debye screening will initially affect the $\psi^{'}$ before the J/ψ and suggest that the

deconfinement regime has been reached at the SPS. On the other hand, various theoretical models have recently been proposed to predict this behaviour utilizing re-interaction and break-up of charmonium in high density matter without invoking deconfinement. None of these attempts can account for the shape of the centrality dependence of the observed suppression.

- So far, no apparent signal from direct photons radiated by quarks in QGP is found. Searches for this radiation were performed at the SPS (WA98, NA45, NA50) but are difficult due to high backgrounds from other sources. For S+Au collisions, WA80 and NA45 established that not more then 5% of the observed photons are emitted directly. For Pb+Pb collisions WA98 has reported indications for a significant direct photon contribution. Preliminary data from NA45 are consistent with this finding, but so far not statistically significant. NA50 has seen an excess by about a factor 2 in the dimuon spectrum in the mass region between ϕ and J/ψ vector mesons. On the other hand the data (NA45) show that in S+Au and Pb+Au collisions the expected peak from ρ vector meson (a particle which can decay into dileptons even before freeze-out) is completely smeared out. Simultaneously, electron pairs (virtual photons) measurements exhibit an enhancement at low to intermediate pair masses (in the mass region between the mass of two pions and 1.5 GeV/c, i.e. around the ρ meson) relative to pairs expected from hadronic decays for central collisions of the heavier systems (S+Au and Pb+Au) at the SPS (CERES/NA45, HELIOS-3 Collaboration). As the electron pairs allow the measurement of the initial quark-antiquark annihilation via the elementary $q\overline{q} \rightarrow e^+e^-$ process (relevant if a QGP is formed), pion annihilation in a high density hadronic medium via $\pi^+\pi^- \rightarrow e^+e^-$, and the leptonic decays of hadronic resonances (such as the ρ meson), this effect is investigated by using different theorethical approaches and ideas such as $\pi\pi$ annihilation, a decreased ρ mass due to partial chiral symmetry restoration and other effects. The ρ is of particular interest as it has a short lifetime compared to the interaction times and it decays very quickly in the presence of the medium (whether QGP or hadronic). Thus it should exhibit signs of possible chiral restoration if there is a reduction of the ρ-meson mass. The clear excess in the mass spectrum of e^+e^- bears the questions: is it thermal radiation from a hot source or rather does it indicate in-medium effects for vector meson resonances? In the latter case, it could be a signal of the onset of chiral symmetry restoration as matter becomes denser.

Summarizing, the results of relativistic heavy ion experiments at the AGS and SPS are quite intriguing. The data from any one experiment are not enough to give the full picture but the combined results from all experiments rather agree and fit. The attempts to explain all of them simultaneously, using established particle interactions have failed, but on the other hand many of the observations are consistent with the predicted signatures of a quark-gluon plasma. Thus, at a special seminar on 10 February 2000, spokespersons from the experiments on CERN's Heavy Ion programme stated that the collected data from seven CERN experiments (NA44, NA45, NA49, NA50, NA52, WA97, NA57 and WA98) give compelling evidence that a new state of matter has been created although this evidence is so far "indirect" [6]. These results present strong incentive for the future planned experiments. It is essential to study this state of matter at higher and lower temperature to fully characterize its properties and definitively confirm the quark-gluon

plasma interpretation. In the nearest future the results will be obtained by the Relativistic Heavy Ion Collider (RHIC) at the Brookhaven National Laboratory in the United States. In 2006 CERN's Large Hadron Collider (LHC) experimental programme will include a dedicated heavy ion experiment, ALICE.

1.3 Experimental hints from unusual cosmic ray events

Cosmic-ray induced reactions can be satisfactorily described in terms of standard ideas below the energy of about 1000 TeV. Above this threshold the global behaviour of cosmic-ray families is hardly explained by smoothly extrapolating the hadron multiple production characteristics which were learnt through CERN collider energies. The families of hadrons and photons, mainly observed by mountain cosmic ray laboratories, exhibit many surprising features such as: rapid attenuation in the atmosphere, multi-core structure with unexpectedly high alignement level, large lateral spread, extremely high energy concentration in the forward angular region (halo) etc. The observed flux value of cosmic ray families is smaller than expected. According to ref. [7] experimental intensity of families at the Pamir is $I(\sum E_\gamma \geq 100 \text{ TeV}) \simeq 0.35 \text{ m}^{-2}\text{y}^{-1} \text{ sr}^{-1}$. The simulated data, based on different simulation codes, give $3 \sim 4$ times higher intensity than observations. In addition, the spectra of high energy showers in families are in younger stage of the shower development, what indicates that majority of observed families originates from main interaction slightly above the observed levels. At energies $10^{15} - 10^{17}$ eV appears the wide spectrum of exotic events hardly explained by the known mechanisms.

The global characteristics of gamma-hadron families are affected by the primary cosmic ray chemical composition and show a high sensitivity to a hadronic interaction model used in the interpretation. Thus, in principle, the problem seems to reduce to a question of whether the data signal a change in the composition of cosmic ray primaries at these energies, or whether they signal a change in the hadronic interactions. Some unusual features of cosmic-ray events could be, in part, understood by the use of a Fe-dominant composition in the primary flux. However, the recent results from Chacaltaya and Tien-Shan ("Hadron" Experiment) instalations operating simultaneously the emulsion chamber and the air shower array also indicate that discrepancy between the predicted (based on conventional models) and observed family flux cannot be reconciled by the heavy-dominant composition of the primary cosmic rays [8, 9]. Moreover, experimental results concerning the composition of primary cosmic ray spectrum seem to exclude this explanation. In fact, the primary flux composition in the energy region above 10^{14} eV can only be obtained by using indirect methods of ground-based detectors looking at showers initiated by the interaction of primary nuclei in the upper atmosphere. Hence, there are substantial uncertainties on the primary cosmic ray composition in this energy region. As a heavy dominant composition does not have convincing observational support [10], it seems that *the introduction of some new mechanism, or a global change of the characteristics of hadronic interactions at around* 10^{16} *eV, especially in the most forward angular region is necessary* to explain the experimental data.

In this work various anomalies such as: exotic events called Centauros, Mini-Centauros, Chirons etc. were reviewed. These events have many common features and they are very frequently connected with the so–called long-flying (penetrating) component. There are

strong indications that they are connected one to the other and they have a common origin.

In fact, the strongly penetrating component has two faces. At first, it has been observed in the apparatus in the form of strongly penetrating single cascades, clusters of showers or the so called "halo". This phenomenon manifests itself by the characteristic energy pattern revealed in shower development in the deep chambers (calorimeters) indicating a slow attenuation and many maxima structure (see chapter 2). The second aspect is connected with the anomalously strong penetrability of some objects during the passage through the atmosphere. In principle, both items can be connected one to the other and could be different faces of the same phenomenon.

The mentioned here anomalies are not rare occurence but they manifest themselves at the 5% level or above. There are many theoretical attempts to explain the observed anomalies, among them the quark-gluon plasma scenario is the very promising one.

As the wide spectrum of exotic events seen in cosmic ray experiments is observed at *forward rapidities*, thus this region seems to be a potential place for the new physics. Unfortunately, the physics in the very forward rapidity region in ultra-relativistic nucleus-nucleus collisions has not been rigorously addressed by theory so far. The main reason is the difficulty of the calculations in an enviroment of finite baryochemical potential. There are, however, some phenomenological and QCD-inspired attempts to predict new phenomena or to explain unusual phenomena already seen. It is expected that this region will contain only a small fraction of the totally produced particles and at the same time the vast majority of the available total energy with the baryon density reaching here the maximum. Figures 1.2 show the pseudorapidity distributions of multiplicity and energy, obtained in simulations (HIJING generator) of 50 central Pb+Pb collisions at LHC energies $\sqrt{s}$ = 5.5 TeV) [11]. There are shown separately distributions of electromagnetic and hadronic component, and the acceptance of the CASTOR detector (see chapter 6) is marked. Figure 1.3 shows distributions of the baryon number predicted by VENUS and HIJING for the same reactions.

Such environment offers the possibility for the appearance of novel, surprising phenomena. In particular, strangelets, the small droplets of strange quark matter are predicted to be formed from the Quark Gluon Plasma, predominantly in a high baryochemical potential environment. Heavy flavour [12, 13] and Super Heavy Particles production, if they exist, may also be seen at very forward rapidities. For instance the new heavy vector bosons V^+, V^-, V^0 with masses up to 6 TeV are theoretically predicted [14]. Another phenomenon which is attracting a lot of theoretical investigation is colour superconductivity at finite baryon density [15]. At relatively low temperature, the baryon rich environment may lead to the formation of Deconfined Quark Matter (DQM) in the core of neutron stars [16]. Also the understanding of cosmic ray exotic phenomena in terms of hadronization of DQM in an extremaly high baryon density environment has been proposed [17, 18, 19].

All these phenomena should be searched for and studied. Unfortunately, most of the present and future nucleus-nucleus experiments are concentrated on exploration of the poor baryon region and doing the "midrapidity physics". In this work the importance of the CASTOR project, as the unique experimental design to explore this interesting region at very high energies planned to be reached at the LHC nucleus-nucleus collisions will be emphasized.

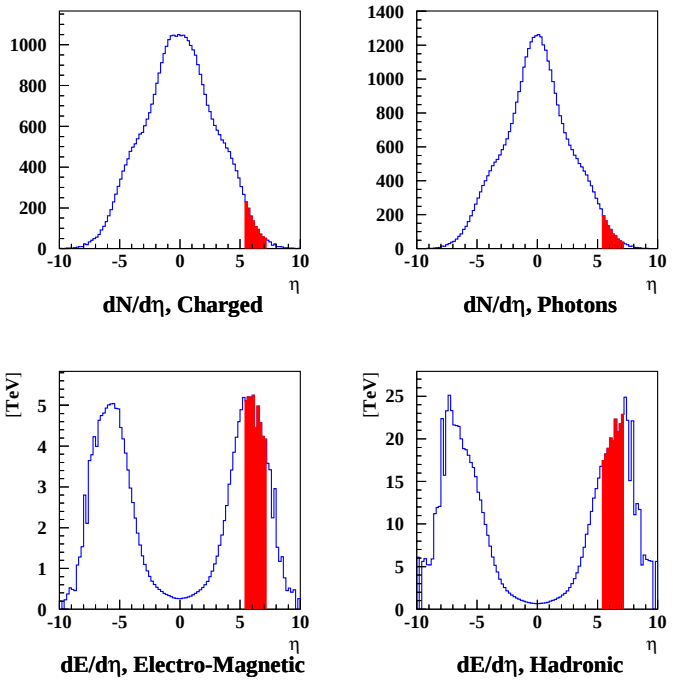

Figure 1.2: Average pseudorapidity distribution of particle multiplicities and energy flow. 50 central Pb+Pb collisions at energy $\sqrt{s} = 5.5$ A TeV were generated by HIJING. CASTOR geometrical acceptance is indicated [11].

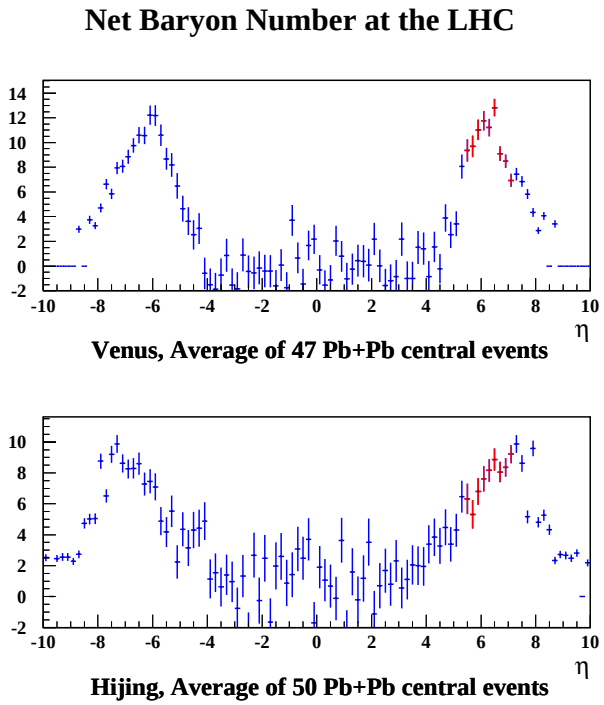

Figure 1.3: Baryon number distribution for central Pb+Pb collisions at energy $\sqrt{s} = 5.5$ A TeV generated by HIJING and VENUS.

Chapter 2

Centauro related phenomena in Chacaltaya and Pamir chambers

The Centauro related phenomena have been discovered and analysed in emulsion chamber experiments investigating cosmic ray interactions at the high mountain laboratories at Mt. Chacaltaya (5200 m above see level) and Pamirs ($\sim$ 4300 or 4900 m above sea level).

In principle the detectors used in these experiments are similar. They consist of three parts: upper and lower chambers, and the carbon target between them. The upper part called the gamma block detects mainly the electromagnetic component. In the lower chamber there are registered mainly hadrons. Both the upper and the lower chambers are sandwiches of the lead absorber and the sensitive layers which are mostly X-ray films, sometimes emulsion plates. Chambers have rather big areas, of the order of several tens m^2 and are exposed for a long time periods, of about one year.

However, the direct comparison and interpretation of the experimental data is difficult because of some differences in the depth and construction of the chambers. Figure 2.1 shows the schemes of Chacaltaya two-storey chamber, a traditional style carbon chamber employed in Pamir experiments and also a schematic view of a homogeneous thick lead chamber (60 or 110/120 cm thick lead). The typical Pamir carbon chambers consist of two (or three) parts: a gamma-block of 5 or 6 cm Pb thick and one (or two) hadron(H)-blocks each consisting of carbon layer of 60 cm thick and 5 cm of Pb. The thickness of a standard Pamir-type carbon chamber amounts to $\sim 1.7\ \lambda_{geo}$ [1], what assures the detection efficiency to be over $\sim$ 60–70 %. Thicker carbon-type chambers (consisting of four hadron blocks) have been also used sometimes. The homogenous lead chambers are simply sandwiches of Pb absorber layers (the upper layer has usually 2 cm Pb and the consecutive ones have 1 cm Pb) and the sensitive material being mainly the X-ray films. The detection efficiency of thickest Pb-chambers is $\sim$ 80–90 %.

Typical two-storey Chacaltaya chamber consists of the upper chamber of 6-10 cm Pb thick, the target layer 20-30 cm of carbon, the air gap (e.g. 150 cm) and the lower chamber of 6-15 cm Pb thick. Some chambers (as for example Chacaltaya chamber no. 19, 20, 21, 22) were covered by several nuclear emulsion layers over all area of both upper and lower chamber. It enables a careful study (under the microscope), of the shower structures. It is essential in classification of the showers (an identification of the photonic and hadronic

[1] λ_{geo} is the geometrical collision mean free path of ordinary cosmic-ray baryons.

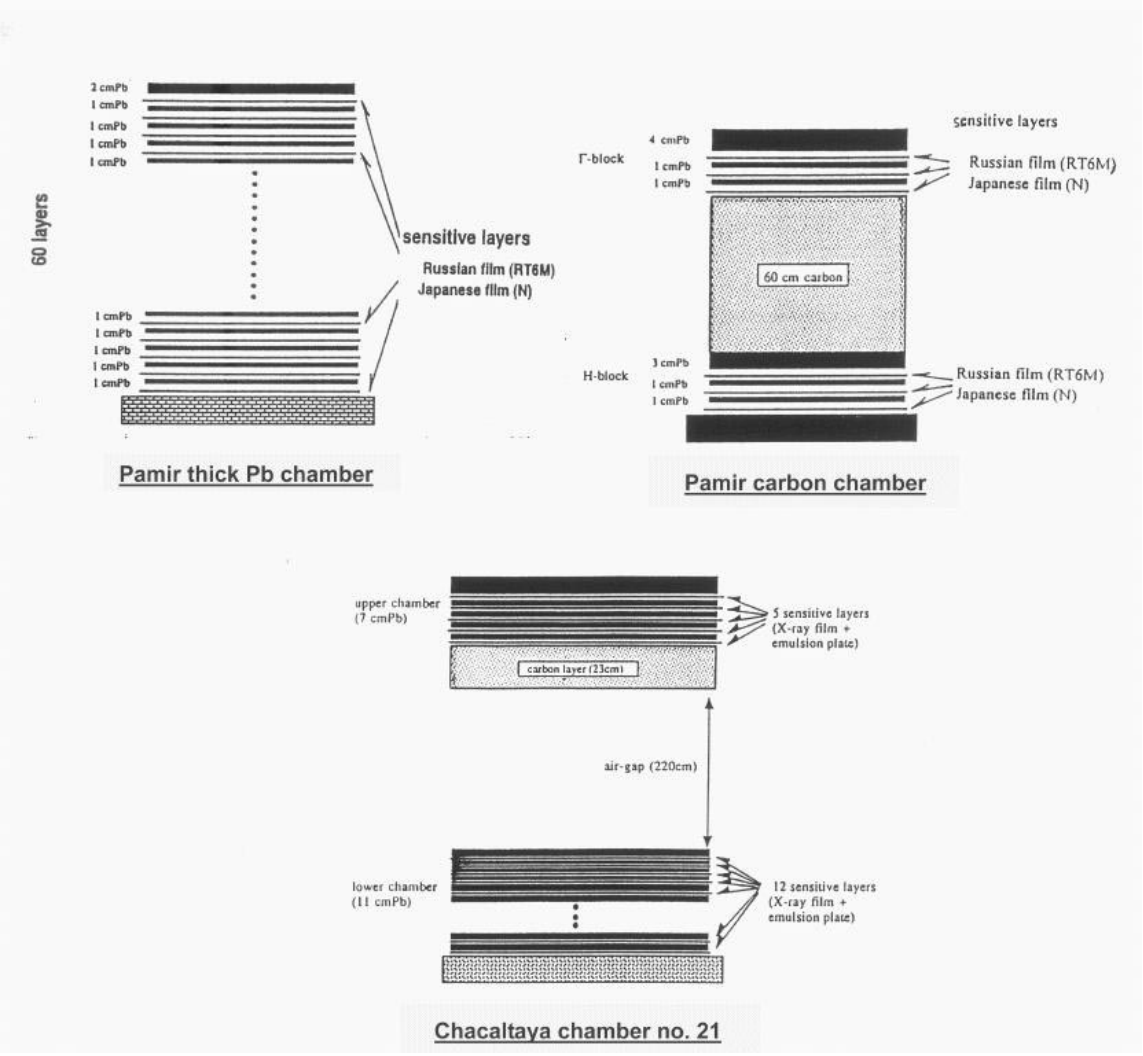

Figure 2.1: Schemes of typical emulsion chambers [20].

cascades) and in the study of the strongly penetrating component.

Typical detected event, called here family, is generated in a collision of a cosmic-ray particle (mostly p or π) with air nuclei at the distance of about 500-1000 m above the apparatus. The collision mean free path of cosmic ray hadrons is about 1200 m and mean free path for pair creation by γ–quanta is about 770 m of the atmosphere at the top of Chacaltaya ($\lambda^{int}_{n-air} = 75$ g/cm^2, $\lambda^{int}_{p-air} = 110$ g/cm^2, 1 c. u. = 37.7 g/cm^2). Keeping in mind these numbers we see that particles born in a typical act of interaction must traverse about 0.5-1 λ^{int} ($\approx$ 2 c.u.) of matter, before reaching the detector. Thus the families born at large distances above the chamber are not "clean" events but they are affected by electromagnetic-nuclear cascade processes in the atmosphere.

Normal events contain about 30% of π^0 mesons. Since each π^0 decays into 2γ there is produced rougly one γ for each charged particle in the primary interaction. As the products of the interaction descend towards the chamber, the fraction of their electronic and photonic content increases through the shower formation, so that a "usual" family (hadrons, gammas and electrons with the common origin) seen in the upper detector is always several times larger than its continuation into the lower detector. In "normal" families, from the energy range $\Sigma E_\gamma = 100$-1000 TeV, the hadronic component constitutes $\leq 30\%$ of the total visible energy. Thus, a big surprise were the events with the contrary situation. Since the upper half of these events did not allow one to predict their lower part, such events were named "Centauros".

At present, rather big statistics of cosmic-ray families with visible energy greater than 100 TeV from Chacaltaya and Pamir-joint experiments exists. The experimental material, suitable for investigation of the above mentioned exotic phenomena, was collected by the Brasil-Japan Chacaltaya Collaboration, starting from the 1970's, when the Centauro I was found. Since 1980, the joint experiment has been conducted at the Pamir, by the Pamir and Chacaltaya groups after Nakhodka Symposium, and a part of the material from the standard type carbon Pamir chambers has been reanalysed in the same manner as in Chacaltaya experiment, with the point of view exotic phenomena. In 1991 a joint analysis, undertaken by Moscow State University and Japan groups using the homogenous thick lead chambers, has been also started. Table 2.1 shows both the statistics reported in ref. [20] and also in the more recent ref. [7] where unusual characteristics of high–energy cosmic–ray families were studied, with CORSIKA simulation code.

Partial analysis, concerning selected subjects, have been done sometimes using higher statistics. In addition some extremely interesting events have been found also in other types of thick chambers (as well as homogenous lead chambers and carbon type chambers consisting of several hadron blocks), see section 2.1.2.

The present experimental results obtained by Chacaltaya and Pamir Collaboration show that hadron rich families occupy more than 20% of the whole statistics and indicate the existence of several types Centauro species, characterized by:

- abnormal hadron dominance (both in multiplicity and in energy content),
- rather low total (hadron) multiplicity, in comparison with that expected for nucleus-nucleus collisions at that energy range,
- transverse momentum of produced particles much higher than that observed in "normal" interactions ($p_T \approx 1.7$ GeV/c for Centauros and 10-15 GeV/c for Chirons,

Table 2.1: Family statistics.

	exposure m^2yr		no. of families $\Sigma E(\gamma) \geq 100\ TeV$	
	[20]	[7]	[20]	[7]
Chacaltaya chambers (5200 m, 540 g/cm^2)	300	300	121	122
Pamir joint chambers (4300 m, 595 g/cm^2)	530	720	173	215
Pamir carbon chambers (joint analysis)	500	528	125	135
Pamir lead chambers (joint analysis)	~ 450		16*	

* families with $\Sigma E_{vis} \geq$700 TeV

assuming the gamma inelasticity coefficient $K_\gamma \approx 0.2$),

- isotropic η distribution.

They can be divided into several groups, such as:

1. Centauros of original type,
2. Mini-Centauros,
3. Chirons,
4. Geminions.

2.1 Centauros of original type

2.1.1 "Classical" Chacaltaya Centauros

History

Centauro, which is mainly characterized by large imbalance between the hadronic and photonic component, has been a puzzle for so many years. The first Centauro [21] was found many years ago, in 1972, in the two-storey Chacaltaya chamber No. 15. It is the most spectacular and indisputable event of this kind. The triangulation measurement (by angular divergence) of shower direction was feasible for the event and it allowed to estimate the interaction height to be 50±15 m above the chamber. It is relatively small distance and this is the reason that the event is clean, i.e. it didn't suffer from the electromagnetic and nuclear cascade in the atmospheric layer above the apparatus. The scheme of the event is shown in Fig. 2.2. In the upper chamber there were observed 7 cascades, identified as

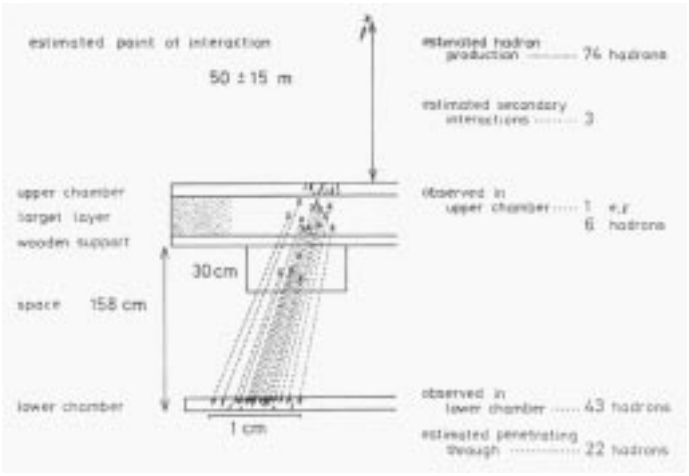

Figure 2.2: Illustration of Centauro I [23].

one atmospheric e/γ and 6 Pb-jets. In the lower part of the detector 43 observed cascades have been classified as 7 Pb-upper-jets, 29 C-jets and 7 Pb-lower-jets.

A "normal" family seen in the upper detector is always several times larger than its continuation in the lower detector. So, the Centauro I event, with the contrary situation, was a very big surprise. The suspicion that the event might have happened during a short period of assembling or removing the chamber was eliminated because the upper detectors were always mounted before the lower ones and the lower detector is always the first to be removed.

After introducing corrections for the hadron detection efficiency and secondary particles generated in the atmospheric interactions above the chamber (A-jets), the Centauro I can be considered as the event with the total interaction energy ΣE_γ= 330 TeV, in which only one electromagnetic (e/γ) particle and 74 hadrons have been produced.

The estimated interaction height allowed to calculate the transverse momenta of produced secondary hadrons. The visible part of the average p_T value is $< p_T^\gamma >= 0.35 \pm 0.4$ GeV/c. It results in the average transverse momentum of a produced hadron $\langle p_T \rangle = 1.75$ GeV/c, taking the gamma-inelasticity factor $< K_\gamma > = 0.2$ [2]

It is very exciting that more recently, in 1997, during the International Cosmic Ray Conference, helded in Durban in South Africa, the next very similar event has been reported [22]. The family consisting of only hadrons, without association of any electromagnetic cascades has been again found in the Chacaltaya chamber. This event has a similar appearance with the original Centauro I, although the hadron multiplicity is smaller ($N_h = 13$) and some authors considered it as rather the clean Mini-Centauro example.

Since the finding of the first event Centauro I a systematic search for such surprising families has been made in the successive exposure of the Chacaltaya chambers and a little

[2]Such value of K_γ factor is usually quoted for nucleons and used by Japan-Brasil Collaboration, basing on assumption that the hadrons born in the Centauro interaction are nucleons. A little higher value, $K_\gamma \simeq 0.4$, is being preferred for pions. In that case, preferred by DCC followers, $< p_T > \simeq 0.875 \pm 0.375$ GeV.

later also in the Pamir chambers. The next four events, found in Chacaltaya chambers, in several years after the discovery of the Centauro I, have been analysed and described in detail in [23]. These well known events we call "classical Centauros".

Multiplicities and energies

The main characteristics of the "classical Centauros" are shown in Table 2.2. There are shown multiplicities (above the energy threshold) and energies of both electromagnetic and hadronic components concerning three stages of analysis of the events. The observed multiplicities (upper part of the table) are the mixture of the particles born in the parent interaction and these generated in secondary atmospheric interactions. Hadronic multiplicities are uncorrected for the chamber detection efficiency. There is shown also a class of cascades detected in the upper chamber, labeled as "unidentified" which in principle could have as well as electromagnetic as hadronic origin. The fraction of the observed hadronic energy to the total visible energy of the event named $Q_h = \Sigma E_h^{\gamma}/\Sigma E_{tot}$ was also calculated. This parameter is now widely used in the analysis of the imbalance between hadronic and electromagnetic components of cosmic ray events.

The medium part of the table contains the above mentioned characteristics, corrected for the hadron detection efficiency. Also separation of electromagnetic and hadronic cascades from the "unidentified" group, by means of statistical procedure, was done. These corrections can be made by using the experimental distribution of the depths of interaction points in the chamber (C-jets, Pb-upper-jets and Pb-lower-jets). The observed distribution was found consistent with an exponential function. Therefore, knowing the thickness of the chamber and the numbers of observed Pb-jets and C-jets, it is possible to estimate the number of hadrons which penetrated through and left the chamber without interaction. At the same time, one knows how many nuclear interactions happened to occur near the top of the upper detector and have been left in the category of "unidentified". Thus, one can estimate the number of arriving hadrons and gammas at the top of the chamber.

Knowing both the number of hadrons arriving at the top of the chamber and the interaction height it is possible to estimate the multiplicity of hadrons produced in the parent Centauro interaction and also the number of secondary atmospheric nuclear interactions (A-jets) during their passage to the chamber. Subtracting the number of expected gamma rays produced in these A-jets from the observed number of atmospheric e/γ in the chamber one can obtain the number of gamma rays produced in the parent Centauro interaction. As it is seen in the lower part of the Table 2.2, the number of gammas or electrons estimated to be produced in the Centauro interaction is practically zero, so the number of neutral pions or other rapid-gamma-decaying hadrons must be negligibly small. The details of such analysis are presented for example in [25] where Centauro IV as a typical case of the event with not too small production height has been studied.

Centauro production heights

Unfortunately, measurements of the heights of interaction points, through the shower geometry, were possible only for a few exotic events found in Chacaltaya chambers, among them for Centauro I and later for Centauro IV. The list of Centauro-type species, for which the geometry measurements were possible is shown in Table 2.3 [26, 27, 28].

Table 2.2: Characteristics of Chacaltaya Centauros.

CHACALTAYA CENTAUROS					
Centauro no.	I	II	III	IV	V
Chamber no.	15	17	17	17	16
Observed in the chamber					
N_γ	1	-	-	-	-
N_{unid}	-	5	26	61	34
N_h	49	32	37	38	31
$\Sigma E_h^\gamma[TeV]$	222	179	169	144	167
$\Sigma E_{tot}[TeV]$	231	203	270	286	285
Q_h	0.96	0.88	0.63	0.50	0.59
					0.72*
Estimated at the top of chamber					
N_h	71	66	63	58	45
$\Sigma E_h^\gamma[TeV]$	321	369	287	220	242
N_γ	1	0	17	51	31
$\Sigma E_\gamma[TeV]$	9	0	66	119	108
Estimated in Centauro interaction					
N_h	74	71	76	90	63
$\Sigma E_h^\gamma[TeV]$	330	370	350	340	350
N_γ	0	0	0	4	0
$H[m]$	50	80	230	500	400
N_{A-jets}	3	5	13	32	18

* value obtained after re-analysis of the event [24]. It is the lower limit as the highest energy hadron was excluded.

Table 2.3: Centauro species with geometry measurement.

Type	*number*	*chamber*	$E_{vis}[TeV]$	$H[m]$	$p_T^{\gamma}[GeV/c]$
Centauro	I	15	230.6	50±15	0.35
Centauro	IV	17	284.8	500^{+206}_{-113}	0.30
Centauro	VII	21	∼6000	∼2000-3000	$\sim 0.35^{*}$
Mini-Cent.	18S18I12	12	356.5	160±30	0.27
Mini-Cent.	139S105I19	19	110.4	300±100	0.33
Geminion**	52I17	19	19	3.0±0.2	2.56
Geminion	70S58I19	19	160	50±15	2.16
Chiron	198S154I19	19	368.7	330±30	1.77
Chiron	212S154I19	19	69.4	$4.2^{+2.2}_{-1.1}$	3.28
Chiron	148S113I	20	312	100±60	2.6±1

* consistent with Centauro I

** Castor-Pollux

The production heights for majority of other events were estimated comparing their respective lateral spreads with that of Centauro I and assuming the same average p_T for produced hadrons. The production heights are mostly higher than that for Centauro I, so it is natural that the events, suffering from nuclear-electromagnetic cascade in the atmosphere, contain stronger admixture of atmospheric gammas and electrons.

Other Centauro properties

- Centauros are observed in the very high energy region. The energy threshold for their production is about 1000 TeV. As the average observed energy (for 5 Chacaltaya Centauros) is 348 TeV, the total incident energy was estimated to be 1740 TeV, assuming the value of inelasticity coefficient $K_{\gamma} = 0.2$.

- Psedorapidity distributions of Centauro species (Centauros, Mini - Centauros and Chirons) are consistent with a nearly Gaussian distribution [29], centered at $\langle \eta_{Cent} \rangle_{lab}^{exp}$ = 9.9±0.2 for Centauros. Generally, experimental characteristics support a formation and a subsequent isotropic decay of a fireball with the hadron multiplicity $N_h = 100 \pm 20$ and the mass $M_{Cen} \simeq 180\pm$ 60 GeV, where the error is mainly due to the uncertainty in the p_T value. The Centauro features based on the fireball model are described in chapter 4.4.2 and they are shown in Table 4.1.

- Centauro origin and the kinematical region in which the phenomenon is observed are still the matter of debate. These questions are more detaily addressed in chapter 4 concerning Centauro models and in chapter 5 regarding the accelerator searches of

the exotic phenomena. Here we would like to emphasize that both these questions cannot be answered on the basis of only experimental data. Some additional assumptions and model speculations are necessary. It should also be noted that both these questions are connected one to the other and the answer is important for the planning of the new collider experiments. Table 2.4 illustrates the problem.

Table 2.4: Average characteristics of 5 Chacaltaya Centauros assuming nucleon-nucleon or nucleus-nucleus collisions.

		nucleon-nucleon	*nucleus-nucleus* $m_{proj} = 60$, $m_t = 14$
Energy (TeV)	$\langle E_{lab} \rangle$	1740	1740
	$\langle E_{cms} \rangle = \langle \sqrt{s} \rangle \simeq \sqrt{2 E_{lab} m_t}$	1.8	6.9
Maximal projectile pseudorapidity	$\langle \eta_{lab}^{max} \rangle \simeq ln(2E_{lab}/m_{proj})$	15.1	11.
	$\langle \eta_{cms}^{max} \rangle \simeq ln(\sqrt{s}/m_{proj})$	7.5	4.8
Centauro pseudorapidity	$\langle \eta_{lab}^{Cent} \rangle$	9.9	9.9
	$\langle \eta_{cms}^{Cent} \rangle$	2.4	3.7

There are shown energies, pseudorapidities and maximal projectile pseudorapidites, calculated both in the laboratory and in the centre of mass system, for two different scenarios of the collision: formation of Centauros in either nucleon-nucleon or nucleus-nucleus collision and assuming the projectile being the medium primary cosmic ray nuclei with a mass ~ 60 and the target with a mass ~ 14, being a medium atmospheric air nucleus. It is clear that answering the question, if Centauros are produced at the midrapidity or rather in the projectile fragmentation region and where in the new colliders should we expect them, depends on a kind of a target and a projectile, which are unknown objects in these experiments. It is seen from Table 2.4 that assuming nucleon-nucleon collision we can expect Centauros produced somewhere between the central and the fragmentation rapidity region. In this case,

the threshold for Centauro formation is close to the Fermilab collider energies. On the other hand, if Centauros are produced in nucleus-nucleus collisions they should be looked for in the projectile fragmentation region. The question of the possible Centauro formation in the new collider experiments (at RHIC and LHC) will be considered later.

2.1.2 Other Centauro and Centauro-like events

Besides the "classical Chacaltaya Centauros", a quite reasonable statistics of Centauro-like (or hadron rich) events has been collected as well by Chacaltaya as by Pamir Experiments. Unfortunately, in contrast to the undisputable Centauro I, some of these events were born at rather large distances from the apparatus, thus they possess the significant fraction of electromagnetic component, which probably have been generated in the nuclear and electromagnetic cascade processes, in the atmospheric layer above the chamber. Besides that the serious difficulties were met during the measurements and analysis of some exotic super-familes (with the very high visible energy, $E_{vis} \geq 500$ TeV) which are very frequently accompanied by the so called "halo". These are the reasons that some events were not so detaily analysed and they are not so spectacular as the Centauro I. We call them *Centauro-like events*. They are not so well known as "classical" Centauros although they carry a big amount of exciting experimental information. Here will be listed and described examples of the most interesting Centauro-like (or hadron-rich) events.

1. *CENTAURO-NEW (C22-Sxxx-I019) [8, 22].*

The new clean Centauro event was reported in 1997 at the 25th International Cosmic Ray Conference in Durban. The event was found in the Chacaltaya two-storey chamber no. 22, consisting of the upper chamber (7 cm Pb), target layer (30 cm CH_2), air space (237 cm) and the lower chamber (11 cm Pb), i.e. of the total thickness $\sim 0.49\lambda_{int}$. It is the family of 31 showers (13 with energy exceeding 1 TeV) of the total observed energy 57.4 TeV (or 51.2 TeV when the energy threshold of 1 TeV is used). No showers in the upper chamber have been found. According to ref. [22] there is no trivial reason for the fact that no showers are observed in the upper chamber (the lower chamber was constructed only after the upper chamber was completed). Hence, the event is considered as clean Centauro (or Mini-Centauro regarding its relatively small energy), without presence of γ rays. It is the second, besides the Centauro I, event of this type.

2. *CENTAURO VI [30, 31, 32].*

The event no. C20-107S-089I was observed in the Chacaltaya two-storey emulsion chamber no. 20. The measurements were restricted to X-ray film observation because the emulsion plates were not in fully satisfactory condition. The observed results, i.e. the domination of hadrons in the high energy region and the exponential $E{\cdot}R$ distribution [3] can be interpreted under the hyphotesis of Centauro interaction. Assumption of the same average transverse momentum of secondary hadrons as that measured for Centauro I ($\langle p_T(\gamma)\rangle \sim 0.35$ GeV/c) leads to the production height of about 800 m. The estimated multiplicities and energies of photonic and hadronic components (for showers with visible energy greater than 4 TeV) at the top of the chamber are: $N_\gamma = 15$, $\Sigma E_\gamma = 95.2$ TeV, $N_h = 40$, $\Sigma E_h^\gamma = 900$ TeV.

[3] E is an energy and R is a distance of a particle from the energy weighted family centre.

The estimated number and energy of hadrons at the interaction point is: $N_h = 80$, ΣE_h^{γ} = 1500 TeV [32].

3. *CENTAURO VII [26, 30, 31].*
The event no. C2187S75I [26, 31] named Centauro VII was the first Centauro with halo. Fortunately, the observed halo has not been developed so well and the energetic showers were distinguishable even on the X-ray film. It has been found in the Chacaltaya two-storey chamber no. 21, consisting of the upper chamber (7 cm Pb) and the lower one (11 cm Pb) with the carbon target (23 cm pitch) and the air gap (2 m) between them. In this event, the detailed study of the shower core structure in nuclear emulsion plates was done. Also the decascading procedure was used to study the longitudinal and lateral characteristics of the event. The family has an extremely large visible energy ($\Sigma E_{vis} \approx 5600$ TeV + 500 TeV (halo) [26]). The interaction height, estimated by triangulation measurements [26], is about 2000-3000 m above the chamber. Such value of the production height results in the average transverse momentum value consistent with the Centauro type events. The event is undisputable the hadron-rich family with Q_h value of the same order as for "classical" Centauros. $Q_h = 0.46$ for $E_{th} = 2$ TeV increasing to $Q_h \approx 0.8$ when assuming the most unfavourable case that all halo energy is of electromagnetic origin and when the analysis is limited to the most energetic cascades, with energies higher than 20 TeV (what seems to be justified by the large production height).

The family is in an old stage of development due to the long distance atmospheric propagation, judging from the existence of a large number of lower energy degraded gamma-rays. However, the family contains, in the central region, several very high energy showers, higher than or close to 100 TeV. Those are confined within the radius smaller than several centimeters from the centre of the family. All of them started the shower development from the upper chamber and were penetrating deeply into the lower chamber, far beyond the expectation from simple electromagnetic cascades. Their transition curves are shown in Fig. 2.3.

This family is sometimes claimed to be the *Chiron-type* interaction because of very large lateral spread of hadrons [31] (the spread of high energy hadrons with $E(\gamma) \geq 40$ TeV is as large as $\langle E(\gamma) \cdot R \rangle \simeq 1300$ GeV·m) and the existence of the *strongly penetrating component*, revealing typical *mini-cluster* configuration. The majority of very high energy penetrating cascades, given in Fig. 2.3 show a typical *mini-cluster* structure. Re-analysis of the event [24] confirmed its exotic character and showed that characteristics of the hadronic secondaries are compatible with assumption of one emitting fire-ball. 4. *CENTAURO "PAMIR" [31, 33, 34].*
Centauro event, marked in [31] as G178H178 or P3' C2 B178 in [33, 34] was found in the carbon-type chamber no. 2 of P-3', consisting of the standard gamma block (6 cm Pb) followed by the carbon target (60 cm C) and the hadron block (5 cm Pb), from USSR-Japan joint exposure at the Pamir. The event shows every feature of a Centauro, i.e. the energy is mainly released into the hadron-induced showers and the average lateral visible-energy spread is much higher for the hadron induced showers than for the γ-ray induced ones. For the hadron induced showers both spectra: the fractional visible energy and the lateral visible energy spread, can be well reproduced by exponential functions. The height of the interaction was estimated to be H = 700± 100 m, from the lateral visible energy

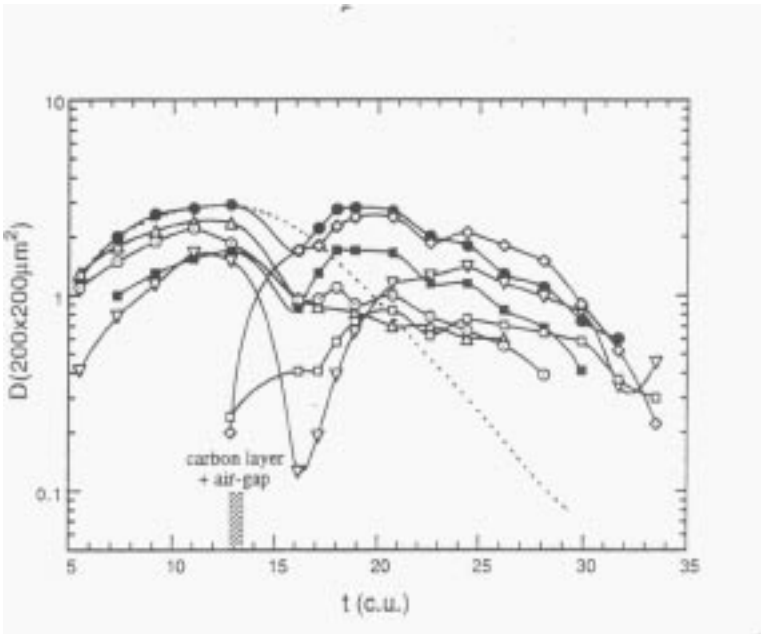

Figure 2.3: Strongly penetrating cascades from Centauro VII [31].

spread of hadrons with $\Sigma E_h^\gamma \geq 4$ TeV and by using the same as for Centauro I $\langle p_T(\gamma)\rangle$ value. Estimated numbers and energies of electromagnetic and hadronic component at the top of the chamber are: $N_\gamma = 55$, $\Sigma E_\gamma = 372.5$ TeV, $N_h = 45$, $\Sigma E_h^\gamma = 700$ TeV. The multiplicity and energy of hadrons estimated at the original interaction is $N_h = 77 \pm 16$ and $\Sigma E_h^\gamma = 1000$ TeV [32] respectively (for showers with the visible energy greater than 2.3 TeV).

5. *ELENA [35].*
Elena is a superfamily with a total measured energy ~ 1700 TeV, detected in the Pamir deep lead chamber of a total thickness of 60 cm, what corresponds to $\sim 3\lambda_{int}$. It has given a rather rare opportunity to observe the transition of particles produced in such high energy interaction through the deep chamber. The majority of superfamilies were detected in relatively thin chambers ($\leq 1.5\lambda_{int}$) what makes impossible the detailed investigation of hadron characteristics.

This event reveals the features of Centauro-type families, such as the wide energy weighted lateral distribution and the large fraction of family energy transfered to hadrons. $Q_h = 0.7 \pm 0.07$, when corrected for hadron detection efficiency, what locates the family well beyond the region of usual fluctuations on the N_h vs. Q_h diagram. Soft spectrum of gamma-rays indicates that the family is "old". The height of the initial interaction point was determined, assuming that $\langle p_T(\gamma)\rangle$ of hadrons is 0.35 GeV/c. It gives the height $\sim 1500 - 2000$ m above the chamber. A similar analysis as that done for "classical" Centauros, i.e. evaluation of the number of hadrons generated in the primary interaction and the number of their interactions in the air above the chamber, does not contradict the scenario of the development of a Centauro-type event occuring at large height above

the apparatus.

The total number of detected hadrons is 31 and among them 4 hadrons undergo in the chamber several interactions.

Especially interesting is the "leading" hadron. It was located at a distance of 7.5 mm from the family energy weighted centre and it was not accompanied by any γ-rays at a distance closer than 1 mm. It started its development rather deeply inside the chamber and escaped through its bottom after passing 35 cm of Pb ($\sim$ 65 c.u.). Three separate maxima are seen in the cascade longitudinal development (see Fig. 2.4).

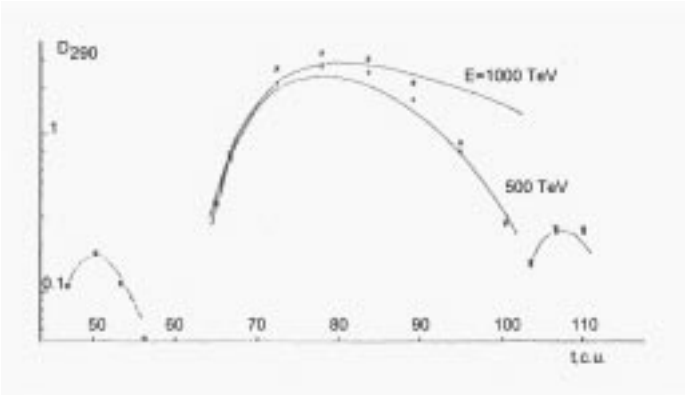

Figure 2.4: Transition curve in terms of optical density D_{290} of high energy cascade detected in family Elena [35]. Black dots are experimental points without methodical corrections, crosses are corrected experimental points. Calculated curves for γ–quanta are also shown.

Dark spots produced on the X–ray films by electromagnetic showers induced by this hadron have large transverse dimensions, $\sim$ 3 mm, and look like a "halo". The estimated energies and the points of origin of the showers producing each of the three "humps" have the following values: $E_1 = 9.8$ TeV, $t_1 = 39.7$ c.u., $E_2 = 500$-1000 TeV, $t_2 = 57$ c.u., $E_3 =$ 20 TeV, $t_3 = 90$ c.u.. The analysis presented in [35] showed that it is difficult to explain such shape of a transition curve , assuming the "normal" interaction of high energy leading hadron. For example, the probability of producing the observed ratio of released energies corresponding to the first two humps by a subsequent interactions of a hadron in usual nuclear-electromagnetic cascade in lead is as small as $\sim (1-4) \cdot 10^{-3}$. 6. *C-K [36, 37].*

The family named here C-K was found in a deep lead chamber "Pamir 76/77", of a total thickness of 60 cm Pb. It has been measured and analysed by the Cracow group. We classified it as a very spectacular Centauro-like event accompanied by the strongly penetrating component. It was the first hadron-rich event with so spectacular evidence for penetrating cascades. Fortunately, it was found in the homogenous type thick lead chamber which gives possibility of the detailed study of the transition curve structures. Comparison of this family with classical Centauros is shown in Fig. 2.5. On the diagram of the number of hadrons N_h vs. the hadron energy fraction Q_h for Chacaltaya events

[23, 38] the event C-K has been marked by the star. For the Chacaltaya events, the hadron part includes C-jets, Pb-jets-lower and identified Pb-jet-upper, and A-jets identified as a shower cluster with association of a hadron in it. Since the effective thickness of the Chacaltaya chambers is about 1.5 nuclear mean free paths, and the "identified A-jets" cover only the A-jets with production heights less than ~ 100 meters, the "hadron energy sum" $\Sigma E_h^{(\gamma)}$ will give an under-estimate on an average. The C-K event has been registered in the deep lead chamber, so that the loss due to penetration is negligible. On the other hand a relatively high threshold for hadrons in Pamir chambers (here it was assumed to be 2 TeV) as compared with the Chacaltaya detectors reduces the number of hadrons. Keeping in mind these two effects it seems that such comparison is roughly reasonable. The hadron-rich nature of the event is evident.

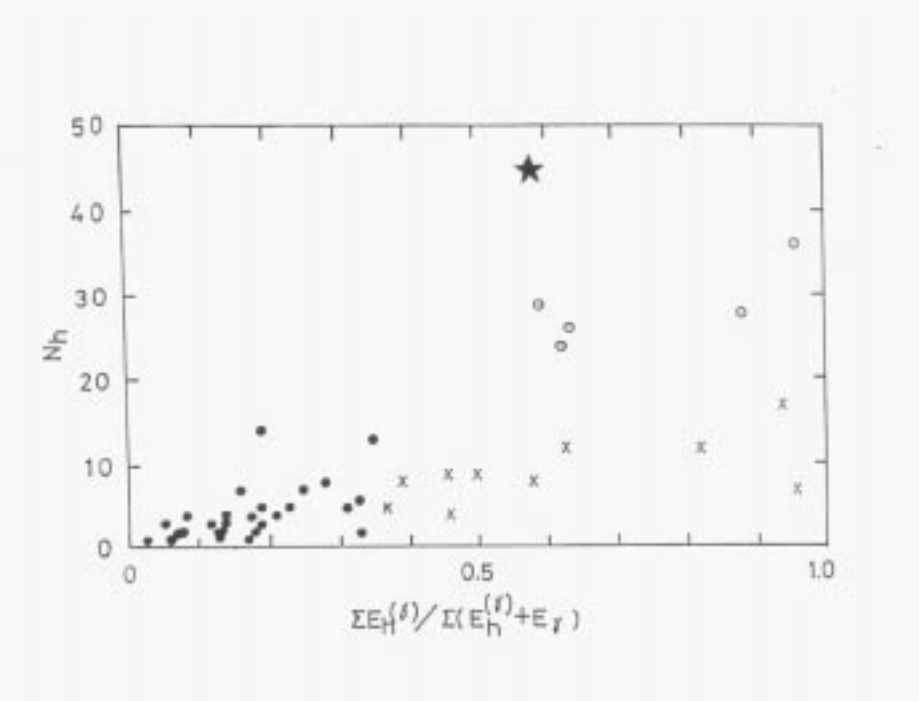

Figure 2.5: Diagram of the number of hadrons and hadronic energy fraction: Chacaltaya events with the total visible energy greater than 100 TeV [38]: ($\circ$) Centauro, ($\times$) Mini-Centauro, ($\bullet$) others; ($\star$) C-K [36].

Among cascades belonging to the family, two cascades reveal unusual features. They were observed not far from the energy weighted centre of the family, in the very close distance one to the other. Both cascades demonstrated a multicore structure. They started their development rather deeply inside the chamber and after passing a very thick layer of lead, escaped through the bottom of the chamber. The features of these cascades are summarized in Table 2.5. Their transition curves reveal surprising features. Both cascades have unexpectedly long range and many maxima character. The longer cascade, shown in Fig. 2.6 penetrated more than 109 cascade units and 11 maxima at its transition curve appeared. The average distance between the neighbouring humps is very small, equals only 10.4 ± 4 c.u.. These features are hardly explained by simulations. According

Table 2.5: Unusual cascades in Centauro-like event C-K.

Cascade no.	*Starts at*		*Finishes at*		*Penetrated*	*Number of*
	c.u.	*layer no.*	*c.u.*	*layer no.*	*c.u.*	*maxima*
197.08	11.8	5	120.7	escape	108.9	11
748.01	48.3	23	120.7	through bottom	72.4	5

to calculations [39], an average cascade initiated by a hadron with energy ~ 100 TeV can be detectable in such chamber only to the depth of 45.5 c.u. (for measurements with diaphragma of a radius of 50 μ). Morever, the many maxima cascade curves are obtained in simulations very rarely. But even in that case, only very limited number of humps can be detected (two-three) and the average distance between them is much larger (23 ± 10 c.u.) than that observed here. Unexpectedly, both unusual cascades penetrate through the whole chamber practically without noticeable attenuation, and a weak growing rather than quenching of the cascades is observed. From this point of view they remind the long-lived cascades discovered by means of the Tien-Shan calorimeter [40].

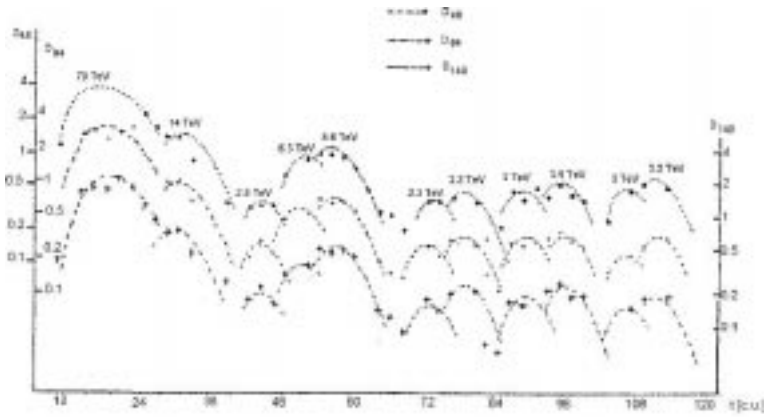

Figure 2.6: Transition curves in X-ray film darkness D (measured in three diaphragms of a radius R = 48, 84 and 140 μ) for cascade no. 197.08. Energy (in TeV units) liberated into the soft component is indicated at each hump (averaged over three estimated values) [36].

7. *P3' C2 201 [31, 34, 41].*

This candidate of Centauro type interaction of the highest energy range, occuring at very high altitude above the apparatus, marked as G201H201 in ref. [31], was detected in

the Pamir joint standard carbon type chamber P3'-C2. It has got the small blackened area (in the radius of about 2 mm on the X-ray film) in the center of the family, being considered as the premature stage of the halo. It is composed of several very high energy showers strongly penetrating into the lower chamber. It is difficult to clearly resolve such a blackened area into individual shower-cores on X-ray film, and therefore this part was separately analysed. The estimated height of the family turns to be ~ 2000 m above the chamber (from the lateral spread of the high energy hadrons and by assuming $\langle p_T(\gamma)\rangle \simeq 0.35$ GeV/c). Such value of the height gives the original multiplicity of hadrons of about 100.

8. *HALINA [31, 42, 43].*

This event has been found among 7 high-energy hadron-gamma families of $\Sigma E_\gamma \geq 800$ TeV in a systematic study of carbon chambers of $\simeq 400$ m^2 year exposure (the Polish part). It was detected in the Pamir-79/80 carbon chamber C42, consisting of the standard gamma block (of 6 cm Pb) and two hadron blocks (of 5 cm Pb) interlayed the carbon target (60 cm of carbon), i.e. the effective thickness of the chamber was ~ 2.3 λgeo. It is a good design for investigation of a hadronic component, as the detection probability of hadrons in the chamber is larger than that of the standard type carbon chamber and it is close to 90%. It is no halo event despite of its high energy.

This event reveals all exotic Centauro features:

- It has hadron-rich nature: the energy fraction of a hadronic component in the peripheral region $Q_h = 0.45$. About 30% of its energy is carried by 106 identified hadrons (with the visible energy greater than 2 TeV).
- Its longitudinal and lateral characteristics cannot be fully explained by usual hadron interactions, even when the contributions of heavy nuclei in primary particles are considered.
- Extraordinary wide lateral spread both in gamma-rays and in hadrons results in the transverse momentum of produced particles $p_T \simeq 1$ GeV/c.
- There are 6 showers which penetrate from the gamma-block to both hadron blocks.

9. *C141G4836 [31, 42].*

It is a hadron-rich event found in the Pamir-85/86 standard type carbon chamber C141. The total observed energy of the event is 2289 TeV and ~ 21% of the energy is carried by 50 identified hadrons. Similarly as Halina this event is no halo family and it is characterized by unusually large lateral spread both in electromagnetic and hadronic component. Usual interactions and normal cascading processes in the atmosphere can not explain all (longitudinal and lateral) characteristics of the event, even if heavy nuclei composition in primary cosmic rays is assumed. According to analysis done in [42] hadron rich nature of the event is seen in the correlation diagrams (N_γ vs. N_h and N_h vs. Q_h) after a decascading procedure. The hadron rich nature of the family is close to that expected for heavy nuclei induced reactions, however, the number of decascaded gamma–rays is appreciably smaller than that in the case of heavy primaries. Heavy primaries induced events give

steeper energy spectrum for both decascaded gamma–rays and hadrons.

10. *ANDROMEDA [44].*
Andromeda was detected in the flat chamber CH-14 (11 cm Pb, 41% hadron detection efficiency) of the Chacaltaya experiment and it is known as the first and most famous example of the superfamily with the huge halo of the radius of about 3.2 cm. Unfortunately, the chamber was not thick enough to study the full development of the halo transition curve and a hadron component of the event. Some authors [38] interpreted a halo in Andromeda as caused by a numerous bundle of high energy atmospheric γ quanta. However, the observed decrease of the intensity of the halo transition curve with the depth in the chamber is less than that expected from a pure electron shower. Besides that the energy spectrum of hadrons is harder than that of electrons/γ-rays and generally its characteristics are found to be inconsistent with the hypothesis of a proton primary with pion multiple production under the scaling model. In ref. [44] the event is claimed to be hadron rich. Estimates of the total energy of the photonic and hadronic component (after corrections for detection efficiency) show that the hadrons carry $\sim 47\%$ of the total energy.

11. *URSA MAIOR [31, 44, 45, 46].*
It was found in the two-storey Chacaltaya chamber CH-15 (64% hadron detection efficiency). Similarly as Andromeda it is the typical halo (with the multi–core structure) super-family. The hadronic component occupies the substantial part of the whole energy (38% after correction for efficiency and above the threshold of the shower spot detection). The study of correlations between hadrons and gamma rays situated the family in the region of big values of hadron number and hadron energy, and outside fluctuations expected from a scaling type model with the proton primary.

12. *MINI ANDROMEDA III [31, 45, 46].*
It was registered in Chacaltaya two-storey chamber CH-19 (59% hadron detection efficiency). The wide halo (with the radius of about 2.2 cm) reveals the core structure. Similarly as in the previous events the chamber is too thin for a study of the full longitudinal halo development and the structures in the halo transition curve. But even at this limited length, the observed attenuation of the halo transition curve is weaker than that expected from a pure electromagnetic origin. In spite of the indications on the very high production altitude (wide lateral hadronic spread) this family is extremely rich in hadrons both in energy fraction and in number. The hadrons occupy $\sim 44\%$ of the total energy (above the threshold of shower spot).

13. *TATYANA [38, 47].*
Tatyana is one of the highest energy events known in the world statistics, extremely interesting and difficult for measurements and analysis. The estimated visible energy of the event is about 11 000 TeV, thus the total energy of the event was estimated to be about 15 000 TeV. The super-family was detected in the Pamir 450-73/74 carbon type chamber. In contrary to the majority of other chambers, it is the extremely deep apparatus, consisting of the standard gamma block and four identical hadron blocks (each consisting of 20 cm carbon layer followed by 5 cm of Pb) what gives in total about 5 λ_{int} or 55 cascade units. It makes possible the direct study of the penetrating power of the family. The halo, occupying the central part of the event easily traversed the whole

chamber, revealing the unexpectedly strong penetrating power. The blackness of the core does not show any sign of attenuation down to the bottom of the chamber, even a rise of the transition curve is observed (see Fig. 2.7).

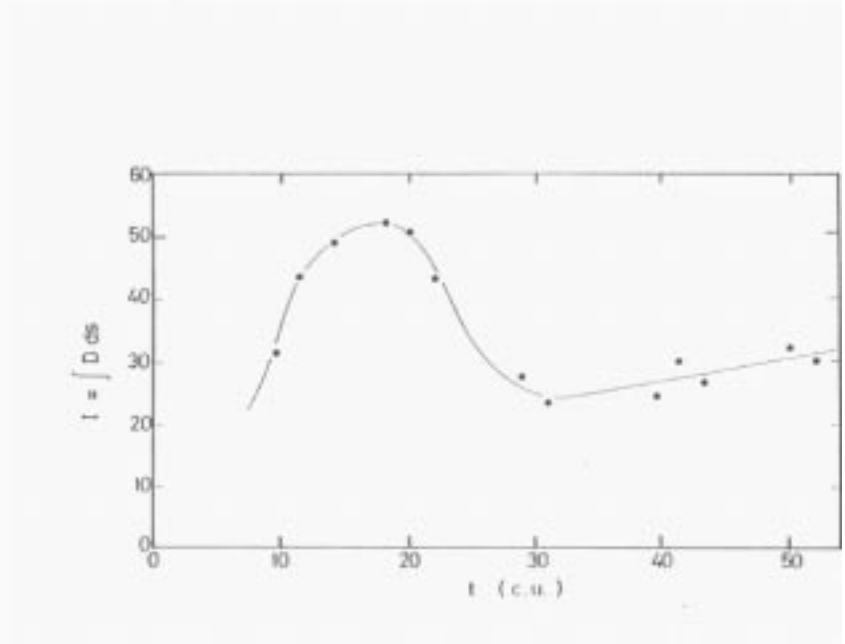

Figure 2.7: Penetrating black core in the family "Tatyana". The curve presents the darkness of the core with halo on the X-ray films with the depth in radiation units in the chamber [38].

The absence of the attenuation of the core through the chamber indicates that the secondary particles are more penetrative than normal hadrons. Outside the core halo region, of a diameter $\sim$ 1 cm, there are numerous showers. There were detected 224 γ–quanta with $\Sigma E_\gamma \sim 3200$ TeV and 66 hadrons with $\Sigma E_h^\gamma \sim 1500$ TeV. Tatyana has been classified as the family with high energy of the hadronic component.

14. *P2-C96-125 [31, 34, 48].*
This event (in ref. [31] marked as G096H125) with a huge penetrating halo was registered in the standard carbon Pamir joint chamber C96 of series P-2. Remarkable feature of the family is the existence of two central clusters carrying 67 % of electromagnetic energy and 64 % of hadronic energy. The event has similar characteristics as Andromeda and M.A. III. [48] and analysis done in [34] put it among hadron-rich events.

15. *P3'-C2-168 [31, 34].*
The event (marked in ref. [31] as G168H167) was registered in the standard carbon chamber C-2 series P3' of Pamir joint exposition. Its hadron dominant character was recognized in [34].

16. *P3'-C2-228 [34].*
Registered in the standard carbon-type chamber C-2 series P3' of Pamir joint exposition.

It is claimed to be hadron-rich family.

17. *P3'-C5-505 [31, 49].*
The family (in [31] marked as G505H505) was found in the standard carbon type Pamir joint chamber. The peripheral region reveals abnormally hadron dominant nature and the very large lateral spread. In the central region there is the strongly penetrating halo. Its characteristics are similar to Andromeda, Ursa Maior and M.A.III.

The hadron dominant character of families registered in Pamir-joint chambers series P3 and P2 was spectacularly presented on the correlation diagram (N_h vs. Q_h) in [34], also in comparison with classical Chacaltaya Centauros and some halo families such as Andromeda, Ursa Maior and U.M.III [49], see also Fig. 3.2 in section 3.1.

The main features of the Centauro–like/hadron–rich events are summarized in Tables 2.6, 2.7 and 2.8.

2.2 Mini-Centauros

Mini-Centauros are events of the same hadron dominant nature as Centauros, the difference being their smaller multiplicity. There were reported by the Brasil-Japan Collaboration 15 atmospheric and 9 produced in the target layer Mini-Centauros [23, 32]. Among 15 atmospheric families there were two favourable cases where the heights of the interaction vertex have been determined through triangulation measurement of shower positions and directions. In these events the direct measurements of the transverse momenta of hadronic showers were possible, giving $\langle p_T(\gamma)\rangle \simeq 0.35$ GeV/c. In searching for Mini-Centauros among C-jets the criterion was imposed that any pair of showers which couple to form a particle of neutral pion rest mass within the experimental error, i.e. $90 \leq m_{i,j} \leq 200$ MeV, where $m_{i,j}$ is the invariant mass of the shower pair, was not found.

The main features of Mini-Centauro events are the following:

1. Hadron multiplicity $N_h \simeq$ 10-20.
2. $\langle p_T(\gamma)\rangle$ value as large as for Centauros ($\langle p_T(\gamma)\rangle \simeq 0.35 \pm 0.10$ GeV/c).
3. Approximately gaussian pseudorapidity distribution.
4. Experimental characteristics in accordance with isotropic decay of the fireball with the mass $M_{fb} \simeq 35$ GeV and average multiplicity $\langle N_h\rangle = 15 \pm 3$.
5. Incident energy $< E_0 >_{lab} \simeq$ 940 (100) TeV for atmospheric (carbon target) Mini-Centauros. These values correspond to $\sqrt{s} = 1.3$ TeV (430 GeV) when assuming a nucleon incidence.
6. Average pseudorapidity in cms system, assuming the proton incidence $\langle\eta\rangle = 3.7$ (they are produced in a little more forward region then Centauros).

The characteristics of individual Chacaltaya Mini–Centauros can be found in [23]. Similarly as Centauros they are sometimes accompanied by the strongly penetrating component. The detailed study of C-jets and Pb-jets from Chacaltaya Mini-Centauros (from chambers no. 17, 18 and 19) revealed the existence of penetrative mini-clusters among

Table 2.6: Centauro-like events.

Event, Refer.	*Collab., Chamber.*		*N*	*Energy* $[TeV]$	Q_h	$\langle ER \rangle$ $[GeV \cdot m]$	E_{halo} $[TeV]$	E_{th} $[TeV]$	*Remarks*
CENT. NEW [8, 22]	Brasil-Japan 2-storey	γ	0	0					
		h	13	51.2	1.			1	
CENT. VI [30, 31]	Brasil-Japan	γ	56	361				4	
			157	644					
								2	
	2-storey	h	28	390				4	
			68	496				2	
		tot		751	0.52	735[1]		4	
				1140	0.44	803[1]		2	
CENT. VII [26, 30, 31]	Brasil-Japan	γ	547	2978				2	Centauro or Chiron
			265	2179				4	
		h	129	2486				2	
	2-storey		74	2328				4	penetr.
		tot		5464	0.46		500	2	cascades
				4506	0.52	842		4	and
					0.8	857[1]		20	mini-clusters, halo
CENT. PAMIR [31, 33, 34]	USSR-Japan	γ	15	95		67		4	
			120	298		28.6		1	
		h	22	444		244		4	
	standard		37	476		173		1	
	carbon	tot		539	0.82	495[1]		4	
					0.62			1	
ELENA [35]	Pamir	γ	78	600		360		4	str.pen.
		h	23	1100		885		4	leading
	deep	tot		1700	0.65±0.05				cascade
	carbon	h	22[2]	300[2]		475[2]		4	
C-K [36]	Pamir	γ	74	306		111		~ 1	str.pen.
		h	55	531		195			cascades
	deep			382[3]					
	Pb	tot			0.64				
		γ	27	198				4	
		h	22	446					
				297[3]					
		tot			0.69				

[1] measured by showers of E(γ) $\geq$ 20 TeV

[2] without leading cascade

[3] energy released only in the first peaks

Table 2.7: Hadron-rich events.

Event, Refer.	*Collab. Chamber*		*N*	*Energy* [*TeV*]	Q_h	$\langle ER \rangle$ [$GeV \cdot m$]	E_{halo} [*TeV*]	E_{th} [*TeV*]	*Remarks*
P3'C2	USSR-	γ	132	1479				4	
201	Japan	h	43	1089				4	penetr.casc.,
[31, 41]		tot		2568	0.42	435[1]	400	4	premature
	standard carbon								halo
HALINA	Pamir								
[31, 42, 43]		γ	171	1630		300	-	4	
	deep		469	2468			-	2	
	carbon	h	65	936		583	-	4	penetr. casc.
			106	1071			-	2	
		tot		2566	0.37	883[1]	-	4	
				3540				2	
C141-	Pamir								
G4836		γ	157	1277		295	-	4	hadron rich
H4784	standard		346	1807			-	2	
[31, 42]	carbon	h	31	415		903	-	4	
			50	482			-	2	
		tot		1692	0.25	1071[1]	-	4	
				2289				2	
ANDRO-	Chacal.	γ	627	4488				1	
MEDA		h	110	1656				1	
[44]	flat Pb		268[5]	(4039)[5]	~ 0.47[5]				
		total					∼21000		
URSA	Chacal.	γ	239	1074				2	single
MAIOR			430	1344				1	cluster
[31, 44]	2-storey	h	38	508				2	
[45, 46]			54	532				1	$\sim$ 1080 TeV
			(84)[5]	(830)[5]	~ 0.38[5]			1	
		tot		1582	0.32	498[1]	$\sim$ 980	2	
M.A.III	Chacal.	γ	192	1701				4	
[31, 45, 46]			441	2370				2	
	2-storey		537	2531				1	
		h	80	1070				4	
			112	1167				2	
			115	1172				1	
			(195)[5]	(1986)[5]	~ 0.44[5]				
		tot		2771	0.39	842[1]		4	
				3536	0.33	866	∼5060	2	

[1] measured by showers of $E(\gamma) \geq 20$ TeV

[5] after correction for detection efficiency

Table 2.8: Hadron-rich events, continuation.

Event Refer.	*Collab. Chamber*		*N*	*Energy* $[TeV]$	Q_h	$\langle ER \rangle$ $[GeV \cdot m]$	E_{halo} $[TeV]$	E_{th} $[TeV]$	*Remarks*
TAT-YANA [47]	Pamir thick carbon	γ h tot	224 66	3200 1500 ~ 11000			~ 6000	~ 1	periph. region str.penetr. halo
P3C96-125 [31]	USSR-Japan standard carbon	γ h tot	40 20	288 579 5437	0.67	1466[1]	4570	4 4 4	data for off halo part (r $\geq$ 1.2 cm) 2 penetr. clusters
P3'C2-168 [31]	USSR-Japan standard carbon	γ h tot	41 15	316 212 528	0.40	1007[1]	-	4 4 4	
P3'C5-505 [31]	USSR-Japan standard carbon	γ h tot	98 49	705 513 10400	0.42	3235[1]	9200	4 4 4	data for off halo (r $\geq$ 2.2 cm) penetr. halo
P3'C2-228 [34]	USSR-Japan standard carbon	γ h tot	30 18	246 236 483	0.60	350 875	-	4 4 4	

[1] measured by showers of E(γ) $\geq$20 TeV

Table 2.9: Mini-Centauros in Pamir-joint chambers, examples.

Event, Refer.	*Collab. Chamber*		*N*	*Energy* $[TeV]$	Q_h	$\langle ER \rangle$ $[GeV \cdot m]$	E_{th} $[TeV]$	*Remarks*
P3'C2	USSR-	γ	3	25		57	4	
223	Japan	h	5	302		172	4	
[34]		tot		327	0.92		4	
	standard carbon							
G544H534	USSR-	γ	18	187			4	
[31]	Japan	h	11	339			4	
		tot		526	0.65	309[1]	4	
	standard carbon							

[1] measured by showers of $E(\gamma) \geq 20$ TeV.

them [50]. This analysis gave also some suggestions on the genetic relations among different types of exotic phenomena.

Families of similar type were reported also by Pamir Collaboration. By a systematic survey in the Pamir chamber in the exposure of ~ 100 m^{2}year [38, 51] six Mini-Centauro events were found among ~ 50 families observed in the Pamir carbon-chambers C18, C19, C24 in "Pamir 78/79" and C34 in "Pamir 79/80". Comparison with simulation calculations showed that these events are beyond fluctuations in the atmospheric nuclear cascade process originating from normal type meson production (see Figures 2a, b, c in ref. [51])

The examples of other than "classical " Chacaltaya Mini-Centauros are shown in Table 2.9.

2.3 Chirons

Chirons are hadron-rich species characterized by the following features:

1. The interaction energy close to that of Centauros and estimated to be ~ 1670 TeV.

2. Rather low hadron multiplicity $N_h \approx 10$–20. The characteristic feature is the existence of *clean hadronic cascades*, not clustered among electromagnetic cascades from atmospheric showering of γ's in the atmosphere.

3. Extremely large lateral spread ($< E(\gamma)R > =$ 10–20 GeV·m, hence $\langle p_T(\gamma) \rangle$ being 2-3 GeV/c, and $\langle p_T \rangle \approx$ 10-15 GeV/c).

4. Pseudorapidity distribution of high energy showers in accordance with isotropic decay of the fireball with the mass $M_{Chiron} \simeq 180$ GeV and centered at $\eta_{cms} \simeq 2.3$ [23].

5. Frequent appearance of strongly penetrating single cores or the so–called mini–clusters (i.e. clusters of particles with very small lateral spread corresponding to very low mutual transverse momentum $p_T(\gamma) \approx$ 10-20 MeV/c). They are observed mainly in the centre of the family.

6. Existence of unusual hadronic component with the short interaction mean free path, as small as $\sim$ 1/3-1/2 of the nucleon geometrical collision mean free path.

The study of C-jets and Pb-jets belonging to the Chiron type families may indicate the existence of the chain of genetic relations [50] among such phenomena as Chiron, Centauro, Mini-Centauro etc.

Similarly as "classical" Chacaltaya Centauros several clean Chiron families have been reported by Chacaltaya group [23]. The first event of this type, Chiron I (family 198S-154I) [20, 38], was found in 1979 in Chacaltaya chamber no. 19. Similarly as Centauro I, it is the clean family for which the altitude of interaction vertex was measured by triangulation method to be 330 $\pm$ 30 m above the chamber. This allowed to measure transverse momenta of observed secondaries and resulting $\langle p_T(\gamma) \rangle \sim$ 1.42 GeV/c. The total visible energy of the event was estimated to be $\sim$ 400 TeV. The characteristics of the individual cascades belonging to the family are shown in Table 2.10. The event shows extremely large transverse momenta of produced secondaries and no π^0 meson emission. Besides that it indicates the existence of penetrating shower clusters which shows similar lateral spread with atmospheric cascades ($\sim$ a few mm in diameter). The transition curves of high energy showers for both single-cores-upper and shower-clusters-upper start development just after entering into the upper chamber, like electromagnetic cascades, however on the other side, they show strong penetrating power, far over than that expected from the pure electromagnetic shower development, see Figure 2.8.

The showers are separated at such large distances to each other that none of the couple of showers which could be attributed to a π^0 meson decay were found. They have been tentatively named "mini-clusters" to distinguish them from pure electromagnetic atmospheric cascades.

Later, two other events were found for both of which the estimation of interaction heights was possible by the triangulation method.

A systematic study of Chiron type interactions was extended to the strong penetrative families with wide lateral spread detected in other chambers. 30 Chiron-type events found in the systematic study of the Chacaltaya chamber no.19 are described in detail in [27, 52]. Other events have been collected in the past several years and the analysis of 82 Chiron-type families (selected out from 120 families from Chacaltaya chambers no. 19, 20 and 22) is presented in [20, 53, 54]. 21 Chiron events among them were found. Four Chiron-type events, found among $\sim$ 60 families with total observed energy greater than 100 TeV from Pamir exposure ($\sim$ 120 m^{2}yr of carbon chambers and $\sim$ 9 m^{2}yr of thick lead chambers) have been reported in [55].

The examples of Chiron-type families, which have been found more recently, are shown in Table 2.11. These are:

1. *Ch18B154S-B133I [56].*

The event was recorded in Chacaltaya chamber No.18. Despite of the large total visible energy (1346 TeV) the family has no halo. It has large lateral spread and it is much more

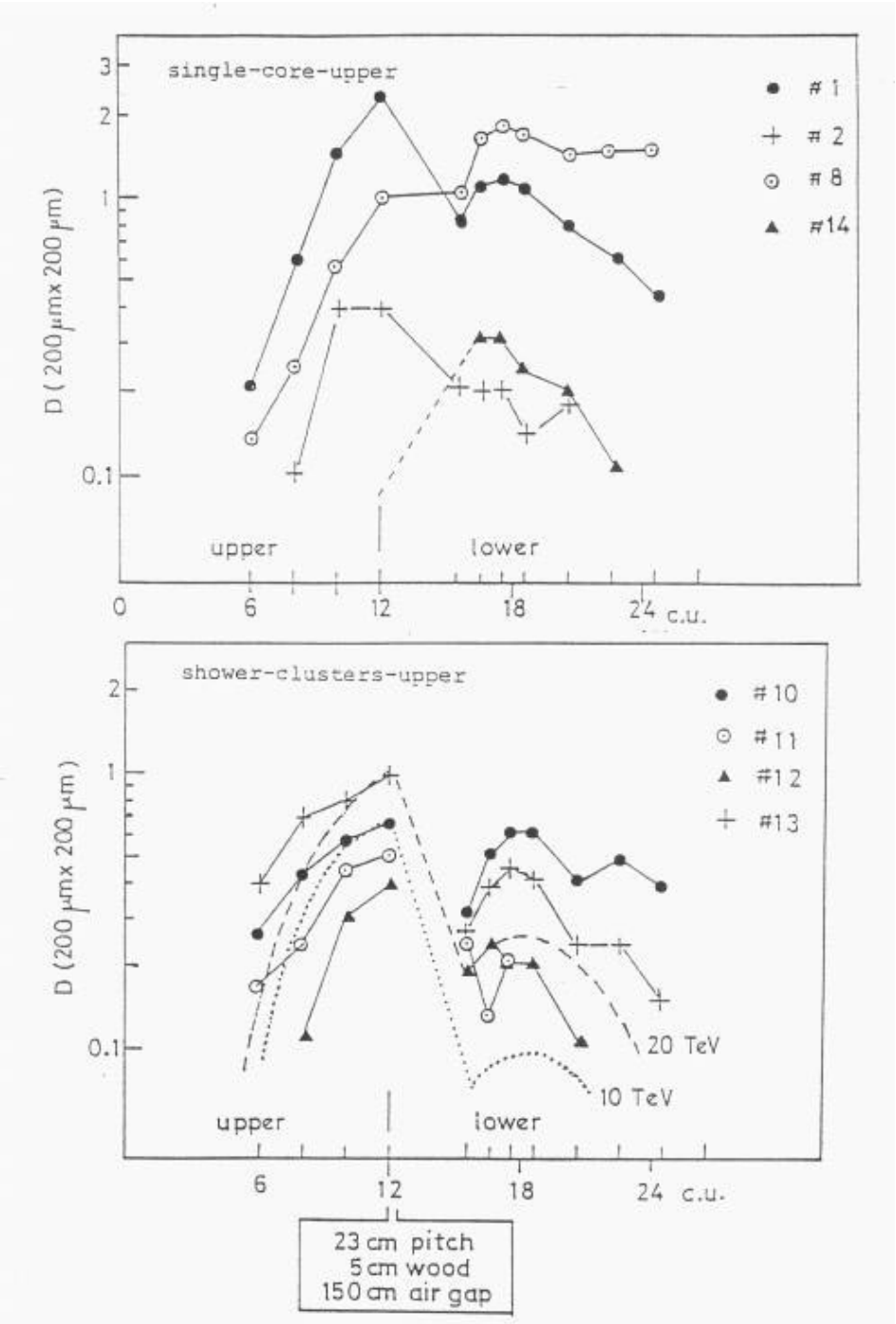

Figure 2.8: Transition curves of high energy showers in Chiron I [20]. The curves expected for electromagnetic cascades are also shown by dotted and dashed lines.

Table 2.10: Chiron I (family 198S-154I).

Shower no.	E_{vis} $[TeV]$	R $[mm]$	$p_T(\gamma)$ $[GeV/c]$	*identification*
1**	90.0	17.0	4.57	Pb-jet-upper(large Δt)
2*	$\geq$13.7	19.5	$\geq$0.80	Pb-jet-upper (large Δt)
3	>13.0	24.5	>0.95	Pb-jet-upper (multi-core)
4*	>17.2	23.5	>1.21	Pb-jet-upper (large Δt)
5	4.7	31.5	0.44	Pb-jet-upper (large Δt)
6	2.9	36.0	0.31	Pb-jet-upper(succesive)
7	10.6	18.5	0.59	A-jet (3 cores)
8**	70.0	7.0	1.46	Pb-jet-upper (large Δt)
9	13.8	18.0	0.74	Pb-jet-upper (multi-core)
10*	39.4	12.0	1.41	A-jet (7 cores)
11*	30.4	31.0	2.81	A-jet (7 cores)
12**	14.2	28.0	1.20	A-jet (2 cores)
13*	40.9	33.5	4.09	A-jet (9 cores)
14	>4.0	40.5	0.48	Pb-jet-upper (large Δt)
15	16.3	20.7	1.01	C-jet

* continue down into the lower chamber.

** it has a collimated core both in upper and lower chamber, and was used for the geometry measurement.

rich in hadron component than usual events. Hadrons carry about 40% of the total visible energy. The most striking feature of the family is the existence of two exotic hadrons within an extremely collimated cluster of showers located in its central part. One gives rise to a Pb-jet in lower chamber. It was found in the downstream of the shower observed in the upper chamber and consists of at least four cores, remaining a mini–clusters. Their average visible transverse momentum is about 2 GeV/c (from measurements of the geometrical convergence between cores at different depths in the chamber). The other gives rise to a pizero-less C-jet (no pair of showers which couples into a π^0 produced in the target layer). Both jets are hardly explained as well as being of "usual" hadron or single "γ-ray" origin.

The event contains also several anomalously collimated bundles of showers. Figure 2.9 shows some examples of the transition curves through the whole depth of the chamber. Dotted lines are the transition curves of pure electromagnetic cascade showers of the same energies expected for such two–storey chamber. It is seen that the observed darknesses in the lower chamber are appreciably larger than those expected for pure electromagnetic shower cases.

2. *P3C1G48H57 [31, 57].*

The event found in the Pamir-joint chamber C1 series P3 is the example of the quasi-clean

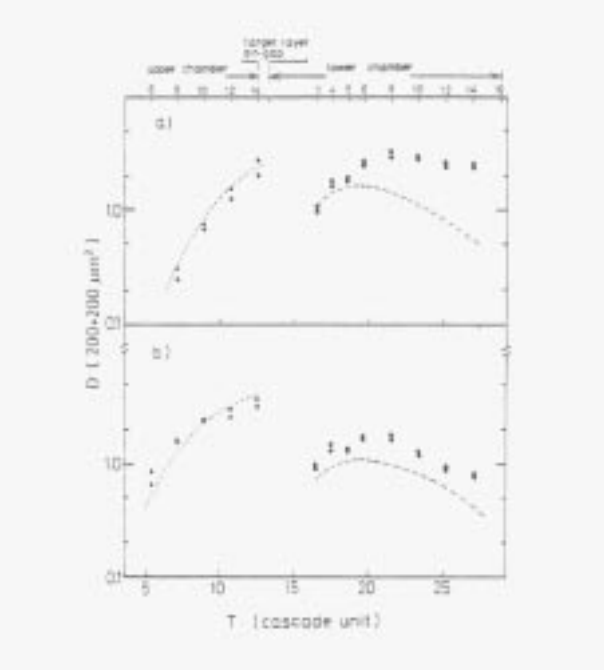

Figure 2.9: Examples of transition curves in the family Ch18-B154S-B133I [56]: a) single-core shower, b) multi-core shower.

family. The analysis of both longitudinal ($f = E/E_{vis}$) and lateral ($E(\gamma) \cdot R$) spectra shows that the majority of high energy secondary particles arrive at the chamber directly. Provided that the interaction height is ∼1 km (≃ one collision mean free path) or less, the present event is the example of particle production with large transverse momenta, $\langle p_T(\gamma) \rangle$ of the order of 2-3 GeV/c or more. Multiplicity of the secondaries at the main interaction is ∼ 10-15. Among high energy showers there are the strongly penetrating ones which after starting development in the gamma block enter further into the lower chamber. Two penetrating clusters with a small lateral spread were also detected.

3. *C22-113S-84I [31].*
This is another example of the quasi-clean Chiron-type family found in the Chacaltaya chamber no. 22. In Figure 2.10 transition curves of high energy showers are shown.

They are far beyond the fluctuation of simple electromagnetic cascades, even though they start shower development in the upper chamber.

4. *P3C4G369H370 [31].*
It is the Chiron type family registered in the Pamir joint chamber C4 series P3, marked as P3'-C4-368 in [53]. Several penetrating mini-clusters emitted with abnormally large p_T values were found among secondaries. The energy weighted spread of these clusters is small, $\langle E(\gamma)R \rangle \simeq$ 10 - 20 GeV·m, while the energy spread for the whole family, when it is measured by cluster energy, shows very large p_T emission, namely $p_T(\gamma) \simeq 2$ GeV/c or more ($\langle E(\gamma)R \rangle \simeq 2800$ GeV·m).

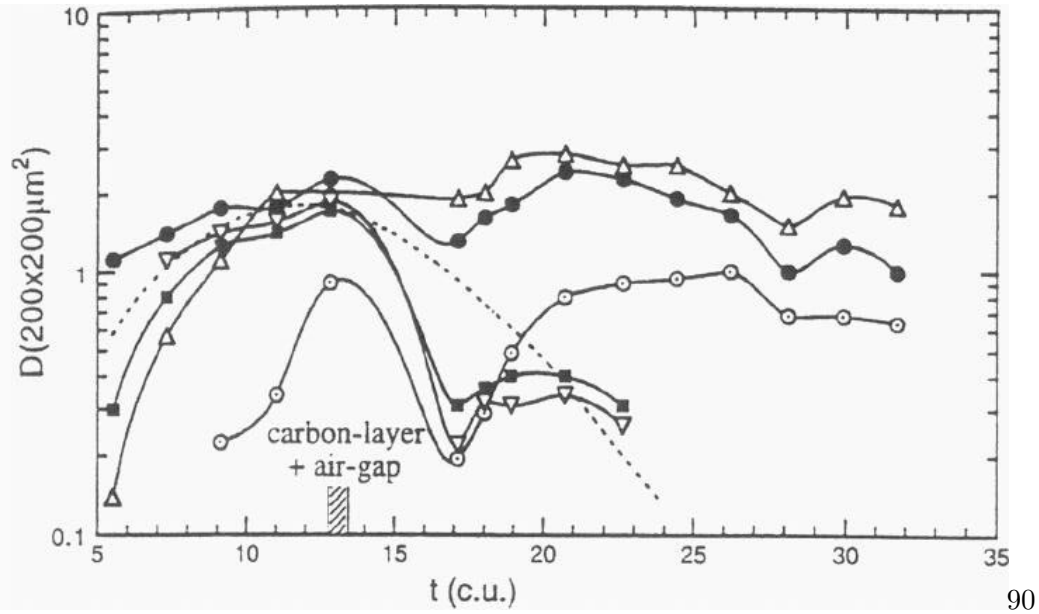

90

Figure 2.10: Transition curves of high energy showers in the family C22-113S-84I [31]. Simulated electromagnetic cascade curve is shown by dotted line.

Since the time of the first finding of the exotic cosmic-ray interaction named "Centauro" it has been even-standing problem whether the produced secondaries from such an exotic events are "ordinary" hadrons or something new. In fact, *secondary hadrons from the Chiron-type interaction reveal very exotic characteristics*:

- *Single or multi-core structure and two very different transverse momentum components.*

  About one half of hadronic cascades is single core structure while the another half develop a multi-core structure at the lateral spread of $\sim 0.1 - 1$ mm, what can be connected with the intrinsic p_T of $10 \sim 20$ MeV/c. These narrowly collimated jets of cascades are called *mini–clusters*. The ratio of $\langle E(\gamma)R\rangle$ of hadronic cascades in the Chiron families to the $\langle\langle E(\gamma)r\rangle\rangle$ in mini-clusters is ~ 300. This is a surprisingly large ratio, telling us that *secondaries in the parent interaction are produced with extra large p_T or mini-clusters are connected with very small transverse momenta phenomena, or both.*

- *Strongly penetrating power.*

  Majority of mini-clusters can not be of electromagnetic origin because of their *penetrating power*. About one half of *mini-clusters* is strongly penetrative. As an example, Figure 2.11 with transition curves of some cascades from Chiron events is shown.

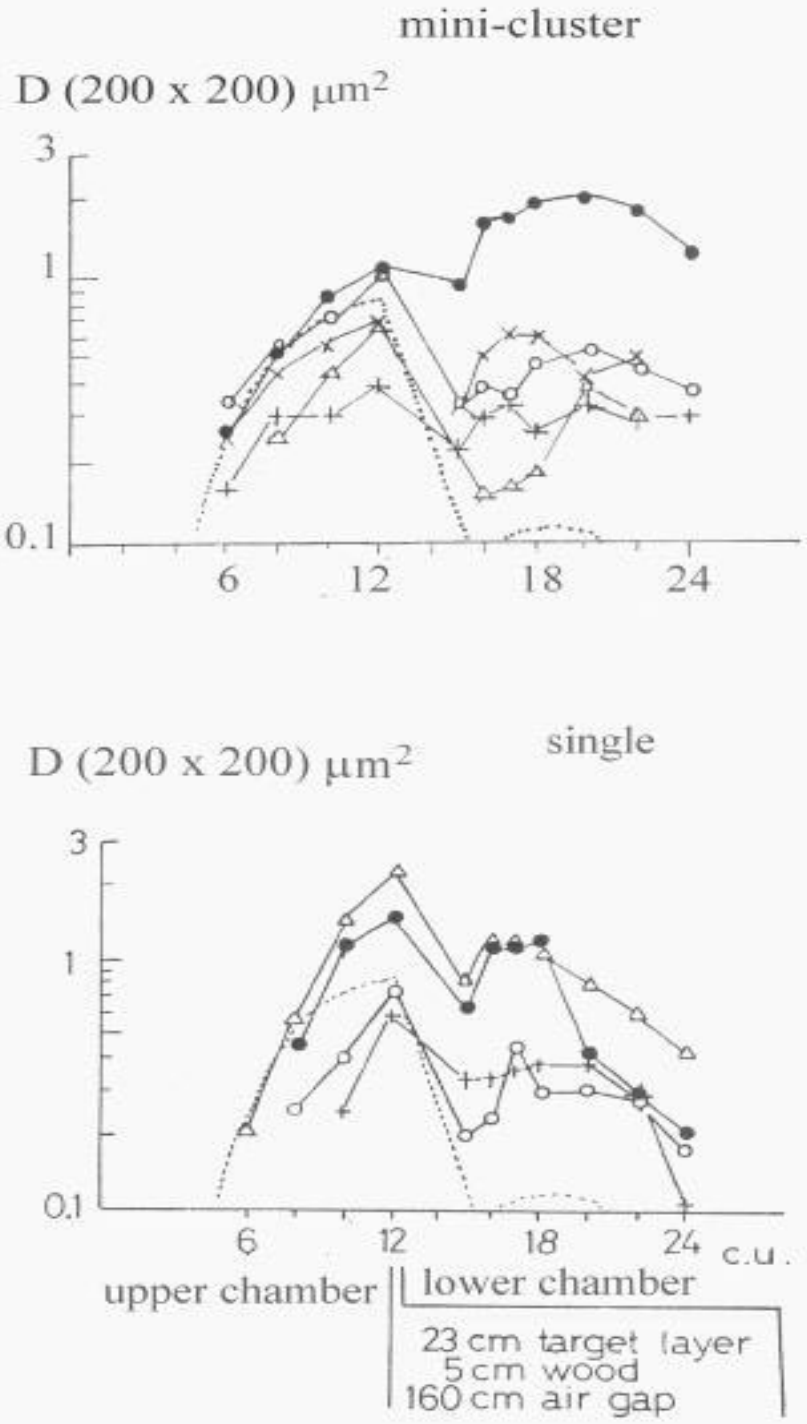

Figure 2.11: Examples of transition curves of cascades from Chiron type families [27].
Upper figure: mini-clusters: (•) no. S-1 in family 150-90I, (○) no. S-1 in family 131S-109I, (△) no. S-2 in family 181S-139I, (+) no. S-2 in family 131S-109I, (×) no. S-10 in family 198S-154I;
Lower figure: single cascades: (•) no. S-1 in family 155S-136I, (○) no. S-3-3 in family 131S-109I, (+) no. S-2 in family 123S-90I, (△) no. S-1 in family 198S-154I.

Table 2.11: Chiron–type events, examples.

Event Refer.	*Collab. Chamber*		*N*	*Energy* $[TeV]$	Q_h	$\langle ER \rangle$ $[GeV \cdot m]$	E_{halo} $[TeV]$	E_{th} $[TeV]$	*Remarks*
B154S	Chacal.	γ	132	818		140			penetr.
B133I		h	24	528		323			cascades and
[56]	2-storey	tot		1346	0.39				mini-cl.
P3C1	USSR-	γ	34	383				4	penetr.
G48H57	Japan	h	5	347				4	clusters
[31, 57]		tot		730	0.48	3141[1]		4	and
	standard carbon								cascades
113S084I	Chacal.	γ	67	513				2	penetr.
[31]		h	25	839				2	
	2-storey	tot		1352	0.62	1362[1]			
P3C4	USSR-	γ	107	1337				4	penetr.
G369H370	Japan	h	26	898				4	multi-
[31]		tot		2235	0.4	701[1]		4	cluster
	standard carbon								

[1] measured by showers of $E(\gamma) \geq 20$ TeV

Figure 2.12 shows the average transition curves of high energy showers, with $\Sigma E(\gamma) \geq$ 10 TeV, from Chiron-type families. For comparison, the average calculated transition curve was shown by dotted line. In calculations it was assumed that 100 gamma-rays of energy greater than 10 TeV enter into the chamber from the atmosphere. The power index of an integral spectrum, γ = -1.3, the same form as observed in the experiment was assumed. One finds that experimental showers demonstrate far stronger penetrating power than that expected in the case of electromagnetic particle incidence. A possibility of the showers being gamma-rays from the ordinary type of meson production have been made implausible as well as from the argument on their penetration, as from isolation and absence of accompanied air showers. If they would be gamma-rays we should expect accompanied air cascades from neutral pions associated with them.

- *Very wide lateral spread.*

  It seems that the high–energy showers from Chiron–type events *are also not usual hadrons* produced through the ordinary multiple meson production, high in the atmosphere. Assumption of $p_T(\pi) \sim 400$ MeV/c for such pions and $k_\gamma \sim 0.3$ for their secondary interactions gives heights H $\sim 4 \sim 8$ km (i.e. 3-5 nuclear mean free paths) for typical $\langle E(\gamma) \cdot R \rangle$ measured in Chiron-type families. Some hadrons could survive such distances, by chance escaping the secondary interactions, but not their majority. Besides that, hadrons produced at such altitudes should be accompanied by air

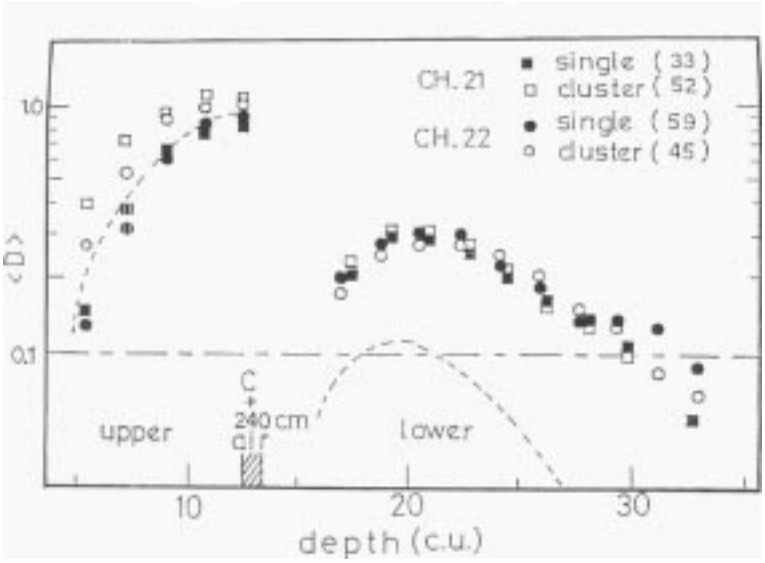

Figure 2.12: Average transition curves of high energy showers of $\Sigma E_{vis} \geq 10$ TeV from Chiron type families [20].

cascades from neutral pions associated with them, what is not observed.

- *Rapid attenuation (large interaction cross section).*

  Another surprising observation is a rapid attenuation of both single high energy "hadrons" and mini-clusters. Majority of them start the shower development just after entering the chamber and their collision mean free path turns to be much smaller than the geometrical value. It is illustrated in Figure 2.13 which shows the result of systematic study [20] of interaction mean free path of high energy secondaries from Chiron type interactions.

  Figure 2.13 gives the distribution of shower starting position in Chacaltaya two-storey chambers, no. 19, 21 and 22. There were selected 222 hadronic showers of $E_{vis} \geq 10$ TeV from 82 families of $\Sigma E_{vis} \geq 100$ TeV. The dotted line in the figure shows the attenuation expected by assumption of geometrical mean free path in the chamber materials. The experimental results indicate the collision mean free path as small as $\sim$ 1/2-1/3 of the geometrical value.

It is worth to note that a similar surprising behaviour have been also found in the study of shower development of the high energy cascades from 17 super-families of visible energy greater than 700 TeV detected in homogenous type lead chambers [54] which have fair advantage for the study of overall transition behaviour of shower development. The high energy hadrons in super families showed shorter attenuation length than ordinary single arrived cosmic–ray hadrons [20, 54]. It was reported [54] $\lambda_{att} = 170^{+47}_{-26}$ g/cm^2 for 143 hadrons of $E_\gamma \geq 10$ TeV, and $\lambda_{att} = 137^{+57}_{-26}$ g/cm^2 for 68 hadrons of $E_\gamma \geq 20$ TeV for hadrons in super–families in comparison with $\lambda_{att} = 252 \pm 30$ g/cm^2 obtained for single-arrived ordinary cosmic–ray hadrons detected in thick lead chambers.

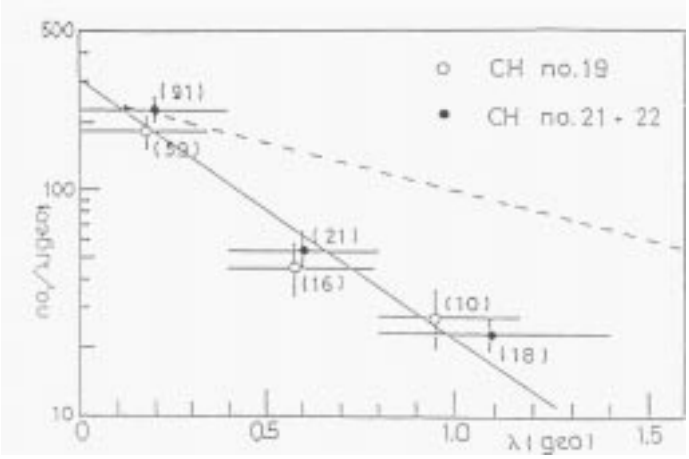

Figure 2.13: Distribution of shower starting positions of high energy showers, measured by λ_{geo} [20].

This result seems to be especially surprising, if one supposes that high energy hadrons in superfamilies are dominantly pions. Then their attenuation length should be larger than that for ordinary cosmic-ray hadrons which are mainly protons. The meaning of this result is clearly seen from the well known relation between the collision mean free path λ_{coll} and the attenuation length λ_{att}.

$$\lambda_{att} = \lambda_{coll}/(1 - \langle(1 - K)^{\alpha}\rangle) \tag{2.1}$$

where K is an inelasticity of the collision and α the power index of energy spectrum of observed hadrons.

In the present case, there were found different power indices of visible energy spectra for ordinary cosmic-ray hadrons ($\alpha = 2.09$) and for hadrons in super-families ($\alpha = 1.16$). Hence, $\lambda_{att} \simeq 1.3$ (1.03) λ_{coll} for K = 0.5 (0.8) for ordinary cosmic–ray hadrons and $\lambda_{att} \simeq$ 1.8 (1.2) λ_{coll} for K = 0.5 (0.8) for hadrons in superfamilies can be expected. So, we should observe longer attenuation mean free path in the case of hadrons in super-families than ordinary cosmic-ray hadrons, if λ_{coll} is the same for both. The majority of the single-arrived hadrons is likely to be protons but most of the hadrons in families are pions. The collision mean free path λ_{coll} of protons is less than that of pions; hence λ_{att} of hadrons in families should be larger than that of single-arrived hadrons. The experiment gives the opposite result and one can estimate that λ_{coll} of high energy hadrons in super-families is about one half of that the one of ordinary cosmic-ray hadrons.

It should be noted, however, that up to now the unexpectedly short mean free path of hadrons was observed only in very high energy superfamilies. Preliminary results [58] of the analysis of showers from 58 families with the visible energy greater than 100 TeV, detected in the Pamir thick lead chamber, gave the value of attenuation mean free path equal to 233 ± 40 g/cm^2, for hadrons with energy greater than 10 TeV.

Results presented here seem to indicate the existence of "the new state of hadrons" which are emitted in the high energy Centauro–type interactions. Authors of ref. [52] suggested, basing on thermodynamical arguments from the fire-ball model, that the secondary particles observed in these exotic events could be some heavy and long–lived particles (with masses $\sim$ 10 GeV and lifetimes $\tau_0 \geq 10^{-9}$ s).

2.4 Penetrating clusters and Halo

Penetrating component, accompanying the exotic events, has been observed in the form of *strongly penetrating cascades, clusters or "halo".*

The term *mini-cluster* [59] is used for stregthening the cluster characteristics which is different from ordinary atmospheric electromagnetic cascade showers, even though the spread of the clusters have a similar dimensions as air cascades. As it has been already said in the previous section, mini-clusters are very narrow collimated shower clusters (of a lateral spread $\sim$ 1 mm or less, $\langle E(\gamma) \cdot R \rangle \sim$ a few TeV·mm, and $p_T \sim$ 10–20 MeV/c). At a first glance they look like pure electromagnetic cascade from the atmosphere. The characteristic which distinguishes them from pure electromagnetic cascade is their strongly penetrative power. Mini–clusters are observed in the most forward angular region and, assuming the production height of the order of $\sim$ 1 km, their emission angles turn out to be of the order of $\sim 10^{-6}$ radians. They show a strong concentration of energy in this very forward region. The fraction of cluster energy relative to the total visible energy of the family is substantially large and the essential amount of energy flow is concentrated within a circle of a radius of a few to several millimeters from the cluster axis. This phenomenon has been discovered in Chiron-type families but it appears also in other Centauro-species (e.g. in Mini-Centauro [50]).

Besides the ordinary mini-clusters (called sometimes also "uni-clusters"), being the isolated single clusters and characterized by relatively small multiplicity, the *giant-mini-clusters (called "multi-clusters")* have been also observed (e.g. giant mini-cluster in Chiron-type family no. 174S-134I [59], found in Chacaltaya chamber no. 19). These are unusual shower core bundles with exceptionally large multiplicities and they are suggested to be the ensembles of ordinary mini-clusters [59]. The analysis [60] of the huge shower cluster spectra suggests its low original multiplicity. A shower cluster starts from a small number ($\sim$ 4-5) of high energy particles with small primordial transverse momenta. Subsequent enhancement of shower core multiplicity, accompanied by softening of its energy spectrum is the consequence of the passage through the atmosphere. The nature of parent particles is unknown. The study of their penetrating power indicates that they are not of pure electromagnetic origin, even if they show such small spread as expected from electromagnetic processes. On the other hand, it seems that they are also not ordinary hadrons. Majority of these showers start developing as soon as they enter into the lead in the upper chamber.

Some examples of hadron–rich giant mini-clusters are shown in Table 2.12. These are:

1. *C22-178S-139I [31].*

It was found in the two-storey Chacaltaya chamber no. 22. The shower cores at the cluster area were scanned in nuclear emulsion plates under the microscope. It is a typical example of the family confined in small dimensions of a spread of the order of several millimeters. It is composed of only three very high energy showers, starting in the upper

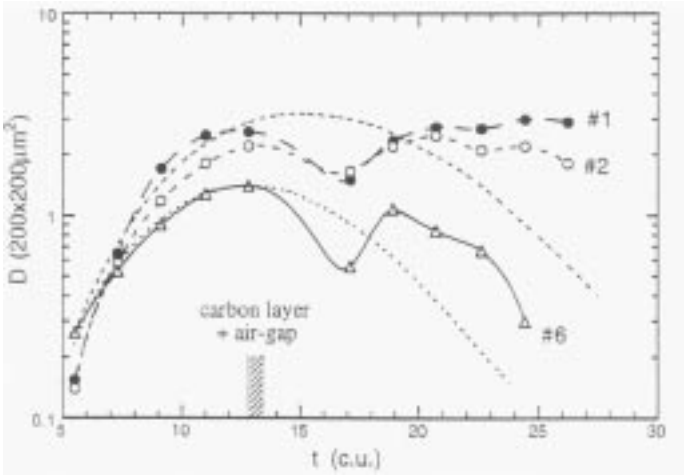

Figure 2.14: Transition curves of the three highest energy showers from the event C22-178S139I [31]. Dotted curves are simulated electromagnetic cascades.

chamber, about 30 low energy showers near the detection threshold energy and one C-jet located approximately at the position corresponding to the one of high energy upper-chamber shower. The transition curves of these three high energy cascades are shown in the Fig. 2.14.

In this chamber there is 30 cm of plastic target and 230 cm of air–gap between the upper and lower chambers. Usually, such air–gap strongly disturbs the transition curve, i.e. significantly reduces the numbers of electrons in the lower chamber, due to the electron scattering through the air–gap. The observed transition curves demonstrate unexpectedly strong penetrating power, indicating that they can not be of electromagnetic origin. It is also questionable if they could be caused by interactions of usual hadrons. The analysis of longitudinal and lateral spectra allows to suspect the existence of a new type particle production, characterized by very small transverse momentum, of the order of $p_T(\gamma) \simeq$ 30 MeV/c, assuming that the main interaction occured at about one collision mean free path, i.e. $\sim$ 1200 m at Chacaltaya, above the detector.

2. *P3C4G454H454 [31].*
Very interesting event with the high energy hadron-rich cluster (of visible energy $\sim$ 1000 TeV) in the centre of the family was found in the Pamir-joint chamber C4 series P3. One observes more than ten high energy shower-cores of visible energies greater than 10 TeV, concentrated within a small area of a radius of $\sim$ 3 mm. A striking feature is the strong penetrating power of the cluster which was observed deeply in the H-block. The longitudinal profiles of penetrating showers show similar transition behaviour as that recognizable in Fig. 2.14. The estimated $p_T(\gamma)$ of high energy showers inside the cluster is as small as $\simeq$ 20 MeV/c, if we assume that the interaction height equals to one collision

Table 2.12: Giant-mini-clusters, examples.

Event Refer.	*Collab. Chamber*		*N*	*Energy* $[TeV]$	Q_h	$\langle ER \rangle$ $[GeV \cdot m]$	E_{halo} $[TeV]$	E_{th} $[TeV]$	*Remarks*
C22	Brasil-	γ	43	229				2	single
178S139I	Japan	h	6	533				2	penetr.
[31]		tot		762	0.70	40[1]		2	cluster
	2-storey								
P3C4	USSR-	γ	22	326				4	hadron
G454H454	Japan	h	23	633				4	rich
[31]		tot		959	0.66	97[1]		4	str.penetr.
	standard carbon								cluster
C19	Brasil-	γ	72	417				2	penetr.
11S021I	Japan	h	10	321				2	cluster
[31]		tot		737	0.44	180[1]		2	(ΣE_{vis} = 465 TeV)
	2-storey								

[1] measured by showers of $E(\gamma) \geq 20$ TeV

mean free path at the Pamir altitude.

3. *C19-11S-21I [31].*
The family was found in the Chacaltaya chamber no. 19. A very high energy shower cluster at the centre is accompanied by a small number of shower cores around it. The central cluster consists of a very high energy single core ($E_{vis} \simeq 140$ TeV), penetrating deeply into the lower chamber. The cluster cascades have similar characteristics as the high energy showers given in Fig. 2.14. The spread of the shower clusters is of the order of a few millimetres in diameter, typical for mini-clusters. The showers found in the far outer region from the central cluster have a hadron-rich composition.

The unusual penetrative nature of mini-clusters have been studied by Chacaltaya , Pamir and also by Chacaltaya-Pamir Collaborations. The results of the study of penetrating component in 17 families with $\Sigma E(\gamma) \geq 100$ TeV, observed in the Chacaltaya chamber no. 19 (24 penetrating showers out of 37 ones in total) and in the chamber no. 18 (16 penetrating showers out of 30 ones in total) supported the existence of unusual showers with strong penetrating power [60, 61]. Similar conclusions have been obtained from the study of penetrating showers registered in the Pamir carbon chamber ("Pamir 79/80" with one carbon block of 60 cm thick) where 187 penetrating showers from 37 families with $\Sigma E_{vis} \geq 100$ TeV were picked up [62]. The detailed analysis of high energy shower-clusters of visible energy beyond 100 TeV observed in Pamir-joint chambers (analysed 173 families of $\Sigma E_{vis} \geq 100$ TeV) is described in [53, 63].

The general conclusions from this study as well as the single-core showers and cluster–

structure ones, are the same for three experiments. They agree that there exist unusual showers with unexpectedly strong penetrative power. Besides that, two very different components of transverse momentum are observed. Shower inducing secondaries are produced with large p_T ($\langle p_T(\gamma) \sim$ 2-3 GeV/c), far beyond that expected from the ordinary type. A low p_T phenomenon, of the order of the electromagnetic one, seems to be responsible for cores generation inside the cluster.

Mini-clusters are considered to be the premature stage of other phenomenon called *halo*. Halo is the diffusion dark spot with dimensions $\sim$ 1-1000 mm^2 observed in the center of families. Sometimes it consists of several hadron cores, spaced very closely together. The first gigantic halo event named "Andromeda" was discovered in the Chacaltaya chamber no. 14 in 1969. Since that time the statistics of halo events have steadily increased and events with different halo configurations have been found by mountain experiments at Mts. Chacaltaya, Pamir, Fuji and Kanbala [44]. About 50% of γ–hadron families with energy $\Sigma E_\gamma \geq 500$ TeV are halo events. The examples of cosmic-ray families in which shower spots surrounding the central halo show abundantly hadron rich composition, the same behaviour as seen in cosmic-ray families of Centauro species, were also found. The halos of anomalously strong penetrative nature (e.g. Tatyana [47]) were observed. The five Chacaltaya families: Andromeda, Ursa Maior, M.A.I, M.A.II and M.A.III [44] are examples of fully analysed halo events.

Many calculations were performed to understand the mechanism of halo formation and its surprising features such as for instance the strong penetration capability. Generally the data show a contradiction between the longitudinal and lateral halo development which cannot be resolved assuming the ordinary cosmic ray composition.

In principle, the nature of super-families show similar characteristics with Centauro species, i.e. unusual hadron rich composition for showers which surround the central halo. There are also strong indications that the relative p_T of hadrons within mini-clusters and halos are in $\sim$ 20-30 MeV/c range, the same as in Chirons. Such properties as: strong penetrative nature and two different components of the transverse momentum invoke the idea that in the extremely high-energy interactions the strongly collimated bundles of particles are frequently produced. They develop in the "halo" after atmospheric degradation.

The other striking feature of halo events is the existence of many-center halos and their alignment along a straight line. Parton-parton scattering naturally leads to the alignment of the final state nucleon fragments with two or more parton jets. However, the observed alignment is reported to be significantly greater than that expected from QCD. Fraction of aligned events in superfamilies was claimed to be between 26-43 % dependently on the type of the chamber (higher for deep Pb chambers) [64]. It has been revealed not only in the Pamir experiment but also in the Tien–Shan large ionization calorimeter and in the emulsion chamber exposed at the Concorde board in the stratosphere. According to recent calculations [64], the explanation of the abnormal fraction of aligned events needs some mechanism of complanar production of hadrons as well as *the existence of highly penetrating particles*. Penetrating component could prevent a destruction of the coplanarity during the development of nuclear cascade in the thick atmospheric target above the emulsion chamber. It has been checked in simulations that assumed mechanism of the coplanar emission is lost in the "normal" process of the nuclear-electromagnetic atmospheric shower development.

There are many other examples of strongly penetrating clusters or halos not listed

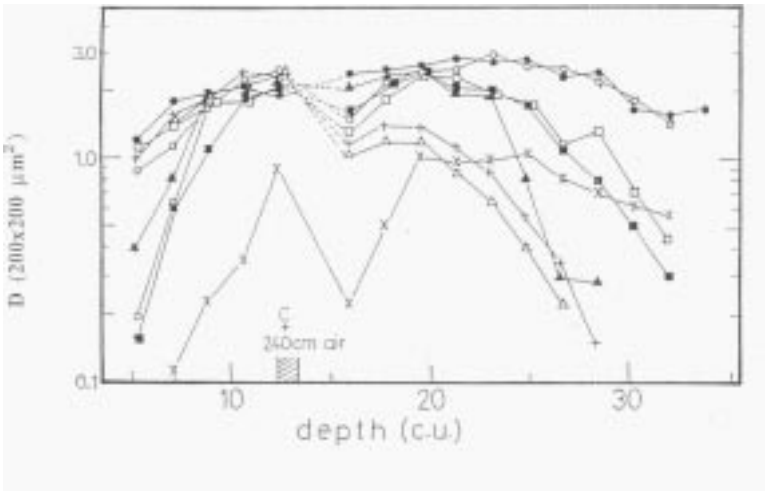

Figure 2.15: Examples of anomalous transition curves registered in Chacaltaya two–storey chambers [20].

here. Unfortunately, serious experimental difficulties in measurements and analysis of halo/cluster events occur frequently. They do not allow for reliable identification of electromagnetic and hadronic parts and estimation of the fraction of hadronic component.

2.5 Anomalous transition curves

Anomalous cascade transition curves have been firstly noticed during the study of Chiron-type families (see section 2.3). Later, they have been encountered also in other events [20, 53] (see sections 2.1, 2.4). Typical examples of long-range cascades (clusters) registered in Chacaltaya two–storey chambers are shown in Figure 2.15.

The common feature for all such showers is that they start their development just after entering the top of the chamber and penetrate through the whole apparatus without significant attenuation. Unfortunately, due to relatively small depth of these chambers and their inhomogenous structure it is impossible to conclude unambiguosly about the exotic nature of individual cascades. In many cases the shape of transition curves could be simply explained by consecutive interactions of the same hadron.

Only statistical analysis of groups of showers may indicate that something unusual happens (see section 2.3). Recently, a penetrating nature of cascade showers observed in the two–storey carbon type chamber was compared with simulated γ–ray–induced and hadron–induced cascade showers. Using QGSJET and modified UA5 model it was shown [65] that about 34% of penetrating showers observed in the two–storey chamber no. 19 are neither γ-ray-induced nor hadron-induced showers. A possible explanation is proposed in connection with "mini–clusters".

Many–maxima structure of cascades have been also observed in carbon chambers of the Pamir experiment. Although thick multi-block carbon chambers constitute only a small fraction of all exposed apparatus some interesting events have been also detected

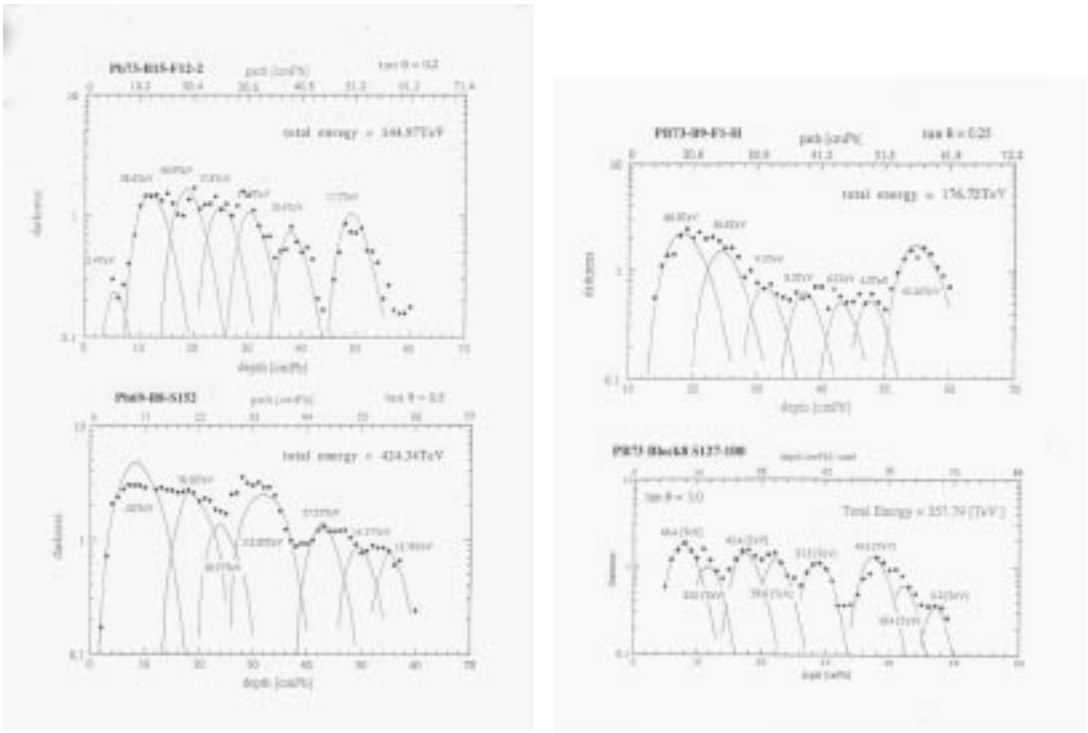

Figure 2.16: Examples of anomalous transition curves registered in thick lead chambers [20].

there [37, 66]. The example is the family N830 [66] detected in the Pamir 76/77 chamber, consisting of a standard gamma–block and four identical sections of hadron blocks (each consisting of 25 cm of rubber and 5 cm of lead with X-ray films as sensitive layers). Among hadron cascades there were observed three high energy ones revealing a multihump structure and traversing tens cascade units through the chamber material.

Homogenous type thick lead chambers are the most appropriate apparatus for the study of penetrability and for looking at anomalies in cascade development. The spectacular examples are exotic cascades detected in the Centauro–like event C–K (see section 2.1). Unfortunately, up to now, rather small area of these chambers have been exposed and analysed. Most of experimental material comes from several thick lead chambers installed at the Pamir in the years 1988-1991 by the MSU (Moscow State University) Group. Some extremely interesting events have been found there and reported in [20, 54]. Some examples are shown in Figure 2.16.

The presented cascades exhibit surprising features, such as many maxima structure and very slow attenuation. Some of them penetrate through the whole apparatus without noticeable attenuation, sometimes even indicating a growing tendency.

Simulation calculations of transition curves in homogenous thick lead chambers have been performed [7, 67, 68] with the purpose to compare the transition behaviour of ordinary hadrons with the experimental one. Some artificial cascades revealed wave–shaped transition curves, showing the successive maxima separated by the depth corresponding to about one collision mean free path or so ($\sim$ 15 cm) in lead. It is, however, much longer

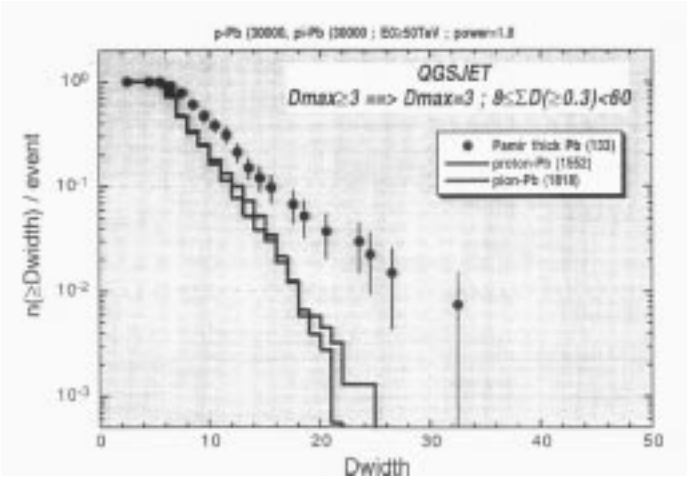

Figure 2.17: Distribution of widths of simulated and observed cascades [7].

distance than experimentally observed one. Generally, the simulated pictures are at the first glance qualitatively different from the experimentally observed curves. More recent simulations, assuming four models of hadron-nucleus interactions (VENUS 4.12, QGSJET, HDPM and modified UA5, all widely accepted as standard models) confirmed the unusual character of long-penetrating cascades [7, 68]. In particular, the widths of experimentally observed cascades and the distribution of the ratio of energy released in the first peak to the total energy of the cascade disagree with those obtained in simulations. As an example, the distribution of the widths of 133 cascades detected in the Pamir thick lead chamber in comparison with the simulated one, assuming the QGSJET model, is shown in Figure 2.17. It is easily seen that both proton and pion induced simulated cascades are much narrower than the experimental ones.

Investigation of the mechanism of transfering the energy into γ–rays, during the passage of the hadron through the chamber, indicate that in simulated events most of energy is released in the first interaction. It again apparently disagrees with experimental observations. Authors of [7, 67, 68] conclude that extensive simulation studies support the existence of exotic long-penetrating cascades. They suggest, as a possible explanation, the extremely collimated hadron bundles, saying, however, nothing about their origin.

It is plausible that the observed strongly penetrating cascades are the same phenomenon as the so–called long-flying component. This effect was firstly noticed [12, 40] in the Tien-Shan lead calorimeter. It was observed that the attenuation length (extension) of the cascade is almost constant up to calorimeter cascade energies of $\sim$ 10 TeV, increasing twice in the energy interval 10-300 TeV. This observation means a nontrivial hadron energy deposit at larger depths in the lead calorimeter. The effect has been later confirmed by the investigation of attenuation of hadrons in deep lead Pamir chambers [69]. At depths corresponding to 3-6 hadron attenuation paths an excess of cascades, which cannot be explained in the framework of a present knowledge about development of hadron-induced cascades in lead, have been observed. An abundance of cascades detected at large depths

($\sim 78 - 192$ c.u.) constitutes $\sim 33\%$ of the total intensity. Distributions of cascade origin points cannot be described as $dN/dt \sim exp(-t/\lambda)$ with the same slope for all depths: $\lambda_{meas} = 212 \pm 19$ g/cm^2 at depths 22-78 c.u., and $\lambda_{meas} = 310 \pm 36$ g/cm^2 at depths 78-192 c.u. [69]. There were considered two explanations of the observed phenomenon:

1. *Hypothesis of copious production of leading unstable particles, having relatively long lifetimes.*
   Generally the phenomenon could be explained by adding to the normal hadron component some particles decaying inside the chamber, at depths somewhere between several tens centimeters and two meters, with energies E $\geq$ 20 TeV. They should carry their energy deeply into lead absorber, practically without spending it in nuclear interactions. Particles with heavy quarks (c, b, t) satisfy these criteria. Among them charmed particles were considered the best candidates: their masses are around 2 GeV/c^2, lifetimes $\sim 10^{-12} - 10^{-13}$ s and the inelasticity coefficient in interactions of charmed particles with nuclei is small. However, for obtaining a satisfactory description of experimental data very large charm cross section production must be assumed. This, so called, "leading charm" hypothesis needs ~ 10 times larger cross section for charm hadroproduction, than resulting from extrapolation of accelerator data, and additionally a small inelasticity coeficient.

2. *Hypothesis of some heavy ($m > 10$ GeV/c^2) and long-lived ($\tau_0 \sim 10^{-8} - 10^{-6}$) s particles, weakly absorbed in the atmosphere.*
   Such particles, if consisting of heavy and light quarks should interact with a cross section approximately similar to that for ordinary hadrons but with a very small inelasticity coefficient.

Chapter 3

Centauro species statistics

3.1 Mts. Chacaltaya and Pamir experiments

The basic question is what is the intensity of Centauro species. The well known numbers, cited in many papers (see for example [70]), are intensities measured by Pamir-Chacaltaya Collaboration and claimed to be of the order of $\sim 10^{-2} - 10^{-3}$ m^{-2}year^{-1} for Centauros and $\sim 10^{-1}$ m^{-2} year^{-1} for Chirons, at the Chacaltaya altitude.

However, it should be mentioned that before giving the statistics of Centauro-type events, the precise definition of such objects should be formulated. If we use very sharp criteria defining such events their numbers will be not very large. Up to now there are reported only two super clean Centauro events, without observed presence of any γ' s, found in the two-storey Chacaltaya chambers, of the total exposure ST = 3.49×10^2 m^{2}yr (for the sensitive solid angle of the emulsion chamber $\Omega = 0.7$). A question of appearance of super clean Centauros have been considered in [8]. The number of cosmic-ray events at energies corresponding to the observed Centauro events was calculated from the formula:

$$I(>\Sigma E_{vis}) = 0.9(\Sigma E_{vis}/100\text{TeV})^{-1.25\pm0.10}/(m^2 \cdot yr \cdot sr). \tag{3.1}$$

Comparing the calculated intensity of cosmic ray events (with $\Sigma E_{vis} = 100 \sim 3000$ TeV) [53] with the total number of observed clean Centauros (i.e. Centauro I and Centauro-New) the probability of appearance of such super pure species have been estimated to be $>10^{-3}$ [8] (see Table 3.1).

Simulations (based on 13714 events) gave probabilities 1.0×10^{-5} and 8.0×10^{-4} for Centauro I and New Centauro respectively. The difference between the experimental and simulated probability of observation of such events indicates that Centauro events cannot be produced by a fluctuation in the multiple particle production and/or in collision mean free path. Figure 3.1 is the diagram of the N_h vs. Q_h for the Chacaltaya families (with $\Sigma E_{vis} \geq 100$ TeV) with the marked contours giving the normalized densities of simulated events.

Similar events, i.e. characterized by the appearance of a family of showers at the certain apparatus layer, deeply inside the chamber, without accompanied showers in the upper part of the apparatus, have been observed [71] also in the deep lead chamber "Pamir 74/75". Unfortunately, in this case it was impossible to exclude the trivial explanation that the observed phenomenon is simply a "usual" family, reaching the chamber during the time of its assembly.

Table 3.1: Clean Centauros from two-storey Chacaltaya chambers.

Event	ΣE_{vis} (TeV)	I $(>\Sigma E_{vis})/$ $m^2 \cdot yr \cdot sr$	*Exp. expected no. of events*	*Experimental probability*	*Simulated probability*
Centauro I	221.6	0.15	1.6×10^2	6.3×10^{-3}	1.0×10^{-5}
New Centauro (Event C22)	51.2	0.90	9.0×10^2	1.0×10^{-3}	8.0×10^{-4}

The sharp definition of Centauro phenomenon can be a little released to include the events in which the observed electromagnetic component is very small. In this case the following numbers as the lower limits of their frequency can be quoted: 7 Centauros, 21 Chirons and 15 Mini-Centauros found in 305 families with $\Sigma E_\gamma \geq 100$ TeV (from Chacaltaya and Pamir joint chambers) [29].

Further extension of the definition to the objects with anomalously high fraction of hadronic component causes that $\sim 20\%$ of all families with the total visible energy $E_{vis} \geq 100$ TeV should be recognized as Centauro–species. This question has been studied carefully in [20, 53] and it is illustrated in Figure 3.2. The analysis was based on the unbiased sample of 429 families from Chacaltaya (open circles), 173 from the Pamir-Joint chambers and 135 from a part of the Pamir chambers of 500 m^2yr (closed circles) with total visible energy greater than 100 TeV. There is shown a scatter diagram of N_h vs. Q_h where N_h denotes the number of hadrons in a family with visible energy greater than 4 TeV. Figure 3.2 b shows 523 simulated families with the total visible energies greater than 100 TeV. In simulations the structure of the chambers was taken into account and normal chemical composition of primary cosmic rays has been assumed. Different marks on the plot refer to families due to different primary cosmic–ray nuclei. The basic mechanism of particle interaction was the production of hadronic clusters and their decay with parameters chosen to reproduce of the CERN UA-5 experiment results. One sees that in the experimental data there exist abundant families with anomalously rich hadron content, sometimes in both the number and the energy fraction. They are beyond expected fluctuations in the distribution from UA-5 type hadronic interactions. None of the simulated families is found to have $Q_h \geq 0.75$ and $N_h \geq 5$, though the experiment shows the existence of families of much richer hadron composition. Among the families there are events with a very large number of hadrons, expressed by a circle and a number in Figure 3.2 a. All those are superfamilies with $\Sigma E_{vis} \geq 1000$ TeV. Among them the family marked as (7) is called Centauro VII, the family marked by C20 is called Centauro VI, both found in the Chacaltaya chambers. Family "Elena" found in the Pamir thick-lead chamber is marked by (E). Other events marked (1)-(6) are superfamilies: P3'-C1-90, P3-C5-505, P2-C96-125, P3-C2-201, P3'-C4-369, found in Pamir-joint chambers, and M.A.III coming from Chacaltaya chamber. Some of them are connected with a strongly penetrative huge halo, what suggests its strong hadronic nature. However, because of the technical

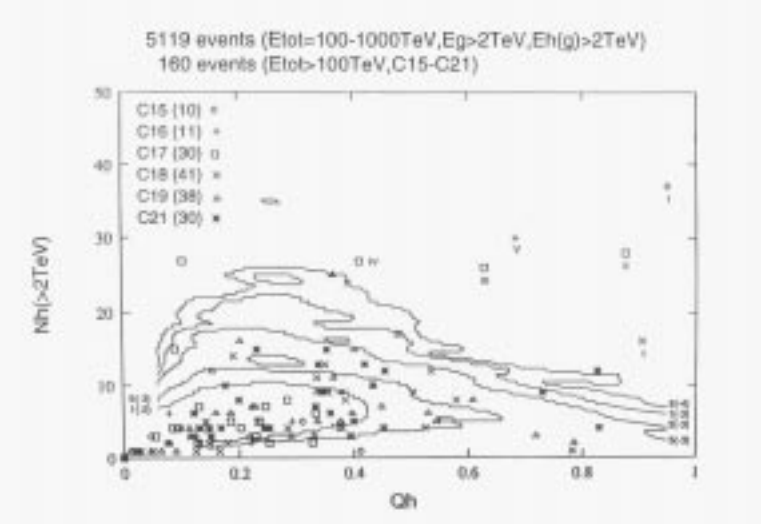

Figure 3.1: $N_h - Q_h$ diagram of families ($\Sigma E_\gamma \geq 100$ TeV) observed at Mt. Chacaltaya (Ch.15 - Ch.21). Centauros are shown by marks (I-V and 1). Contours give the normalized density of the simulated events [8].

problems with measurements of the halo, presented results include only the analysis of the off-halo part. The characteristics, of both the off-halo part and estimations of the halo region, are published in [31, 53]. The off-halo part of superfamilies shows tendency of hadron-dominant nature in either N_h and Q_h or both, even though these superfamilies are estimated to have been produced at high altitude. From the study of the off-halo part the large value of p_T can be also concluded.

It is important to note that there are no significant differences among three experiments. The figures (a) and (b) tell us that such anomalously rich hadron content is neither caused by the incidence of heavy nuclei in the primary cosmic rays, nor by the superposed fluctuations of ordinary-type hadronic interactions. The anomalously hadron-rich families constitute a substantial part of the unbiased observed samples, at least $\sim 20\%$.

The effect of the anomalous hadron dominance in families is much enhanced if the analysis is restricted to the events generated at the distances not far from the top of the chamber. In [53] the events have been selected with rather small lateral spread, i.e. with $\langle E^* R^* \rangle \leq 300$ GeV·m, after applying the "decascading" procedure for γ-rays. There were found 69 families from the Chacaltaya and 173 from the Pamir and Pamir-joint chambers satisfying the above condition. The result is shown in the plots on the right side of Figure 3.2.

These conclusions have been supported by the more recent, extensive simulation studies [7] based on four different models of hadron-nucleus interactions (VENUS, QGSJET, HDPM and modified UA-5) and by using the CORSIKA code for simulation of nuclear–electromagnetic cascade development in the atmosphere. The enhancement of hadron–rich families can not be explained by widely accepted models of "normal" interactions. The question of abnormal dominance of hadron component has been studied separately also

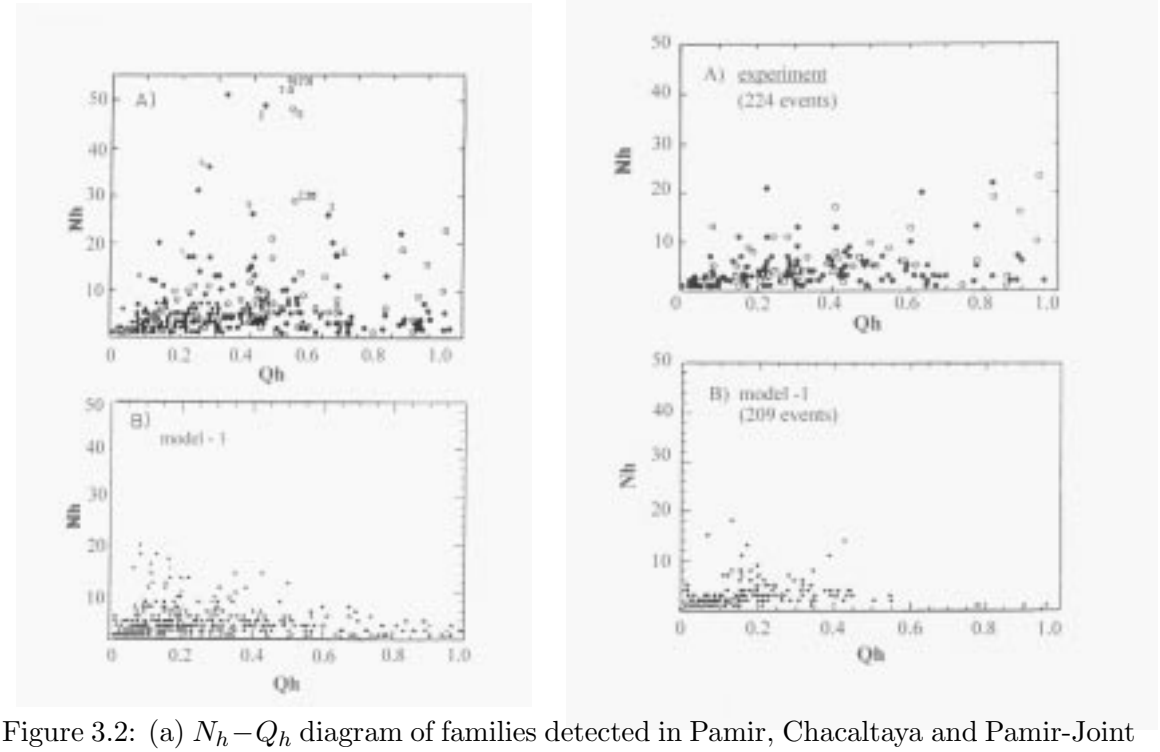

Figure 3.2: (a) $N_h - Q_h$ diagram of families detected in Pamir, Chacaltaya and Pamir-Joint chambers, (b) The same for the simulated families. Different marks signify the different primary cosmic-ray nuclei: (•) proton, (○) α, (◇) CNO, (×) heavy, (+) Fe, [53]. Plots on the right side are for the families selected under the criterion that the average of the lateral spread after decascading is smaller than 300 GeV·m.

for ultra high energy events. In [31] has been presented the systematic analysis of 75 families with $\Sigma E_{vis} \geq 500$ TeV detected in Chacaltaya two-storey chambers (300 m^{2}yr), Pamir-joint chambers (~ 530 m^{2}yr) and in the part of the Pamir exposition (~ 500 m^{2}yr). Among presented families, four Centauro–type, two Chiron-type, and ~ 10 other hadron-rich events could be noticed. The families coming from homogenous type lead chambers (110, 60 and 40 cm of Pb thick from a total exposure ~ 450 m^{2}yr) have been also separately analysed. The list and characteristics of 17 superfamilies with $\Sigma E_{vis} \geq 700$ TeV and 40 families with $100 \leq \Sigma E_{vis} \leq 500$ TeV are shown in [54]. Among them at least three events with $Q_h \geq 0.5$ are present.

3.2 Mts. Kanbala and Fuji experiments.

The Centauro like event named "Titan" has been reported in 1977 by Mt. Fuji experiment [23, 72]. The authors emphasized its large p_T and hadron–rich character. It was suggested that all secondaries are hadrons. A systematic search for Centauro events has been done later [73] in the thick-type lead chambers [1] by the China-Japan Collaboration. The total exposure was ~ 130 m^{2}yr at Mt. Kanbala (5500 m a.s.l.) and ~ 380 m^{2}yr at Mt. Fuji (3750 m a.s.l.). Among 30 hadron families (with the total visible energy greater than 100 TeV) coming from thick lead chambers exposed at Mt. Fuji and 100 families coming from Mt. Kanbala chambers no candidates of Centauro events have been found. The upper limit of the fraction of such events was estimated to be 3% (95% c.l.) in the hadron families with energy greater than 100 TeV. The puzzle of the nonobservation of Centauro events by these experiments still remains a mystery. Several reasons, such as differences in experimental conditions, in emulsion chamber designs and data analysis procedure used by different Collaborations can be suspected. In particular, the following reasons should be mentioned:

1. *Some differences in hadron identification procedure.*
   Mt. Kanbala and Mt. Fuji groups classified hadrons and γ–rays only statistically by referring to the starting depth of showers. In the Chacaltaya and Pamir experiments additional criteria have been used, based on differences in development (lateral and longitudinal) of hadronic and electromagnetic cascades. Not only showers observed in the lower chambers were regarded as hadrons. Showers from upper chambers have been studied under the microscope and some of them consisting of well–resolved cores or revealing many–maxima structure in the longitudinal development were also identified as hadrons.

2. *Difference in exposure altitude.*
   Mt. Fuji laboratory, giving the main part of the experimental data to the Centauro problem study, is located at the much lower altitude than Mt. Chacaltaya or Pamir. If Centauro species were born in nucleus-nucleus collisions or if they are the "strongly penetrating objects" produced at the top of the atmosphere or somewhere in the extra-galactic region then the decrease of their flux with the atmospheric depth is quite plausible.

3.3 JACEE Experiment.

The Japanese-American Cooperative Emulsion Chamber Experiment, JACEE, has flown emulsion chambers with baloons near the top of the atmosphere. Despite of a small area and short time of exposure, as compared to Chacaltaya/Pamir Experiment, a few events of anomalous γ/charged ratio have been observed by JACEE Collaboration. However, these events differ in some essential points from classical Centauros. The anomalies were noticed at incident energies lower than that estimated for "classical" Centauros and unusual

[1] Mt. Kanbala and Mt. Fuji groups mostly used Pb and Fe chambers with the total thickness of 10-70 c.u.. The flat type chambers which constitute the most part of the exposed apparatus are not suitable for the Centauro problem study.

γ/charged ratios were observed only in the limited $(\eta - \phi)$ phase space region. Besides that, an excess of photons (anti–Centauro), in contrary to the hadron excess observed in Centauros, was claimed. The examples are:

1. 4L-II-27 event [74] of incident energy of 80 TeV, yielded 149 charged particles and 120 γ's. Almost all γ–quanta were produced in a narrow jet in the extreme forward direction. The γ/charged ratio is 2.6 $\pm$ 1.1 in the region of pseudorapidity 5.5 $\leq \eta \leq$ 7.5, what is a significant deviation from the expected ratio of $\sim$ 1. The analysis presented in [74] showed an anomaly at the 5-10% level among 41 studied events with $E_0 \geq 40$ TeV.

2. The event, with ΣE_γ = 15.4 TeV, described in [75, 76] was initiated by a singly charged primary. The collision occurred within the detector. Almost all leading particles were γ–quanta. Photons appear to cluster into two groups. The leading cluster consisted of about 32 γ's with $\langle p_T \rangle \simeq 200$ MeV and only one accompanying charged particle. A possibly distinct cluster had three times as many photons as charged hadrons (about 54 photons versus 17 charged). This event is one out of a sample of about 70.

3. The event presented in [77] is a peripheral collision of Fe nucleus (E $\simeq$ 9 TeV/nucleon) in emulsion. There were found 27 γ–quanta with $\eta \leq 6$. As they came from pair conversions at only 0.8 radiation lengths, one can expect that the total number of photons was about 50. At the same time, only 6 charged particles (out of 21 charged tracks detected in the whole angular region) falled in the same kinematical range.

In all these events there was observed a tendency to a group emission of π^0 mesons. Such π^0 groups, having similar directions and momenta, could be signs of a formation and a subsequent decay of the chiral condensates. It should be mentioned, however, that these events were found in emulsion by scanning for the leading photon showers, so there was a "trigger bias" in favour of a large neutral fraction. It would be interesting to hear something about anti-Centauros from the mountain-top emulsion chambers. Here, there is, however, even much more stronger "trigger bias" in favour of gamma families, and thus the interpretation of data, from this point of view, is a complicated exercise. It is rather difficult to identify anti–Centauros unambigously, with exception of unusual and rare events in which the interaction vertex is close to the top and clearly resolved in the chamber.

3.4 Summary of the Centauro species statistics

Summarizing results of cosmic ray emulsion chamber experiments, it can be stated that Centauro–type anomalies have been observed by several different Experiments and Collaborations, working under different experimental conditions and using various types of chambers. Examples of detected unusual events were given in the previous sections. However, the systematic search for Centauros, by using the same criteria, have been made only for the part of the exposure from the three experiments : Chacaltaya Collaboration, Pamir-Collaboration and Pamir-Joint Chambers. China-Japan (Mt. Kanbala) and Mt. Fuji Collaborations, in their systematic Centauro search, used different type of chambers

Table 3.2: Centauro statistics

Laboratory	*Altitude* $m\ (g/cm^2)$	*Chambers*	*Exposure* m^2yr	*No. of families* $E_{vis} \geq 100TeV$	*No. of Centauros*	*Ref.*
Mt. Chacaltaya (Brasil-Japan)	5200 (540)	two-storey carbon	300	121	$\sim 8^*$	[53, 31]
Pamir (USSR-Poland)	4300 (600) or 4900	carbon type	500	135	$\sim 3^*$	[53, 31]
Pamir (Russia-Japan)	4300	carbon type or thick Pb	530	173	$\sim 2^*$	[53, 31]
Mts. Kanbala (China -Japan)	5500 (520)	thick-Pb	130	30	-	[73]
Mt. Fuji (Fuji Coll.)	3750 (650)	thick-Pb	380	100	-	[73]

* $\sim$ 20% hadron rich families in the sample

and different criteria of data analysis. Table 3.2 shows the statistics of "unambigious" Centauros found only in that part of experimental material where systematic and uniform searches were done.

It should be emphasized, however, that extension of the "Centauro" definition to all hadron–rich species causes that about 20% of events among the families with the total visible energy $\Sigma E_{vis} \geq 100$ TeV can be regarded as Centauro–like anomalies.

Chapter 4

Centauro explanations

The possibility that fluctuated air showers mimic Centauro type events seem to be the most natural suspicion. This question has been studied by many authors (see for example [78, 79]). Recently, very carefull analysis of this problem, by using the most modern simulation tools, as CORSIKA code (and four different models of hadron-nucleus interactions: VENUS, HDPM, QGSJET and modified UA5), has been done by M. Tamada [7]. All considered models fail in describing Centauro species. In particular none of models was able to explain the experimentally observed fluxes of hadron-rich events. They fail also in describing many characteristics of events, such as anomalous hadron-gamma correlations (e.g. N_h vs Q_h), mini-cluster and giant-mini-cluster structures etc.

Especially, no one has succeeded in reproducing the Centauro I event. The possibility that a heavy nucleus interacting in the lower part of the atmosphere could give rise to Centauro I type event was considered for example by Acharaya and Rao [79]. They have shown that, in principle, it would be possible to reproduce the event, though the total number of such events expected in the global data sample is $\sim 2\times10^{-5}$ what is in apparent discrepancy with the observed flux of Centauros. Similarly, in [8] (see also the previous chapter) the probability of finding a "clean" Centauro event, like Centauro I or Centauro New, among simulated events was found to be several order of magnitude smaller than the experimental one.

The suspicion that Centauro like phenomena would arise from nucleus-nucleus collisions was examined in many works. Keeping in mind that there is a negligible probability that nucleus would penetrate so deeply into the atmosphere B. Mc Cusker [80] suggested that a small fraction of iron nuclei from a primary cosmic-rays would survive passage through several hundred g·cm^{-2} of the atmosphere and produce Centauro events. But P. B. Price et al. [81] showed (taking into account various chains of fragmentation) that the flux of surviving heavy nuclei is too low by a factor of $\sim 10^{-10}$ to account for Centauros.

So, it is widely believed that Centauro related phenomena could not be due to any kind of statistical fluctuation in the hadronic content of normal events.

Therefore, new type of interaction or the creation of a new kind of matter is conjectured to be responsible for these extremely unusual phenomena. In the last years many interesting models have been proposed by different authors. It would be difficult to describe or even list all of them. Some of them are amenable to experimental verification in accelerator conditions, the other ones seem to be unamenable. Some of them (e.g. [82]) assume that the exotic objects of unknown origin are present in the primary cosmic

ray spectrum and they are seen as Centauros during their penetration through the atmosphere. The other ones assume that the exotic events are produced in extremely high energy hadron-hadron (e.g. [83]) or nucleus-nucleus (e.g. [17, 18]) interactions. Many of them incorporate the strong penetrability as the main feature of the phenomena. For instance, in [18] we avoid the problem of very small flux of heavy nuclei at the mountain level, by conjecturing that the initial collision of the heavy cosmic-ray nucleus does occur very high in the atmosphere. The fireball created in the central collision of a heavy nucleus with air nucleus is a very dense object which penetrates several hundred g·cm^{-2} of the air before exploding into fragments.

The widespread opinion that *the likely mechanism for Centauro production is the formation of a quark-gluon plasma* was incorporated in a lot of proposed models. Other exotic attempts, as for example the color-sextet quark model [84], based on Pomeron physics in QCD were also developed. It needs adding to the Standard Model an additional flavour doublet of color sextet quarks.

All proposed explanations are based on two different believes. In the first case it is assumed that mostly baryons are the products of Centauro type events. Such picture is incorporated for example in diffractive-type fireball models (see sections 4.2 and refs. [32, 83, 85]) and in scenarios with strange quark matter (see section 4.4 and refs. [17, 18, 19, 70, 82, 86]). In the second case, particles produced by the Centauro mechanism are suppose to be mainly mesons and there are numerous attempts to explain Centauros as different types of isospin fluctuations [87]-[96]. According to refs. [88, 90] large isospin fluctuations could be due to the Bose nature of the emitted pions and a laserlike (so-called PASER) mechanism is considered to be responsible for Centauro formation. The other theoretical speculations predict large isospin fluctuations arising from formation of localized regions of misalignment vacuum which become coherent sources of a classical pion field. In particular, formation of disoriented chiral condensate (DCC) [75, 91, 92, 94, 95] is suggested to be a possible explanation of Centauro-like phenomena (see section 4.4). It seems, however, that all these attempts have at least one common difficulty. It has been shown in ref. [97] that families produced at mountain altitudes are insensitive to any isospin fluctuations.

In this section some of the models will be shortly described. The most attention will be given to the strange quark matter fireball [17, 18] model which, in our opinion, gives the best chance for simultaneous explanation of different Centauro-related phenomena. It has been used also as the basis for the designing and simulation calculations done for the CASTOR experiment at the LHC.

4.1 Exotic extraterrestrial glob of matter

In [82] it was postulated by Bjorken and Mc Lerran that Centauro could be a metastable glob of highly compressed quark matter present in the primary cosmic ray spectrum. These globs could have radii of several fermi and contain several hundred quarks. Since the mean transverse momenta of the Centauro decay products are several times larger than the normal value typical of a nucleus it can be expected that the glob would have radii $\sim$ 3 - 5 times smaller than that of an ordinary nucleus and a very high density, $\sim 30 - 100$ times that of ordinary nuclear matter. If the binding energies of the constituents in the

dense nuclear matter are the same order as the transverse momenta, then the glob should be characterized by both the binding energy much higher than that of conventional nuclear matter and by the reduced geometrical cross section, allowing it to penetrate deeply into the atmosphere. To develop this idea authors of ref. [82] used the crude liquid-drop model. They formulated the stability condition and described the evolution of the glob during its penetration through the atmosphere.

The energy of the glob is generally a function of its baryonic number N and it was taken to be sum of the three terms :

- *the volume term*, αN, where α is an extensive parameter, arising from repulsive quark interactions and being for the bag model with no interaction $\sim$ 900 MeV,
- *the surface term*, $\beta N^{2/3}$, which reduces the strength of the repulsive quark interactions owing to the presence of a surface. It destabilizes globs of arbitrary large N and induces a condensation down to globs of finite baryon number.
- $\Delta(N)$ *term*, which summarizes all the finite-size corrections to $E(N)$, not already included in the previous terms.

$$E(N) = \alpha N - \beta N^{2/3} + \Delta(N) \tag{4.1}$$

If $E(N)>Nm_p$, the globs are not absolutely stable with respect to decay into nuclear matter. Thus the stability condition with respect to single-nucleon emission is:

$$\frac{dE}{dN}<m_p \tag{4.2}$$

and hence

$$\frac{2}{3}\beta N^{-1/3} - \frac{d\Delta}{dN}>\alpha - m_p \tag{4.3}$$

The globs are always unstable for baryon number N greater than some limiting value N_0. For $N<N_0$ they are stable with respect to nucleon emission unless, for some baryon number N_c the term $d\Delta/dN>\frac{2}{3}\beta N^{-1/3} + m_p - \alpha$. In this case the system would be metastable for $N_c<N$ and $N<N_0$ and would spontaneously decay for $N<N_c$ or $N>N_0$.

Upon entering the atmosphere, the glob collides with air nuclei with the collision length ~ 30 g/cm^2 (for $R_{glob} \sim R_{air}$). Such process heats the glob, and it cools either by radiation of mesons or evaporation of baryons. The boiling of baryons decreases the baryon number, what can remove the glob from the metastability region into stable on unstable region. In the former case the glob will explode and in the latter one it will collide with air nuclei until it is evaporated. Thus in some cases the glob could be characterized by *a large degree of penetration and short interaction length*, leading to a considerable deposition of energy in the atmosphere. To estimate both the energy transferred to the glob per collision and the evaporation, a simple model of a glob consisting of an ideal degenerate Fermi gas of quarks was used. Taking the quark-proton cross-section to be $\sigma_{qp} \sim 12$ mb, $k_F \sim 1$ GeV and assuming the collision of the glob of the baryon number $N \sim 100$ with the air nucleus ($N_{air} \sim 14$) authors of ref. [82] obtained that the fractional energy loss of a glob $\Delta E/E$ is ~ 3 %. For the gamma factor $\sim 10^3 - 10^4$, the glob loses somewhere between $10^3 - 10^5$ GeV/collision and (omitting the possibility of explosion and assuming a collision length ~ 30 g/cm^2 as appropriate for $R_{glob} \simeq R_{air}$) it could easily penetrate a distance $X \sim 6000 - 8000$ g/cm^2 in the atmosphere and reach the sea level.

In ref. [82] were also discussed two other variants: the glob containing an unconfined massive quark or being a fractionally charged hadron with large baryon number. In the former case, the glob would have the quantum numbers of a quark. As the quark in such a model is expected to be a complex object of a relatively large mass and size, its long-range color field should attract nucleons via an induced color dipole moment and help to compress the quark matter to the required high density. Below a certain baryon number, the binding energy per nucleon will monotonically increase, causing that the "stripped glob" consisting of an unconfined quark and a few tightly bound nucleons would penetrate to sea level. There are, in fact, rather serious experimental constraints on this hypothesis as it leads as well to unacceptable flux of quarks at sea level as to an unacceptable rate of horizontal air showers (with zenith angle $>70^0$).

The picture proposed in [82] has the following difficulties:

- Problem of the glob origin;
- Unacceptably large rates of fractionally charged quarks and/or horizontal air showers at sea level;
- Adequate explanation of the absence of pions.

4.2 Diffractive fireballs

Numerous phenomenological models (e.g. [17, 83]) assume that a fireball plays a role of an intermediate state for Centauro production. They were inspired by some experimental characteristics of exotic events which can be satisfactorily explained by means of the fireball scenario. All of them postulate the production of "exotic" clusters, the differences concern the type of a projectile and the mechanism of evolution and decay of the fireball.

An example is the scenario [32, 83] in which Centauros and Mini-Centauros are proposed to be a result of isotropic decay of "exotic" fireballs coherently produced in a diffractive dissociation process. In this phenomenological model a nucleon-nucleon collision at $\sqrt{s}$ ~1.8 TeV can create a diffractive superheated fireball with a mass $\sim$ 180 GeV in the forward region centered around pseudorapidity $|\eta_{cms}| = 2.2$ and with a spread $\Delta\eta = \pm$ 0.7. The high p_T reflects the temperature of the phase transition. Within this model the unusual hadron-electromagnetic asymmetry is assumed to be caused by a phase transition, similar to the DCC hypothesis, due to the superheated fireball conditions (with, however, the identification of the hadrons as nucleons). In principle, there is no explanation why pion emission should be suppressed in the quark-gluon plasma. The cross-section for a diffractive event with this mass was predicted to be $\sim$ 0.33 mb. Full Monte Carlo simulation of Centauro like events was carried out using this model [32, 85]. The code consists of two parts : *Code Nucleus + Exotic Algorithm. The Code Nucleus* describes the nucleus-nucleus collisions, using the superposition model. The nucleon-nucleon collision was described by the UA5 algorithm, based on codes for non difractive and single diffractive interactions. *The Exotic Algorithm* was a code that included the exotic channel, i.e. a diffractive production of a baryonic fireball and its isotropic decay into baryons. The total inelastic cross section was assumed to be:

$$\sigma_{in} = \sigma_{normal} + \sigma_{exotic} \tag{4.4}$$

with $\sigma_{normal} = \sigma_{ND} + \sigma_{DD} + \sigma_{SD} \simeq \sigma_{ND} + \sigma_{SD}$ where $\sigma_{ND}, \sigma_{SD}, \sigma_{DD}$ and σ_{exotic} are the cross sections for non-diffractive, single diffractive, double diffractive and exotic processes respectively.
The branching ratio of "exotic diffractive channel" (Centauro and Mini-Centauro) was chosen to increase with incident baryon energy as

$$P_{exotic} = 0.333 log(E_N/100TeV) \tag{4.5}$$

This model successfully reproduces the kinematics of cosmic ray exotic events. Morever, it also permits to reproduce the experimental data for electromagnetic family flux. In opposite to "normal" diffractive events where the majority of secondary particles are pions, in exotic diffractive events the secondary charged particles were assumed to be only nucleons and antinucleons. Multiplicity of nucleons was generated using a Poisson distribution with $\langle N \rangle = 100$ for Centauro and $\langle N \rangle$ =15 for Mini-Centauro. The inclusion of exotic process in nuclear interaction of cosmic ray particles with atmospheric nuclei, reduces the expected electromagnetic family flux, because the production of π^0's in Centauro like events is suppressed by some unknown mechanism. It has been shown that in the extremely high energy region ($E_0 \geq 10^5$ TeV) a dominant exotic channel is consistent with experimental data from emulsion chamber experiment. The model also allows to understand the negative search for Centauro events at $Sp\overline{p}S$ CERN collider and some results of Tevatron experiments. It introduces the energy threshold for Centauro production connected with the point of the phase transition ($\sqrt{s}_{th} \sim 2000 \pm 500$ GeV), which is much higher than energy of $Sp\overline{p}S$ experiments ($\sqrt{s}$ = 540 - 900 GeV) and comparable to that of the Fermilab collider ($\sqrt{s}$ = 1.8 TeV). The negative results for Centauro search in some Tevatron experiments operating in the central rapidity region (e.g. CDF experiment) were also expected from this model [85], as the Centauros are assumed to be produced close to diffractive dissociation region.

4.3 DCC

4.3.1 Centauros as DCC manifestation

The QCD phase transition from normal hadronic matter to the Quark-Gluon- Plasma, manifests itself in two forms: deconfinement transition and chiral symmetry restoration. One of the interesting consequences of the chiral transition is the formation of a chiral condensate in an extended domain, such that the direction of the condensate is misaligned from the true vacuum direction. The formation of these so called Disoriented Chiral Condensate (DCC) domains in high energy collisions of both hadrons and heavy ions, has been proposed by many authors [75, 91, 92, 94, 95], however, this subject is a quite speculative one. There is no compelling argument that DCC must exist, but there is no compelling argument that it does not exist.

Simplified versions of the chiral effective theory are the linear and non-linear sigma-models. In the framework of the linear sigma model the Lagrangian can be expressed in terms of the order parameter a four-component vector field $\Phi \equiv (\sigma, \vec{\pi})$, which is a combination of the scalar field σ of isospin 0 and the vector pion field $\vec{\pi}$ of total isospin 1. The isoscalar condensate is identified with σ, while the isotriplet condensate is formed of the flavour combinations: $\overline{d}u$, $(\overline{u}u - \overline{d}d)/\sqrt{2}$ and $\overline{u}d$ are the π^+, π^0 and π^- fields

respectively. A natural hypothesis is, in the context of the linear sigma model, that the chiral field initially vanishes (at least in the average). At low temperatures the chiral symmetry is spontaneously broken. In order to break chiral symmetry, but not isospin symmetry, the minimum chosen is that for which the σ field acquires a vacuum expectation value: $\langle\sigma\rangle = f_\pi, \langle\vec{\pi}\rangle = 0$. In other words the potential, V(Φ), has a minimum in the σ direction and all the directions of $\vec{\pi}$ are equally populated. This leads to the isospin symmetry of pions. As the system goes through the chiral transition and then rapidly expands and cools, it may also roll down from the unstable local maximum of V(Φ) to the nearly stable values of one of the pion directions. The ordinary vacuum has chiral order parameter in the σ direction (it has no isospin). Isotopic vector $\vec{\pi}$ in DCC can point in arbitrary direction, and DCC could have the same energy as vacuum, if we would not have surface term of "chiral domain", resulting from its finite volume. *A disoriented chiral condensate (DCC) is thus a piece of vacuum which is disoriented from the σ direction to a direction with $\vec{\pi}$ components. When the DCC domain makes contact with the ordinary vacuum, it coherently radiates pions with isospin determined by the direction of disorientation in order to restore the σ direction.* For example, if the disorientation was in the π^0 direction, only π^0's would be emitted.

The imporant question is, what are the basic signatures of DCC? The main features of that disoriented piece of quark matter result directly from its definition. In both descriptions, the linear and non-linear sigma models, DCC can be defined as a cluster of pions, coherently produced, with anomalously large fluctuations in the neutral fraction. Pions from a DCC domain will be emitted at low p_T and will have a distinct distribution pattern compared to the normal pion production mechanism without DCC. An important feature of this radiation is coherence, which means that the multiplicity distribution of produced particles should be of Poisson–type, and there will be no Bose-Einstein enhancement. A DCC almost by definition will consist of a cluster of pions with almost identical momenta and in its own rest frame will have approximate spherical symmetry. Assuming some transverse boost for DCC, and the internal relative velocities of the pions within a DCC cluster, smaller than the transverse boost velocity, it should look like in the laboratory frame as a colorless minijet.

A convenient quantity to characterize a DCC is the fraction of neutral pions per event

$$f = \frac{N_{\pi^0}}{N_{\pi^0}+N_{\pi^+}+N_{\pi^-}}.$$

In a DCC model the probability of finding a given neutral fraction is

$$P(f) \simeq \frac{1}{2\sqrt{f}} \tag{4.6}$$

in the limit of large number of pions.

In generic particle production, that is, production by mechanisms other than DCC, producing a pion of any given charge is equally likely to isospin symmetry, so that f is binomially distributed with mean $\langle f\rangle = \frac{1}{3}$. Hence, a basic signature of DCC production is the presence of very large event-by-event fluctuations in the fraction of produced neutral pions. There should be also a significant low p_T enhancement. Other DCC signatures include various effects on pion pair correlation.

Thus, the best detector for finding DCC should cover a wide range of pseudorapidity η and azimuthal angle ϕ. It should count both charged pions and photons and accept pions down to as low p_T as possible ($p_T^\gamma \sim m_\pi/2$). The segmentation of the detector, both in η and ϕ is required, for constructing the f distribution in bins ranging from very small sizes, up to "bins" containing the whole event.

Searching for DCC is connected also with the correlation question, although it is not understood completely what correlation structure of the distribution chiral order parameter is likely to be. Z. Huang and X. Wang [96] found (basing on a linear σ model) that a rapidity interval in which the pion field is correlated in isospin direction could be as large as $\sim$ 2 - 3 rapidity units and the cluster structure of pions radiated from the coherent pion field may occur anywhere in the whole rapidity region. According to [75] the natural correlation length for DCC is of the order of 1-2 units of rapidity. However, this is yet an unsolved theoretical issue. One can imagine, for example, a piece of a DCC centered at rapidity of +1 , and another one centered at -1 with a different chiral order parameter and having some small overlap at rapidity 0. The question is how do the two pieces interact? Will there be a tendency to create a common alignment, or will they form independent domains? As it was suggested in [75] there is even a remote possibility that the nonlinearities of the linear sigma model are strong enough to promote long-range correlations in rapidity, i.e. to create a semiclassical structure which produces the phenomenology of a soft Pomeron. The formation time and corresponding correlation length have been also estimated in [92] by non-linear sigma model and quenching approximation. The correlation length was estimated as $\sim$ 8 fm in nuclear collisions at 200 GeV/nucleon (taking WA80 data). This large value reflects the coherence of the source. The ratio of "anomalous" correlation length, related to a DCC mechanism, to the "ordinary" correlation length was estimated as $\sim$ 5.6 [92, 98].

As we see the interest of particle and nuclear physics in coherent states stems also from the fact that the concepts of spontaneous broken symmetries and condensates are connected with coherent states. The topics of coherence, correlation and fluctuation are connected one to the other and they can be studied also by analysis of the multiplicity distributions, by using different kinds of multiplicity distribution moments [99].

Some signs of the existence of the long range correlations we have reported [100] already in 1991, in NA35 data (sulphur-sulphur central collisions at 200 GeV/n). We have studied multiplicity distributions and their second moments in various rapidity intervals, following the methods proposed by R. C. Hwa [101], P. Carruthers and others [102]. In opposite to the intermittency, the so-called coarse grain fluctuations were investigated. The dependence of the normalized moment $f_2/\langle N\rangle^2$ [1] on the width of the rapidity interval allows to estimate the length and the strength of correlations. Our observations may indicate the appearance of weak, long range correlations, with the length $\xi \gg 3$ rapidity units. Another piece of experimental information comes from our fractal analysis and the entropy study [103] done for the same set of data. The entropy for central $^{32}S-S$ collisions is bigger than expected from models and mostly concentrated in the central rapidity region which may suggest a higher concentration of chaoticity at midrapidity. A coherent domain could be connected rather with fragmentation region, as it can be expected in the case of Centauro events, assuming their production via DCC domain formation.

[1] $f_2 = \langle N(N-1)\rangle - \langle N\rangle^2$ where N is the particle multiplicity

To answer the basic question, if a DCC scenario could be able to explain all Centauro related phenomna needs, however, very carefull studies. Some doubts can be mentioned at once. At first, it seems that using a DCC scenario it would be rather difficult to explain simultaneously both the large transverse momenta observed in the Centauro species and the existence of a strongly penetrating component. The anomalously high $\langle p_T \rangle$ of the particles produced in Centauro type events seems to be the main problem. Assuming even that the value of the gamma inelasticity factor, k_γ is closer to 0.4 than 0.2, as it was taken in cosmic-ray papers, the obtained $\langle p_T \rangle \simeq 0.875 \pm 0.375$ GeV. This value seems to be still too high to be connected with a DCC mechanism. On the other hand, one can not rule out that the narrow and strongly penetrating clusters, observed in Chiron type events, are produced by a transversally boosted DCC. It cannot be excluded that the coherently emitted groups of DCC pions may have a net transverse drift velocity, forming the "colorless" jet. J. Bjorken [104] speculates that the relative p_T of the pions in the "colorless" jet may be under 100 MeV, what is very close of that measured for cosmic-ray mini-clusters observed in Chiron type events.

The other question concerns the existence of charged DCC, i.e. the events in which the orientation of the vacuum is orthogonal to the π^0 direction. Bjorken [75] considered this idea, as more speculative than ordinary DCC, however, he did not exclude it. He proposed the scenario where for example the positive charge DCC is produced at negative η , and the negative charge DCC is produced at positive η, with a "domain wall" in between. He found that the width of the dipole layer could be about 1-2 units of rapidity. Assuming that charged DCC could be formed, both Centauros and anti-Centauros should be observed in the same experiment. As it has been already mentioned, the experimental situation is surprising. Both extremes are claimed to be seen in cosmic ray data but by two various experiments and in different energy range. There were found some anti-Centauro like events by JACEE Collaboration and no Centauros. There are Centauros and no reported anti-Centauro events in Chacaltaya and Pamir experiments. Figs. 3.1 and 3.2 do not show any excess of γ–rich events when the observed families are compared with the simulated ones. It allows to doubt if Centauro and DCC are the same phenomenon. On the other hand, it should be mentioned that the analysis of γ-hadron families detected at mountain laboratories from the point of view of disoriented chiral condensates done in ref. [98, 105, 106] does not exclude a small contamination of DCC clusters among normally produced particles (see the next subsection). However, this result is inconsistent with the conclusion contained in [97] where authors demonstrate that artificial families produced at mountain altitudes are insensitive to any isospin fluctuations. Their simulations showed that all scenarios of isospin fluctuations lead to essentially the same characteristics of families registered at mountain altitudes. In other words, the cascading process in the atmosphere "kills" the characteristic features of the main interaction. It suggests that Centauros should originate from strongly penetrating projectiles.

4.3.2 DCC search in γ-hadron families

.

In 1996, a Brasil emulsion group reported [98] an analysis of several tens cosmic ray events of visible energy greater than 100 TeV from Mt. Chacaltaya. They plotted the number of observed hadrons against the energy fraction of hadronic component (N_h vs.

Q_h) and compared the experimental diagrams with the simulated ones. Artificial families were constructed for two different models. The first scenario which does not include an anomalous channel was called "ordinary interaction" model. It was based on two separate algorithms for non–diffractive and single diffractive interactions used by the UA5 group for the description of nucleon-nucleon collision. The single diffraction cross section was taken to be 19%. The second model included an anomalous production (DCC) in the diffractive channel. This description needs the inclusion of coherent emission of pions from a large domain of disoriented chiral condensates in the *leading particle region* because hadron rich families are observed in the form of a narrow cluster concentrated in the forward rapidity region.

It was shown that N_h vs. Q_h distribution does not match Monte Carlo simulation based on UA-5 data. Experimental distributions were better simulated by a Monte Carlo which included 24% DCC production rate in the leading particle region. On the other hand, a significant discrepancy between the experimental family flux and results of simulations should be mentioned. Even the model including the anomalous channel (DCC) fails in description of such global characteristics as the family flux observed at mountain altitudes. The question of unusual transverse momentum observed in hadron-rich families was not investigated by authors of [98].

More recently, a more advanced analysis, using the robust observables have been done [105, 106]. The robust observables $r_{i,j}$ are constructed through the ratios of normalized bivariate factorial moments $F_{i,j}$. As it has been shown in [107], they are sensitive to DCC admixtures in multiple production.

$$r_{i,j} = F_{i,j}/F_{i+j,0} \tag{4.7}$$

where

$$F_{i,j} = \frac{\langle N_{ch}(N_{ch}-1)...(N_{ch}-i+1)N_\gamma(N_\gamma-1)...(N_\gamma-j+1)\rangle}{\langle N_{ch}\rangle^i\langle N_\gamma\rangle^j} \tag{4.8}$$

For example:

$$r_{1,1} = \frac{\langle N_{ch}\rangle\langle N_{ch}N_\gamma\rangle}{\langle N_\gamma\rangle\langle N_{ch}(N_{ch}-1)\rangle} \tag{4.9}$$

The basic difference between generic production and DCC production is that in the former case the generating function depends only upon one variable, while for DCC it depends nontrivially upon two. Thus the factorial cumulants are very convenient tools for distinction between the distributions. If a distribution of ratio of neutral to all pions, f, is governed by a binomial distribution, as it is observed in standard pion production, called generic pion production, then

$$F_{i,j} = F_{(i+j),0}. \tag{4.10}$$

Therefore many ratios of the $F_{i,j}$ are expected to be unity:

$$r_{i,j}(generic) = \frac{F_{i,j}}{F_{(i+j),0}} = 1, \tag{4.11}$$

and particularly for $i \geq 1$ and j=1.

$$r_{i,1}(generic) = 1. \tag{4.12}$$

If on the other hand a distribution of f is of the form $p(f) = 1/(2\sqrt{f})$, as predicted by a DCC mechanism, then in the semiclassical limit

$$r_{i,1}(DCC) = 1/(i+1). \tag{4.13}$$

Thus the values of $r_{i,j}$ below 1 could be the indicators of a DCC formation. The results presented in [105] were based on analysis of 59 γ-hadron families, with ΣE_{vis}>100 TeV, detected in thick lead chambers, of 57 m^{2}year exposure. Such chambers give opportunity to study hadronic component with high precision and detection probability close to one. The robust observables have been calculated for real and simulated families and compared one to the other. It was concluded that there are peculiar clusters of pions with large asymmetries in the neutral pion fraction distribution, absent in the artificial families.

Similar conclusion has been obtained in [106] where 139 γ-hadron families with energies 100 TeV <ΣE_{vis}<700 TeV, from Pamir experimental data, have been analysed. Here the behaviour of robust observables as a function of the visible energy of a leading jet, obtained after decascading procedure, was studied. The authors of refs. [105, 106] explain the observed deviation from the simulated characteristics as a copious production of pions from a DCC domain, formed in the far-forward angular region. It should be noted, however, that the production rate of DCC, estimated in [98] as 21-24% for the leading particle region, is not sufficient to explain the global characteristics, such as the energy spectra of families. For the whole inelastic channel this value was estimated to be less than 5%.

The presented analyses [98, 105, 106] have been done in the whole region of the experimentally accessible phase space. More information could be achieved from the study of robust observables in pseudorapidity and/or azimuthal angle bins of different sizes. Some hints can be taken from our earlier studies of multiplicity fluctuations in pseudorapidity bins [108]. The analysis has been done for several events, coming from the similar type thick lead chamber of the Pamir experiments. Strong fluctuations have been revealed in the high energy (ΣE_{vis}>100 TeV) photon and hadron families. Here, the multiplicity fluctuations have been studied, by means of scaled factorial moments, separately for photonic and hadronic component. Such result, however, may also indicate on fluctuations of the ratio of photon to hadron multiplicity in analysed bins (DCC domains). Some difficulties in interpretation of experimental data are connected with discrepancies between various simulation studies. Authors of [98, 105] conclude about the existence of non-statistical fluctuations in the neutral fraction. This conclusion is based on disaccordance of experimental and simulated characteristics, based on the "normal" model production and Monte-Carlo calculations of the cascade processes through the whole atmosphere. On the other hand, authors of [109] claimed that strong fluctuations observed in atmospheric families are primarily determined by fluctuations in the atmospheric cascades themselves, and there is no need for changing the act of elementary production. The problem needs further investigation.

4.4 Strange Quark Matter

Colour single states observed so far consist of three quarks (baryons), three antiquarks (antibaryons) or quark–antiquark pairs (mesons). Such objects are described by the Standard Model which does not forbid the existence of colour single states in a bag containing an

integer multiple of three quarks. In such quark matter bags all the quarks are free within the hadron's boundary, so such states are inherently different from nuclear ones that are composed of a conglomerate of A = 1 baryons. Quark matter states composed of only u and d quarks are known to be less stable than normal nuclei of the same baryon number A and charge Z since they do not decay into quark matter. The strange quark matter (SQM) is a matter with strangeness per baryon of the order of unity, thus containing a comparable fraction of up, down and strange quarks. If it ever exists, may be a stable ground state of a QCD instead of the nuclear matter. The fact that SQM is absolutely stable does not contradict the ordinary experience that matter is, for the most part, made of ordinary nuclear matter. The reason is that changing the ordinary matter to SQM one, a large number of u and d quarks need to convert to s quarks, which would require a very high order weak interaction and therefore it is highly improbable [110]. On the other hand, the existence of ordinary nuclear matter shows that quark matter consisting of only u and d quarks is unstable. Adding a third flavour introduces another Fermi well and thus reduces the energy relative to a two–flavour system what can make the system stable. The most stable configurations would have roughly equal numbers of up, down and strange quarks with charges of +2/3e, -1/3e and -1/3e, respectively, therefore minimizing the surface and Coulomb energies. A major destabilizing factor is the large mass of the strange quark. The anticipated mass range for this kind of matter may lie between the masses of light nuclei and that of neutron stars of $A \simeq 10^{57}$. Some astrophysical mechanisms can convert very large stars into strange stars. Strange matter being the part of the cosmic radiation is called sometimes strange quark *nuggets* or *nuclearities*. Smaller amounts of strange quark matter are usually called *droplets* of strange quark matter, or simply *strangelets*. The existence of stable SQM was postulated by Witten [110]. He also suggested the possibility of production of small lumps of SQM, strangelets with $10^2 <$ A $< 10^6$, in today's universe by quark(neutron) stars, which could convert to more stable SQM stars. They could permeate the Galaxy and reach the Earth.

SQM could have important cosmological consequences for today's universe which arise from the possibility that the early universe has undergone a first-order phase transition from SQM to nuclear matter. There are also some speculations [111] that its existence could have important technological implications. They are connected with a possibility that in some conditions the small metastable SQM drops could be "rapidly grown" to a larger stable size, feeding in neutrons or light nuclei and getting out energy in photons. There were described a number of reasons, theoretical as well as experimental, why such a scenario is exceedingly unlikely [111]. It is argued that the experiments at RHIC and LHC do not represent a threat to our planet. Very large safety factors can be derived for example from the survival of the Moon and the observed rate of supernovae.

Many authors investigated conditions for SQM stability (see for example [112, 113, 114]. The practical measure of stability of a strangelet is provided by the so called separation energy dE/dA, i.e. the energy which is required to remove a single baryon from a strangelet. If $dE/dA > m_N$ then strangelet can evaporate neutrons from its surface. Contrary to normal nuclei, SQM stability increases with A and the threshold of its stability is close to $A_{crit} \sim 300$. Some calculations, based on QCD and the phenomenological bag model [114, 115] (up to the baryon number A = 40) suggest that strange quark matter may be metastable or even completely stable for a wide range of bag model parameters values ($B^{1/4} \sim$ 150-170 MeV). Generally, for higher bag parameter values there are less

long–lived strangelets and they are shifted towards higher values of baryon number A, strangeness factor f_s and towards higher negative charges. There are also predictions that quite small strangelets might gain stability due to shell effects [116, 117]. They are called "magic strangelets". However, due to the lack of theoretical constraints on bag model parameters and difficulties in calculating colour magnetic interactions and finite size effects, experiments are necessary to help answer the question of the stability of strangelets. The properties of some forms of hypothetical strange matter, as small lumps of strange quark matter (strangelets) or hyperon matter (metastable multihypernuclear objects MEMO's) have been discussed by many authors (see for example [113, 114, 115, 118]) with special emphasis on their relevance to the present and future heavy ion experiments. Different aspects of strange quark matter physics are described in the recent reviews [16, 119, 120].

Searches for SQM have been made on terrestrial matter [121], cosmic rays and astrophysical objects [122]. The searches resulted in low limits for strangelets in terrestrial matter, but on the other hand some data could be understood by assuming the presence of strangelets in cosmic rays [18, 19, 70, 86, 123, 124] (see the next section). It is postulated that the millisecond pulsar SAX J1808.4-3658 is a good candidate for a strange star [125]. Several strangelet candidates have been reported in cosmic ray experiments [126, 127, 128]. There are a lot of experiments looking for strange quark matter in heavy ion collisions. They are mostly based on such discerning property of strangelets as an unusual charge to mass ratio ($Z/A \ll 1$). The strange counterparts of ordinary nuclei are searched for in high-energy collisions at Brookhaven [129] and at CERN [130]. For example experiment E864 published the final results of a search for charged and neutral strange quark matter produced in interactions of 11.5 GeV/c per nucleon Au beams with Pt or Pb targets. Searches were made for strange quark matter with $A \geq 5$ and proper lifetimes greater than 50 ns. They found 90% confidence level upper limits of approximately 10^{-8} per central collision for both charged and neutral strangelets. Also high efficiency searches at the CERN-SPS by the NA52 experiment found no evident SQM event. To date no experiment has published results indicating a clear positive signal for strangelets. Although experiments were able to set upper limits on the existence of strangelets in the range of sensitivity of the experiments, they were not able to answer the question concerning their existence. There are several definite reasons for this. The main ones are that the experiments are sensitive only to metastable strangelets with proper lifetimes greater than $\sim 5 \cdot 10^{-8}$ s and they look for strangelets in the midrapidity region. Most of experiments (except the E814) used focusing spectrometers which, for a given magnetic field setting, have a good acceptance only for a fixed momentum and charge of the produced particle. Therefore, the production limits obtained in these experiments are strongly dependent upon the production model assumed for lumps of strange quark matter. The present status of strange quark matter searches, both in cosmic ray and in accelerator experiments is presented by R. Klingenberg in his review [131].

According to the picture which we proposed in [18] strangelets could be remnants of the decay of slightly-strange quark matter fireball, produced in central collisions of primary cosmic ray nuclei. We have developed this idea and in [19] it has been shown that, in fact, the characteristics of the strongly penetrating many maxima cascades can be successfully explained by assuming the strangelet scenario (see subsection 4.4.2).

4.4.1 Extraterrestrial strangelets

Strangelets have been discussed, in the context of Centauros, by several authors [18, 70, 86, 97]. However, in contrary to our picture [18], where they are postulated to be produced in nucleus–nucleus collisions, some authors have considered the possibility that *strangelets are a component of primary cosmic rays*. After penetration deeply into the atmosphere they could decay, evaporating nucleons and producing Centauro-type events. In principle, the ideas presented in [70, 86, 97] are very close to the old picture of Bjorken and McLerran [82]. The main difference is the proposed Centauro-fireball (strangelet) cross section.

S. B. Shaulov in [70] has presented a rather qualitative disscussion of the presence of strangelets in the primary cosmic rays. The important assumption made here was that relatively large value of strangelet cross section can be combined with high intensity of strangelets in primary cosmic rays. In Bjorken's scenario the glob matter density was taken $\sim$ 30-50 times of normal nuclear matter what results in its small interaction cross section. The density assumed in [70] was only about two times that of normal nuclear matter. In a consequence, strangelets considered here have radii close to these of normal nuclei ($R_{str} \simeq 10$ fm for a strangelet of $A_{str} = 1000$), and a relatively small interaction length ($\lambda_{int} \simeq 10$ g/cm^2, corresponding to geometrical cross section of the strangelet with air nuclei) [2]. Their absorption length, being the function of the interaction length, the fraction of energy lost in the collisions with the air nuclei and the power index of the strangelet mass spectrum, was estimated to be $\lambda_{abs} \simeq 250$ g/cm^2. The dissociation length, describing the total strangelet desintegration, due to its central collisions with air nuclei, has been estimated to be $\lambda_{diss} \simeq 5000$ g/cm^2. Similarly as in [82] the evaporation of neutrons was assumed to be the main channel of strangelet energy loss and the energy fraction evaporated in a single act of collision was estimated in similar way. It was obtained that in one act of a collision several neutrons can be evaporated and a strangelet loses energy of several GeV (in its own rest frame).

In this work it was postulated that the new penetrating component, carrying a large part of energy through the atmosphere, could qualitatively explain a chain of anomalous phenomena such as:

- *Extensive Air Shower (EAS) spectrum "knee"*
  The break in the cosmic ray spectrum, observed at about 10^6 GeV, was detected about 40 years ago and its nature is still unknown. All attempts to connect it with a peculiarity of the cosmic ray acceleration, changes in the composition or the violation of the scaling, have failed. In [70] it is claimed that the "knee" in the EAS spectrum naturally originates if the strangelet spectrum has the maximum at the energy higher than 3 PeV and the strangelet intensity in the maximum is similar to the nuclear one.

- *Large variety of anomalies observed in individual events*
  Such phenomena as: Centauro, Chiron, Geminion, halo, penetrating component could be natural manifestation of the strangelet evaporation during its passage through the atmosphere. Also mini-clusters frequently observed in Chirons could

[2] It seems to be in disagreement with our simulations. Long range many-maxima cascades can be explained only by assuming a small strangelet cross section, resulting from estimated large value of quark-chemical potential, see subsection 4.4.2.

be natural consequence of small p_T evaporation processes. Within this scenario, however, it is hard to understand the appearance of high transverse momenta secondaries in such events.

For consistency of this picture the beginning of strangelet spectrum near $E_0 \sim 10$ PeV with the power index ≥ 3 should be assumed.

G. Wilk and Z. Włodarczyk presented in [86, 97] the picture of propagation of lumps of Strange Quark Matter through the atmosphere, similar to the one described in [70, 82]. In opposite to [18] and [82] they argue, however, that strangelets are of almost normal nuclear sizes. This statement results from the value of strangelet quark chemical potential assumed by authors of [86] to be $\mu_q \sim 300$ MeV. Such value disagrees with that estimated in [17], from Centauro experimental characteristics, and being $\mu_q \sim 600$ MeV. According to refs. [86, 97] the strong penetrability of strangelets is not caused by their small geometrical radii. Strangelets penetrating deeply into the atmosphere are formed in many consecutive interactions with air nuclei, when the mass number of the incident, very heavy lump of SQM is successively diminished. Big primary strangelets can penetrate very deeply into the atmosphere until their baryon number A_{str} exceeds some critical value $A_{crit} \sim 300 - 400$. Below this value they simply disintegrate into nucleons. Such decay could imitate Centauros. According to [86] Centauro events observed at the mountain altitudes would require a primary strangelet of $A_0 \simeq 1000-2000$. For the mass spectrum of the form $N(A_0^{str}) \sim exp(-A_0^{str}/130)$ the model explains the smaller number of Centauros detected at Pamir altitude (~ 600 g/cm^2) than at Chacaltaya (540 g/cm^2). Simultaneously, as it was already mentioned, the authors of ref. [97] claimed that their simulations indicate the insensitivity of families detected at mountain altitudes to any isospin fluctuations. It could mean that the explanation of Centauros needs the presence of some very strongly penetrative projectiles in primary cosmic rays. The model passes over in silence the question of high p_T of Centauro-like phenomena.

It is important to note that all proposed pictures of the strangelet penetration through the matter and its successive destruction in the consecutive collision acts should be connected with the observation of the large cloud of the low energy nucleons from the destroyed target nuclei. Interesting, the extremely long delay (> 0.5 msec) neutrons have been recently observed [123] in large Extensive Air Showers ($N_e > 10^6$) by the neutron monitor working in conjunction with EAS instalation "Hadron". This phenomenon appears at primary energies higher than 3×10^{15} eV and it is observed close to the EAS axis. As the tentative explanation of this phenomenon one can propose the arrival of a new type of primary cosmic ray particles, like strangelets, with gradual dispersion of their energy along the whole atmosphere.

Also muon bundles of extremely high multiplicity observed by ALEPH detector (in the dedicated cosmic–ray run) could originate from strangelets collisions with the atmosphere [124].

The old experimental results are also worth to recalling. Anomalous massive (A=75...1000) and relatively low charged objects (Z=14...46), which could be interpreted as strangelets, have been observed. These are :

- Two anomalous events, with charge $Z \simeq 14$ and mass number A$\simeq$ 350 and $\simeq$ 450 (what can be consistent with theoretical estimate for Z/A ratio for SQM), observed

in primary cosmic ray by counter experiment with the balloon (at the depth $\sim$ 9 g/cm^2) [126];

- The so–called Price's event [127] (detected at the depth $\sim$ 3-5 g/cm^2) with Z $\simeq$ 46 and A $>$ 1000, regarded previously as a possible candidate for a magnetic monopole. It turned out to be also consistent with the small Z/A ratio in SQM;

- The so–called Exotic Track event with Z $\simeq$ 20 and A $\simeq$ 460 [128]. It was observed in the emulsion chamber, exposed to cosmic rays with the balloon at the atmospheric depth of only 11.7 g/cm^2 at zenith angle of 87.4^0. It means that the projectile causing that event traversed $\sim$ 200 g/cm^2 of the atmosphere. It is in contrast with the previous events where the corresponding depths were of the order of 5-15 g/cm^2 of the atmosphere only.

If the Cenaturo-like events are really caused by strangelets then the Exotic Track event could be an argument supporting their strongly penetrative power. It is rather impossible for normal nuclei of A $\sim$ 460 to traverse $\sim$ 200 g/cm^2 of matter without fragmentation. The Exotic Track event motivated the balloon JACEE [132] and the Concorde aircraft [133] experiments (at the depth 110 g/cm^2) intended to search for strangelets with long mean free paths. The idea of both experiments is based on two distinctive characteristics of strangelets: their small geometrical radii and small Z/A ratio when compared with those of ordinary nuclei. The assumed interaction mean free path λ_{str} of strangelets in the atmosphere was of the order of $\sim$ 124-59 g/cm^2 for strangelets of $A_{str} \simeq$ 100-1000. These values are close to those for protons at comparable energies ($\lambda_{protons}$ = 60-70 g/cm^2 and much higher than those for normal nuclei ($\lambda_{nucleus} \simeq$ 3.8 g/cm^2 for A =100). The results of both experiments are, so far, negative: no evidence for strangelets with $Z \geq$ 30 that survived a travel of 100 g/cm^2 in the atmosphere was found. It should be noted, however, that these experiments fail in detecting high mass and small Z objects because of Z/β detection threshold in CR-39 films.

4.4.2 Strangelets formed in the Centauro fireball

At present, several types of models are used to describe the strangelet production in heavy ion collisions [118, 134, 135]. They can be classified into two categories: strangelet production by coalescense of hyperons or by production following a quark-gluon plasma creation. In a very popular coalescense model, an ensemble of quarks, which are products of nucleus-nucleus collisions, form a composite state which fuses to form a strangelet [134]. The formation of a quark-gluon plasma is not needed in this scenario, as hyperons coalesce during the late stage of the collision forming a doorway state for strangelet production. Such scenario favours the production of low mass strangelets in the midrapidity region, formation of strangelets with $A \geq 10$ is rather unlikely. Thermal models further assume that chemical and thermal equilibrium are achieved prior to final particle production [135]. Coalescense and thermal models usually predict lower strangelet cross section than models postulating a formation of a QGP state. Greiner et al. [118] suggest that once a QGP droplet is formed, almost every QGP state evolves into a strangelet by means of the strangeness distillation mechanism. Distillation process provides a possibility for producing more stable large strangelets since the QGP would lose energy by meson emission possibly resulting in a strangelet of approximately the same A as the QGP droplet.

In [17] the model of Centauro production in nucleus-nucleus collisions has been proposed. We have developed this model in [18] postulating the formation of incident quark-matter fireball, in collisions of the primary cosmic ray nuclei with air nuclei, at the top of the atmosphere, and its subsequent transformation into relatively long-lived strange quark-matter droplet. In order to survive passage from the upper atmosphere downward to the Chacaltaya (Pamir) altitude, the Centauro fireball should have a large mean free path ($\lambda \geq 150$ g/cm^2) and/or lifetime $\tau_0 \sim 10^{-9}$ sec. Then the hadronization of the Centauro fireball will occur close to the detector.

Our picture [18, 19] is based on models involving an intermediate quark-gluon plasma state and the distillation process as separation mechanism of strangeness and anti-strangeness, as described for heavy ion collisions in [118]. We consider baryon-rich environment where the QGP contains a lot of quarks and gluons from the initial nuclei. Since the production of $u\overline{u}$, $d\overline{d}$ pairs is strongly prohibited in such environment, the main process is the formation of $s\overline{s}$ pairs by gluon fusion, $g + g \rightarrow s + \overline{s}$. The QGP cools by emitting hadronized π's and K's. The larger amount of up and down quarks with respect to the anti-quarks results in a higher chance for a $\overline{s}$ quark to find u or d quark and form a K^+ or K^0 than for s-quark to form the anti-particle counterparts. Thus, antistrange quarks are emitted and the remaining part of the QGP is enriched by strange quarks. If such multi-quark state is stable the strangelet can be born, if not it decays with emission of presumably hyperons.

The model avoids the problem of the very small flux of cosmic ray nuclei at the mountain top level and additionally contains very exciting suggestion of the simultaneous interpretation of both Centauros and long-flying component. The strongly penetrating component could be the sign of the passage of strangelets, formed at the last stage of the Centauro fireball evolution, through the matter. We have studied this hypothesis in detail and the results are described in [19].

The model explains most features of Centauro events. It could likely explain also the observed low family flux. Such features of the exotic fireball, as its strong penetrating power and its decay predominantly into baryons could cause a decrease of the electromagnetic family flux.

Characteristics and time evolution of Centauro fireball

The development in time of the Centauro fireball has been described in details in [18]. The scheme of its evolution is shown in Fig. 4.1. A similar fireball development was proposed by C. Greiner et al. [118] in the context of heavy ion collisions. Here are summarized the main points which are essential from the point of view of a possible connection of Centauros with long–flying component and their detection in future collider experiments.

1. *Formation of a quark–matter fireball.*
   The fireball is created in central collisions of ultrarelativistic ($E_{Lab} \sim 1740$ TeV) medium–heavy cosmic–ray nuclei with air nuclei, in the baryon–rich, projectile fragmentation region. At the moment of creation it consists of u, d quarks and gluons only. It has very high matter density, hence high binding energy. Due to its very strong binding its lifetime is assumed to be $\sim 10^{-22}$ s. Large baryochemical potential suppresses the production of $\overline{u}$ and $\overline{d}$ quarks because

$$N_{\overline{q}} \propto exp(-\mu_q/T) \tag{4.14}$$

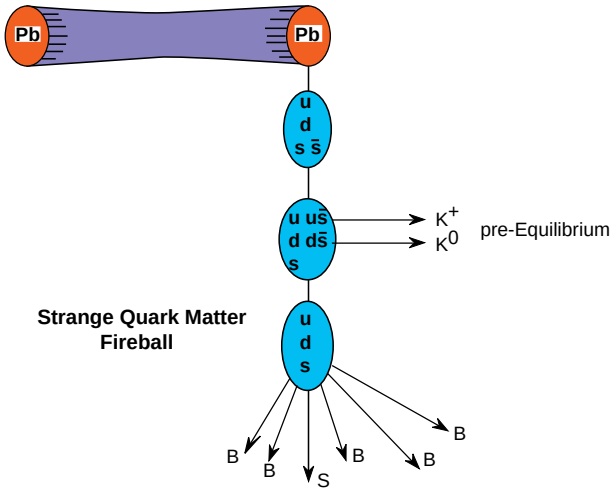

Figure 4.1: Centauro fireball evolution scheme [136].

In addition the production of quarks is also strongly prohibited due to the Pauli blocking. Thus, the very high baryochemical potential prohibits the creation of $u\overline{u}$ and $d\overline{d}$ quarks, resulting in gluon fragmentation $g \rightarrow s\overline{s}$ mainly.

2. *Chemical equilibrium*
   The state of (partial) chemical equlibrium may be approached in a time interval $\Delta\tau > 10^{-23}$ s, the relaxation time for $g \rightarrow s\overline{s}$. During this time the fireball has a chance to emit several $K^+(\overline{s}u)$ and $K^0(\overline{s}d)$ carrying away all strange antiquarks and positive charge, and lowering somewhat the initial temperature and entropy. Kaons are quickly emitted due to their small mass and high thermal velocity. They are not observed in emulsion chambers because they are lost in electro-nuclear cascade process in the atmosphere.

3. *Strange quark matter state*
   After emitting kaons the fireball is a mixture of u, d and s quarks. In absence of $\overline{u}$ and $\overline{d}$ quarks, s quarks can not be emitted quickly. This may cause the transformation of *the initial quark–matter fireball* into *a lightly strange quark matter state* (with the value of strangeness to baryon ratio $\rho_s/\rho_b \sim 0.06$). It is still characterized by very large density, low temperature and the value of charge to mass ratio ($Z/A \sim 0.4$) less than that of the original quark–matter fireball.

   The fireball has a finite excess of s–quarks and due to their stabilizing effects [110, 118] it could become *a long–lived state* capable to reach the mountain top level before decaying.

4. *Hadronization*
   The mechanism of strangeness separation suggested by Greiner et al. [118], can cause the strange quark content of the Centauro fireball to form low–mass strangelet(s). The total energy per baryon can be lowered assembling the nonstrange quarks into

pure nucleonic degrees of freedom and leaving the strange quarks in a strange matter droplet, its strangeness fraction being enriched to $f_s \simeq 1$. Such state would be a mixture of two phases: pure nucleonic matter and strange quark–matter cluster. The Centauro fireball finally could decay into non–strange baryons ($< N_h > \sim 75$) and strangelet(s) having very high strangeness–to–baryon ratio ($f_s = N_s/A \sim 1$), very low charge–to–baryon ratio ($Z/A \sim 0$), and a small mass number ($A_{str} \sim 10 - 15$). The strangelet temperature is expected to be lower than that estimated for Centauro fireball. Strangelets could be identified as highly penetrating particles, frequently accompanying the exotic cosmic–ray events.

This scenario is based on the experimental Centauro characteristics derived from five "classical Chacaltaya Centauros". Using these experimental characteristics the *thermodynamic quantities* have been estimated [17].

The main observed and estimated characteristic quantities of Centauros have been summarized in Table 4.1. These Centauro characteristic quantities were calculated assuming an ideal two–flavour QGP and should be understood as rough estimates.

More realistic picture needs introducing *three flavours (u,d,s) interacting quarks*, realistic *strangeness equlibration factor* and using the full equation for $\varepsilon(T, \mu_q, \alpha_s, \gamma_s)$. The energy density can be calculated from the formula [138, 139]:

$$\begin{aligned} \varepsilon_{qgp} &= (\frac{37}{30} - \frac{11a_s}{3\pi})\pi^2 T^4 + (1 - \frac{2a_s}{\pi})3\mu_q^2 T^2 + \frac{3}{2\pi^2}(1 - \frac{2a_s}{\pi})\mu_q^4 + \\ &+ \gamma_s(\frac{18T^4}{\pi^2}(\frac{m_s}{T})^2 K_2 + 6(\frac{m_s T}{\pi})^2(\frac{m_s}{T}K_1). \end{aligned} \tag{4.15}$$

The entropy per baryon

$$S_b = S/\rho_b \tag{4.16}$$

where the baryon density

$$\rho_b = \frac{2}{3}(1 - \frac{2a_s}{\pi})(\mu_q T^2 + \frac{\mu_q^3}{\pi^2}), \tag{4.17}$$

and the entropy

$$\begin{aligned} S &= \frac{1}{3}\frac{\partial \varepsilon}{\partial T} = (\frac{74}{45} - \frac{44a_s}{9\pi})\pi^2 T^3 + 2(1 - \frac{2a_s}{\pi})\mu_q^2 T + \\ &+ \gamma_s(\frac{3m_s^3}{\pi^2}K_3 + \frac{12m_s^2}{\pi^2}TK_2 + \frac{m_s^4}{\pi^2 T}K_2 + \frac{5m_s^3}{\pi^2}K_1 + \frac{m_s^4}{\pi^2 T}K_0), \end{aligned} \tag{4.18}$$

where $K_i(m_s/T)$ are i–order modified Bessel functions and γ_s is the strangeness equlibration factor.

Using these formulas, it is seen that the Centauro fireball with values of the temperature, quarkchemical potential and energy density estimated previously to be T =130 MeV, μ_q = 600 MeV and ε = 2.4 GeV/fm^3, is not the ideal QGP fireball because the strangeness equilibration factor is estimated to be less than unity and strong coupling constant is expected to be greater than zero. The estimated thermodynamical quantities are consistent rather with the picture of "constituent quark matter " formation. That is, a state of deconfined constituent quarks, somewhat massive and interacting, *not* an ideal quark-gluon plasma, which has undergone a chiral phase transition. Taking for this quark

Table 4.1: Summary of observed and estimated thermodynamic and kinematical quantities characteristic of the cosmic–ray Centauro events [17, 18].

"Centauro" event	
Hadron multiplicity $< N_h >$	64–90, $< 75 >$
γ multiplicity	0
Average total incident energy	$< E > \geq$ 1740 TeV
Total interaction energy in "60+14" c.m.	$\sqrt{s} \geq$ 6760 GeV
Total interaction energy in N–N c.m.	$\sqrt{s_{N-N}} \geq$ 233 GeV
Incident nucleus rapidity in laboratory frame	$y_{pr} = 11.03$
Midrapidity of "60+14" system	$y_{c.m.} = 6.24$
Laboratory pseudorapidity of emitted baryons	$< \eta_{cnt} > = 9.9 \pm 0.2$
Width of pseudorapidity distribution	$< \Delta\eta_{cnt} > \simeq 1 \pm 0.2$
Average transverse momentum	$< p_T > = 1.75 \pm 0.7$ GeV/c
Mass of fireball	$M_{fb} = 180 \pm 60$ GeV
Volume of fireball	$V_{fb} \leq$ 75 - 100 fm^3 (*)
Energy density of fireball	$\varepsilon_{fb} \geq 2.4 \pm 1$ GeV fm^{-3} (*)
Baryochemical potential of fireball	$\mu_b = 1.8 \pm 0.3$ GeV
Temperature of fireball	$T_{fb} = 130 \pm 6$ MeV
Quark density of fireball	$< \rho_q > = 8 \pm 3\ fm^{-3}$
Baryon density of fireball	$< \rho_b > = 2.7 \pm 1\ fm^{-3}$
Strange quark density	$\rho_s \sim 0.14\ fm^{-3}$
Antiquark density	$\rho_{\overline{q}} \sim 3.6$ x $10^{-3} fm^{-3}$
Gluon density	$\rho_g \sim 0.6\ fm^{-3}$
Entropy density	$S \sim 16.4\ fm^{-3}$
Entropy/baryon density	$S/\rho_b \sim 6$
Strangeness/baryon density	$\rho_s/\rho_b \sim 0.06$
Final charge/baryon	$(Z/A)_f \sim 0.4$
Net strangeness	$N_s - N_{\overline{s}} \sim 14$
Predicted particle ratio	N(pion)/N(nucleon) $\simeq$ 7x10^{-6}
"Centauro" strangelet	
Mass	A $\sim$ 10 - 15
Charge/baryon	Z/A $\sim$ 0
Strangeness/baryon	$f_s \sim 1$

* according to [137] $V_{fb} = 27 \pm 16$ fm^3 and $\varepsilon_{fb} = 6.7 \pm 3.6$ GeV/fm^3

matter state the strong coupling constant $\alpha_s \simeq 0.5 - 0.6$ and $\gamma_s \simeq 0.4$ one obtains the Centauro point located at the phase diagram close to the QGP phase, at the in-between region of the ideal QGP phase connecting with chiral phase transition and the Hadron Gas Phase as it is shown in Figure 4.2. Lattice QCD calculations at zero baryochemical

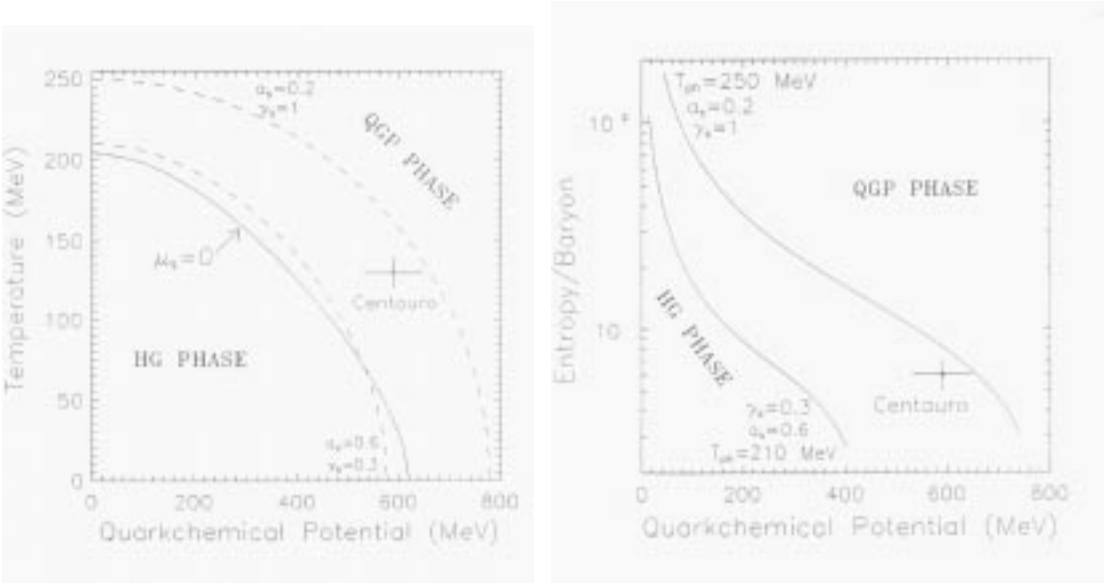

Figure 4.2: Location of the Centauro point (T, μ_q) on the phase diagram for two temperatures: $T(\mu_q = 0)$= 250 and 210 MeV (dashed curves). Solid curve is for $\mu_s = 0$ in the hadron gas. The plot at the right side shows entropy per baryon versus quarkchemical potential, for two phase curves [139].

potential [140, 141] and relativistic mean field theory chiral calculations in dense nuclear matter [142] predict a phase transition to an ideal quark–gluon plasma, at a temperature of about 250 MeV $\sim 2T_{cr}$ [141] (T_{cr} being the critical temperature for deconfinement [140] and density of about $18\rho_0$, respectively). The phase curves have been drawn assuming a simple MIT bag EOS for three quark flavours and realistic boundary conditions:
the upper curve for $T(\mu_q = 0) = 250\,\mathrm{MeV} \simeq 2T_{cr}$ and for $\alpha_s = 0.2$, $\gamma_s = 1$;
the lower curve for $T(\mu_q = 0) = 210\,\mathrm{MeV} \simeq 1.6T_{cr}$ and $\alpha_s = 0.6$, $\gamma_s = 0.3$. The upper curve denotes the (approximate) limit of the ideal QGP phase, whilst the lower one the effective upper limit of the Hadron Gas phase [139].

Penetrability question

According to this model, Centauro events are produced in central collisions of ultra-relativistic cosmic-ray nuclei with air nuclei. A collision of the medium-heavy cosmic-ray nuclei occurs at the top of the atmosphere. Thus the Centauro fireball must possess features allowing it to reach the mountain-top altitudes ($\sim$ 500 g/cm^2) without interaction with air nuclei or spontaneous decay during its flightpath of about 15 km. This

requirement creates the following questions:

- what is the magnitude of the interaction length λ and the lifetime τ of the Centauro fireball, resulting from the existing experimental data?
- do they not contradict the requirement of traversing of about 15 km before the fireball decays?
- what are the theoretical reasons which could allow such long flightpath?

These questions we considered in [18] and the stability question has been studied more recently also in [137].

Experimental constraints on λ or τ

An estimate of the value of the interaction length of the Centauro fireball can be obtained from the comparison of the observed rate of Centauro events, detected at the mountain top level, after Centauro fireballs decaying, with the results of experiments looking for heavy penetrating particles, assuming that Centauro fireballs before their decays may be identified with such objects. On the one hand, it seems that the large flux of Centauro events detected in Chacaltaya and Pamir emulsion chambers suggests a long interaction length of the Cenaturo fireball, allowing it to reach the mountain top level. On the other hand, the negative results of the experiments looking for heavy penetrating particles at White Mountains and Mt Norikura by means of CR–39 films could be explained, by assuming a short interaction length of Centauro fireball, allowing for its decay before reaching the mountain top altitude [143]. However, the careful analysis of that seeming contradiction [18] shows that the interaction length of the Centauro fireball, λ_{Cnt} larger than 150 g/cm^2, is in accordance with the results of both kind of experiments.

The long interaction length of Centauro fireball could be connected with the very high binding energy and the reduced geometrical cross section (the estimated volume of the fireball [18] is more than six times smaller than that of the ordinary nucleus with A=75).

If the Centauro fireball is an unstable state spontaneously decaying with the probability P(x) after travelling a distance x $\approx$ 15 km, then the lifetime τ_0, in its own frame, can be calculated from the formula:

$$\tau_0 = \tau/\gamma_{FB} = -Mx/p\, ln P(x) \tag{4.19}$$

where τ is the lifetime in the observer's frame and $\gamma_{FB} = E/M$.
Taking [18] average kinetic energy $E \simeq 1740$ TeV, mass $M \simeq 180$ GeV, momentum of the Centauro $p \simeq 1700$ GeV/c and assuming $P(x) \sim 10\% - 50\%$ we obtain the *mean life* τ_0 of the Centauro fireball of the order of 10^{-9} s.

If the Centauro fireball is a metastable state decaying spontaneously, it should have a mean lifetime of the order of 10^{-9} s to survive a flightpath of about 15 km and reach the mountain top altitudes. This means that the fireball could decay via weak interactions,

since strong decays occur within $\sim 10^{-23} - 10^{-24}$ s. Even so, the lifetime of 10^{-9} s is unrealistically long for a nonstrange, normal quark matter state.

Theorethical justifications of the long flightpath, i.e. stability question

We estimated [18] that the interaction length of the Centauro fireball in the atmosphere $\lambda_{Cnt} \geq 150$ g/cm^2 is in accordance with different experimental observations. This is an extremely long interaction length. It is about 1.6 times larger than that of a nucleon and about 35 times larger than that of a normal nucleus of a comparable mass number. The long lifetime and small cross section could be attributed to its very high binding energy and much reduced geometrical volume. The very high baryochemical potential and the transformation of the intial quark matter state into a partially-strange quark matter one, with increased spatial concentration of quarks due to the extra fermion flavour, result in an increase of the binding energy. Extremely large density and binding energy and the small volume may result in the formation of a (meta)stable state. However, the problem is open and according to our present knowledge rather far from satisfactory and quantitative solving. The main questions are:

1. *Radius (and volume) question.*

   - The long penetration length of the Centauro fireball through the atmosphere suggests the small geometrical cross section of that object, i.e. very small radius. Assuming, in accordance with the results of cosmic ray experiments, the average interaction mean free path of nucleons with the air nuclei being $\langle \lambda_{p-air} \rangle = 110$ g/cm^2 and $\langle \lambda_{n-air} \rangle = 75$ g/cm^2 for protons and neutrons respectively we can easily estimate that the ratio of the radius of a nucleon to the radius of the Centauro fireball should be:

   $$R_{nucleon}/R_{Cnt} = \sqrt{\sigma_{nucleon}/\sigma_{Cnt}} = \sqrt{\lambda_{Cnt}/\langle \lambda_{nucleon} \rangle} \simeq 1.27 \qquad (4.20)$$

   Assuming further that $R_{nucleon} \simeq 1.15$ fm and $R = r_0 A^{1/3}$ we can expect $R_{Cnt} \sim 0.9$ fm and $r_0^{Cnt} \sim 0.22$ fm (for A = 75). In other words, the experimental observation suggests that the Centauro fireball radius could be about 5.5 times smaller than that of a normal nucleus of corresponding A.
   - The other estimate of the Centauro fireball radius can be done by using its volume value, $V_{Cnt} \simeq 75$ fm^3 as obtained in [17]. Assuming the spherical shape of the fireball we get $R_{Cnt} = 2.6$ fm and $r_0^{Cnt} = 0.62$ fm. These values seem to be overestimated in comparison with the previous ones.
   - Another estimate taken from [137] gives $R_{Cnt} = 1.86 \pm 0.36$ fm and $r_0^{Cnt} = 0.44 \pm 0.08$ fm.

   Summarizing, the radius question from the point of view of "experimental" estimates, the situation is rather unclear. Different estimates locate the Centauro fireball radius in the range : $R_{Cnt} \sim 0.9 - 2.6$ fm and $r_0^{Cnt} \sim 0.22 - 0.62$ fm.

2. *Stability curves.*
   The main question is if extreme conditions, such as a very high quarkchemical potential and reduced volume, can cause the (meta) stability of the object. A general

condition for DQM (Deconfined Quark Matter) bag stability comes from the equalization of the internal (quark- gluon) and external (bag) pressure. The formulas for thermodynamical quantities of strangelets being in mechanical equilibrium can be found for example in [119]. They have been derived assuming the massless u, d and s-quarks of equal chemical potentials μ, and $\alpha_s = 0$. Strangelets are in mechanical equilibrium at fixed temperature T and baryon number A when

$$BV = (\frac{19\pi^2}{36}T^4 + \frac{3}{2}\mu^2T^2 + \frac{3}{4\pi^2}\mu^4)V - (\frac{41}{216}T^2 + \frac{1}{8\pi^2}\mu^2)C \qquad (4.21)$$

where extrinsic curvature $C = \oint(\frac{1}{R_1} + \frac{1}{R_2})dS$ ($C = 8\pi R$ for a sphere), and V and B are the volume and bag model value constant respectively.
In this case

$$A = (\mu T^2 + \frac{1}{\pi^2}\mu^3)V - \frac{\mu}{4\pi^2}C \qquad (4.22)$$

The stability curves obtained from this formula are shown in Fig. 4.3.

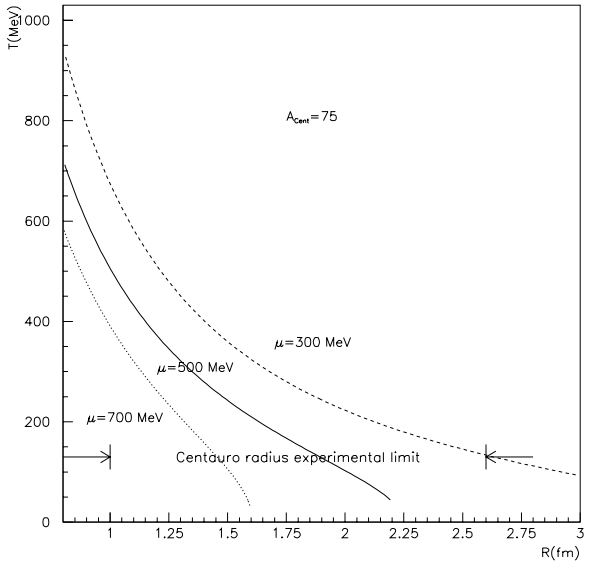

Figure 4.3: Stability curves plotted as T versus R for fixed μ_q = 300, 500, 700 MeV for a strangelet with A=75.

There is plotted the temperature T as a function of the radius R for three values of quark chemical potential (μ = 300, 500, 700 MeV) and baryon number A=75. There is drawn also the experimentally estimated Centauro fireball radius limit. It is well inside the "stability region" for the Centauro fireball with parameters close to experimentally obtained values, i.e. T=130 MeV and μ = 600 MeV.

According to the model [17, 18] the Centauro fireball is supposed to be, however, only the slightly strange quark matter glob. It has been concluded in ref. [137] that Centauro fireball quantities, such as T = 130 MeV, μ_q = 600 MeV and $R_{Cnt} = 1.86$

$\pm$ 0.36 fm are within one standard deviation from the stability conditions, thus it might be possible that the Centauro fireball is a metastable state.

In the context of discussing of Centauro fireball stability it should be stressed that there are also some predictions concerning the possibility of the existence of stable collapsed nuclei [144]. A collapsed nucleus is a highly dense nuclear matter state, the nucleon density being more than 20 times larger than that corresponding to a normal nucleus, with binding energy per nucleon of hundred MeV and even up to the nucleon mass (for T=0). In this condition, a collapsed nucleus is a cold deconfined quark matter state, with the radius r_0 estimated to be 0.4 fm, which is close to that of the Centauro fireball.

It should be mentioned, however, that these attempts need about two times larger bag pressure than the value required for stability of a strangelet at T = 0. For instance, $B^{1/4} \sim 375$ MeV is needed for the stabilization of the quark-gluon plasma bag with T=130 MeV, $\mu_q = 600$ MeV, A=75 and R= 1.62 fm [137].

Strangelets from the Centauro-fireball

At the last stage of the Centauro fireball evolution, due to the strangeness distillation mechanism a strangelet can be formed. The characteristic features of such quark–matter nuggets can be estimated by using the above mentioned quark–gluon plasma model describing the experimental Centauro characteristics. On the other hand they can be derived independently from the analysis of the strongly penetrating cascades, assuming that they are due to a strangelet passage through the apparatus.

The excess of strange quarks in the Centauro fireball is mainly caused by the pre–equilibrium emission of the K^+ and K^0 mesons which carry $\overline{s}$ quarks away. We assume that the total number of $s\overline{s}$ pairs created in the Centauro fireball volume V approximately equals to the number of emitted K^+, K^0 mesons and it can be estimated from the formula:

$$N_{K^+ + K^0} \simeq N_{s\overline{s}} = \rho_{\overline{s}} V \tag{4.23}$$

where $\rho_{\overline{s}}$ is s–antiquark density and depends on the temperature by the relation [145]:

$$\rho_{\overline{s}} \simeq 0.178 (\frac{T}{200\text{MeV}}) K_2 (\frac{150\text{MeV}}{T}) \tag{4.24}$$

For T=130 MeV which is the temperature for cosmic-ray Centauros, $\rho_{\overline{s}} \simeq 0.14$ fm^{-3}. Taking a volume of the Centauro fireball V $\sim$ O(100 fm^3) the number of created $s\overline{s}$ pairs (and thus emitted kaons) will be $\sim$ 14. After the pre–equilibrium emission of kaons, a strange quark matter metastable object with a small Z/A ratio is formed. It is a mixture of u, d and s quarks and experimentally it can be identified by its Z/A ratio less than that of the ordinary nuclear matter. The change of Z/A ratio, because of kaon emission can be calculated from the formula

$$(\frac{Z}{A})_f = (\frac{Z}{A})_i - \frac{\Delta Q}{A} \tag{4.25}$$

where the net change of the charge

$$\Delta Q = N_{s\overline{s}}((Q_u + Q_d)/2 + Q_{\overline{s}}). \tag{4.26}$$

Assuming the quark charges $Q_u = 2/3, Q_d = Q_s = -1/3$, $(Z/A)_i \simeq 0.5$ and the temperature T $\sim$ 130 MeV we evaluate $(Z/A)_f \simeq 0.4$. In the extreme case when all produced strange quarks became constituents of the strangelet and $N_s/A_{str} \simeq 1$, we can expect the final explosion of the Centauro fireball into non-strange baryons and accompanied *emission of a small strangelet characterized by* $A_{str} \sim 10 - 16$. Its very high strangeness-to-baryon ratio implies also very low charge-to-baryon ratio (Z/A $\sim$ 0).

Strongly penetrating cascades as signs of strangelets

The hypothesis, that the strongly penetrating cascades can be produced by a strangelets, announced in [18], was developed in [19] where the possible connection between the very penetrating component, frequently accompanying the cosmic ray exotic phenomena, and the hypothesis of the formation of strangelets in the process of strangeness distillation was studied.

Several possible decay [110, 113, 114, 118, 146] and interaction [86] modes of a small strangelet were considered and its travelling through the homogenous–type thick lead chamber was simulated.

Unstable strangelets

Objects decaying via strong interactions in the timescales typical for strong processes ($\tau_0 \lesssim 10^{-20} s$)were called unstable strangelets. Although a variety of such processes is expected [110, 113, 114], the most important one is a *strong neutron emission* $S \rightarrow S' + n$ in which a strangelet S emits a neutron, yielding a daughter strangelet S' with parameters changed by $\Delta A = -1, \Delta Y = -1, \Delta Z = 0$. Strong proton emission is similar to neutron emission except for the Coulomb barrier. For this reason, proton emission is unimportant in comparison to neutron emission. Another important baryon emission mechanism could be α-emission. α particles have large binding energy per baryon, making α decay energetically favourable in a wide range of strangelet parameters. However, α decay is expected to be negligible as compared to other possible processes because of two reasons supressing it: the Coulomb barrier and a small probability of finding an ensemble of up and down quarks resembling an α particle. For these reasons, in our picture we have assumed that a strangelet, being a remnant of an explosion of the Centauro fireball, decays via neutron evaporation. [3]

Unstable strangelets decay very fast, practically at the point of their formation. For strangelets with $\tau_0 \sim 10^{-20} s$ and a Lorentz factor $\gamma \sim 10^4 - 10^5$ the estimated length of the decay path will be of the order of $\sim 10^{-5} - 10^{-6}$ cm, what is very small in comparison with the estimated heights of the Centauro fireball explosion (H $\sim$ 100 - 1000 m above the chamber). Thus the considered picture resolves into a simple case of a bundle of nucleons entering the chamber. Assuming additionally that all nucleons are evaporated with momenta close one to the other we get a bundle of strongly collimated nucleons. If the relative transverse momenta of neutrons are of the same order as those observed in mini-clusters, i.e. $p_T(\gamma) \sim 10$ MeV/c, then the average lateral distances between neutrons, at the chamber level, are estimated to be of the order $\sim$ 100 - 1000 μm. Thus, depending

[3] What concerns the decay of a strangelet via hyperon emission, it seems that they are too massive to be emitted. However, even if it is possible, the final picture should not be essentially different from that when the emission of nucleons is assumed. Both the bundle of nucleons and hyperons falling into the chamber will give similar long-range cascades.

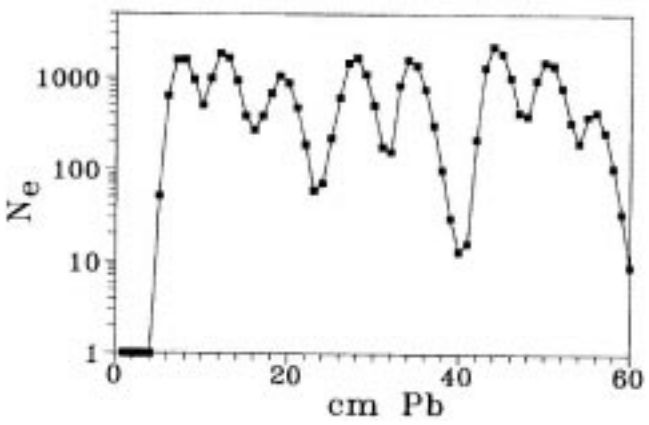

Figure 4.4: Example of simulated transition curve produced by an unstable strangelet decaying into a bundle of 7 neutrons, recorded in the thick lead chamber. Neutron energy $E_n \simeq E_{str}/A_{str} \simeq 200$ TeV). Numbers of electrons N_e are counted within the radius of 50 μm.

on the formation height and the energy, a decaying strangelet will produce in the chamber the picture resembling a mini-cluster or one single long-range cascade (if the relative distances between the decay products are smaller then the lateral resolution of the used detectors). The development of nuclear-electromagnetic cascades, caused by such neutron bundles, in the typical homogenous lead chamber with detection layers placed every 1 cm of the lead absorber was simulated. It has been found that the bundle of several ($\sim$7) neutrons generates the many–maxima long-range cascades, very similar to the long-flying component observed in cosmic-ray experiments. A typical simulated event is shown in Fig. 4.4.

The impression of the strong similarity between the simulated and observed transition curves has been confirmed by investigation of the relative distances and the distribution of energy contained in the successive humps. The comparison of the simulated characteristics with these obtained from analysis of the experimental long range cascades presented in [54] is shown in Fig. 4.5.

Metastable strangelets

Metastable strangelets are commonly assumed to decay with a lifetime $\tau_0 \lesssim 10^{-4}$s. They decay via weak interaction processes, of which the most important is *the weak neutron decay.* As it involves a weak interaction flavour-changing process, $s+u \leftrightarrow u+d$, it should be much slower than a strong neutron decay. Generally, however, lifetimes of small metastable strangelets are not predicted precisely at present and they are still a matter of debate [118, 146]. Thus, in principle, a wide range of possible lifetimes of metastable strangelets should be taken into account. For the purpose of our work two extreme possibilities and the intermediate case can be admitted:

- *Lifetimes short enough for decaying of a strangelet above the chamber.*
  In that situation the same final result as in the case of unstable strangelets can be

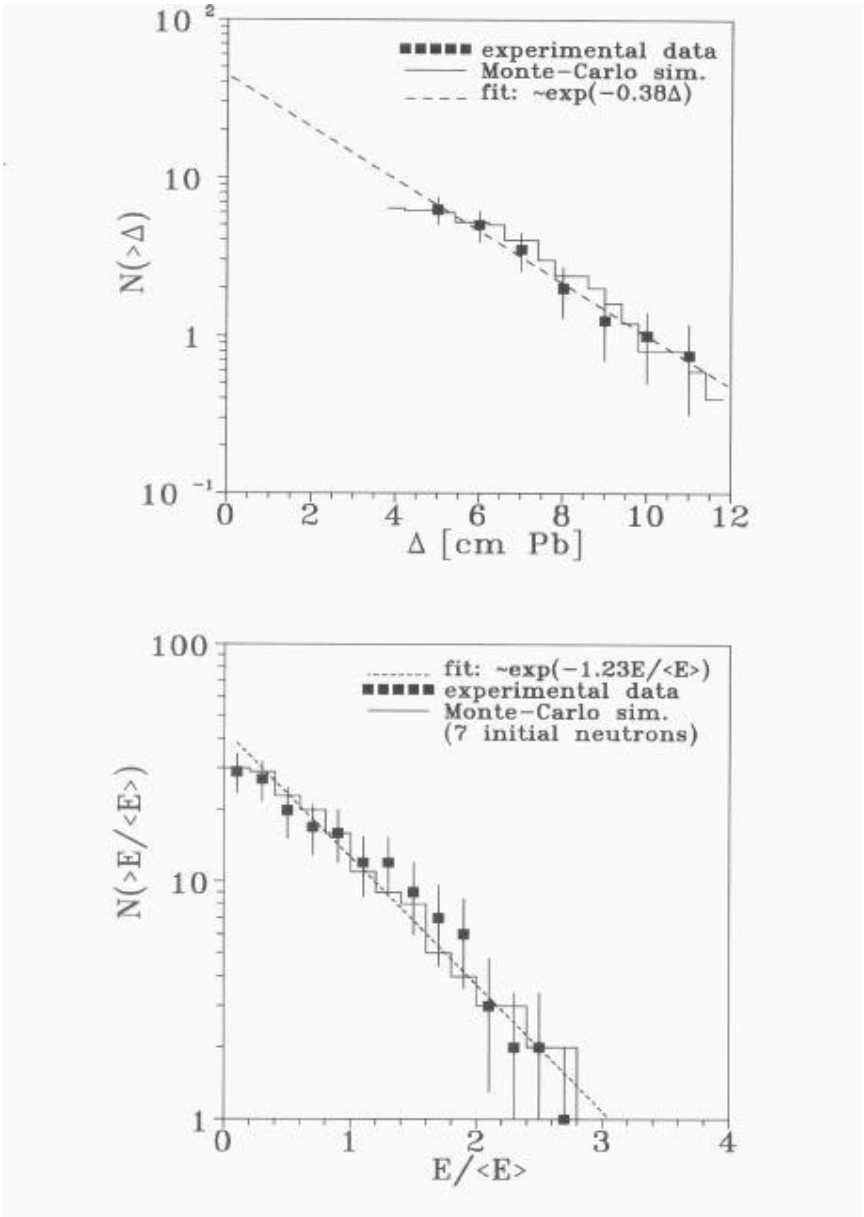

Figure 4.5: Similarity between the experimental data taken from [54] and simulated cascades produced by a bundle of 7 neutrons (full histogram): (a) distribution of mutual distance between the consecutive maxima; (b) distribution of ratios of the energy contained in the particular maxima to the average energy of the humps.

expected.

- *Lifetimes long enough for a strangelet passage, without decay, through the air layer above the chamber and the chamber itself.*
  The situation is analogous to the case of "stable" strangelets, which will be considered later.

- *Intermediate case.*
  A strangelet penetrating through the chamber can successively evaporate neutrons. Neutrons interact with nuclei of the lead absorber producing the many-maxima cascades in which the distances between the successive humps are strongly correlated with the time interval between the successive evaporation acts. Assumption of a strangelet lifetime $\tau_o \sim 10^{-15}$s leads to the formation of the long-range many-maxima cascades similar to these observed in the experiment. Example of such transition curve, produced by a strangelet with $A_{str} = 15$, during its passage through the chamber, is shown in Fig. 4.6. In principle, the picture of successive evaporation of neutrons via the weak strangelet decay could also explain the appearance of a long flying component, when the assumed lifetimes are of the order $\sim 10^{-15}$s. This hypothesis involves, however, some hardly acceptable points:

  – Required lifetime $\tau_0 \sim 10^{-15} s$ seems to be too short for the weak neutron decay process (much shorter than for example the lifetimes of both weak semileptonic and weak nonleptonic decays, estimated in [147] on the basis of the Berger - Jaffe mass formula [113] for strangelets of $A_{str} = 15$).

  – The picture assumes that a strangelet decays successively inside the chamber. Thus, it concerns objects produced at a very small distance from the chamber or just inside it. In the case of strangelets produced in typical cosmic-ray families (at heights $H \sim 100 - 1000$ m above the chamber) it seems unclear why they do not decay in the air layer, above the apparatus.

Stable strangelets

The weak radiative decays ($u + d \longleftrightarrow s + u + \gamma$) and weak leptonic decays ($d \longleftrightarrow u + e^- + \overline{\nu}_e$, $s \longleftrightarrow u + e^- + \overline{\nu}_e$) are expected to be slower than a weak neutron emission. The rate of the radiative decay is inhibited by the electromagnetic coupling constant and all β-decays by the three-body phase space. Additionally, the strangeness changing β process is suppressed by the Cabibbo factor. S. A. Chin and A. K. Kerman [114] estimated that hyperstrange multiquark droplets, having the strangeness to baryon ratio $f_s = 2.2$ - 2.6 can be the subject of weak leptonic decays only and their lifetime is estimated to be longer than $\tau_0 \sim 10^{-4}$s. We call them "stable" strangelets. Such long-lived objects, if produced in the high energy cosmic-ray families should pass without decay through the apparatus. We have considered the simplified picture of their possible interaction in the chamber matter. The idea is similar as described by G. Wilk and Z. Włodarczyk in [86], where the passage of a strangelet through the atmosphere has been considered.

The strangelet is considered as an object with the radius

$$R = r_0 A_{str}^{1/3}$$

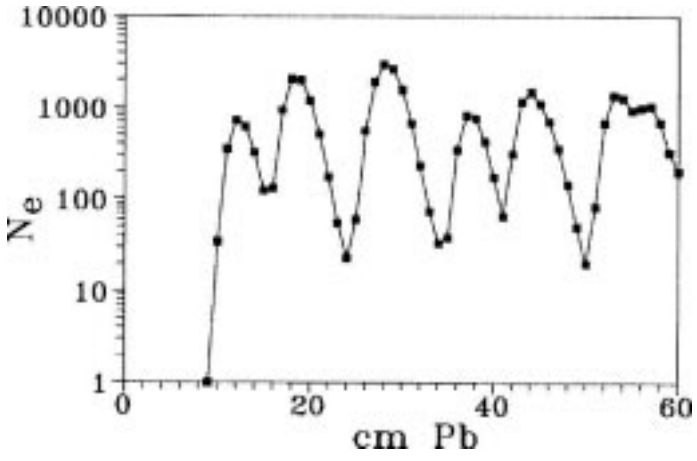

Figure 4.6: Example of simulated transition curve obtained under the assumption of the successive evaporation of neutrons from a metastable strangelet passing through the lead chamber ($A_{str} = 15, E_{str} = 200$ A TeV, $\tau \sim 10^{-15}$ s).

where the rescaled radius

$$r_0 = (\frac{3\pi}{2(1 - \frac{2\alpha_c}{\pi})[\mu^3 + (\mu^2 - m^2)^{3/2}]})^{1/3} \tag{4.27}$$

μ and m are the chemical potential and the mass of the strange quark respectively and α_c is the QCD coupling constant.

The mean interaction path of strangelets in the lead absorber

$$\lambda_{s-Pb} = \frac{A_{Pb} \cdot m_N}{\pi(1.12A_{Pb}^{1/3} + r_0 A_{str}^{1/3})^2} \tag{4.28}$$

Penetrating through the chamber a strangelet collides with lead nuclei. In each act of collision, the "spectator" part of a strangelet survives continuing the passage through the chamber and the "wounded" part is destroyed. The process is ended, when in the successive interaction the whole strangelet is destroyed. Particles, generated at the consecutive collision points, interact with lead nuclei in usual way, resulting in the electromagnetic-nuclear cascade, developing in the chamber matter.

Penetration of a strangelet with mass number $A_{str} = 15$ through the chamber, assuming two different values of the chemical potential: $\mu = 300$ MeV and 600 MeV (what, for $\alpha_c = 0.3$, corresponds to the geometrical cross section $\sigma_{s-Pb} = 2513$ mb and 1854 mb respectively [4]) was simulated. In both cases, many maxima cascades can be produced. Example of the transition curve obtained in the process of successive interactions of a strangelet in the chamber matter is shown in Fig. 4.7.

[4]The experimental value of cross section of cosmic ray nucleons interacting with lead nuclei $\sigma_{n-Pb} = 2030 \pm 190$ mb [54].

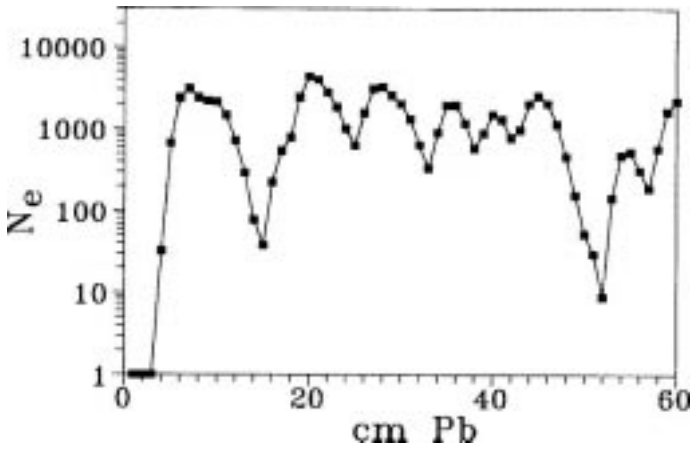

Figure 4.7: Example of simulated transition curve recorded in the lead chamber produced by successive interaction of a long-lived strangelet with lead nuclei ($A_{str} = 15$, $\mu_q = 600$ MeV).

Calculations done in [19] showed that the long-range cascades observed in the thick homogenous lead/emulsion chambers could be the result of a strangelet penetration through the apparatus. Their strong penetrating power can be connected both with the small interaction cross section (in comparison with nucleus of comparable A) of the strangelet and with the big concentration of its energy in a narrow region of phase space. This energy could be liberated into conventional particle production in many consecutive evaporation or interaction acts. In this context, the Centauro-like event with abnormally long cascades found among its secondaries, described in [36, 37], could be regarded as an event, in which strangelets were generated as remnants of the strange quark matter fireball. It seems that also numerous hadron-rich families accompanied by highly penetrating cascades, clusters or halo could be explained by assuming the same mechanism of the formation of a strange quark matter fireball and its successive decay into predominantly baryons and strangelet(s). However, stronger experimental support, especially in the form of hadron-rich events accompanied by the long-flying component, appearing in a form of anomalous long-range cascades, and registered in the thick lead chambers, would be very much required.

It is seen that several possible pictures of a strangelet penetration through the chamber, which give the long-range many-maxima cascades similar to these observed in the cosmic-ray experiments, exist. At this stage of investigations two pictures seem to be the most plausible ones:

- The scenario in which short-lived strangelets (unstable or metastable ones), via strong or weak decays, produce a strongly collimated bundle of neutrons entering the chamber. The successive maxima, seen as the structures of a transition curve could be the result of interactions of these neutrons in the chamber material.

- The scenario in which the long-lived ("stable") strangelets penetrating through the chamber interact with the absorber nuclei.

However, to distinguish between these two scenarios a more precise detector and higher event statistics are necessary.

Chapter 5

Search for Centauros in accelerator experiments

Centauros and/or related phenomena have attracted a lot of attention since the early 80's. Several accelerator experiments have been already performed to search for such unusual events. There are also some current and future experiments which are going to look for these phenomena, what is illustrated in Tables 5.1 and 5.2.

5.1 Past experiments at CERN SPS collider

The first accelerator searches for the Centauro phenomenon have been performed many years ago (in 1981-1986) at the SPS CERN $p\overline{p}$ collider by the **UA1** experiment [148] (at energy $\sqrt{s}$ =630 GeV) and by the **UA5** Collaboration [149] (at energy $\sqrt{s}$ = 546 and 900 GeV). Both experiments looked for Centauros in the central rapidity region (UA1 at $|\eta| \leq 3$ region and UA5 in wider pseudorapidity interval). The UA5 detector consisted of two streamer chambers, placed on opposite sides of the beam pipe. Charged particles left there tracks which were photographed for analysis. Photons were detected through conversions in a lead-glass plate, placed between the beam pipe and the upper streamer chamber. In the last search the UA5 detector was significantly improved. The geometrical acceptance of the large streamer chambers was about 95% for $|\eta| \leq 3$, falling to zero at $|\eta| = 5$. The lead-iron-scintillator calorimeter was situated at 90^0 and covered the interval $|\eta| \leq 0.9$ and azimuthal angle $\Delta\phi \simeq 30^0$. In the latest analysis upper limits of 0.1-0.5% at 95% c.l. have been placed on Centauro production. No indication of Centauro production was observed.

The negative results of UA1 and UA5 experiments have several possible alternative explanations:

- The energy threshold for the production of such objects is higher than $\sqrt{s} = 900$ GeV, what corresponds to the incident energy in the laboratory frame E_{lab} higher than 431 TeV, when assuming a nucleon projectile. This explanation seems to be especially convincing, as the average incident energy of cosmic–ray Centauros has been estimated to be $\sim$ 1740 TeV. The separate question concerns Mini-Centauro species which, in fact, have been observed in cosmic ray experiments in a lower energy region. In this case the reason of their nonobservation by UA1 and UA5 experiments

may be the existence of "genetic relations" between different exotic phenomena (see e.g. [50]).

- Centauros are produced in the projectile fragmentation region, thus the above mentioned experiments, limited to the central region, were unable to find them.
- Centauros can not be born in nucleon-nucleon collisions. This would support the hypothesis of the formation of Centauros in nucleus- nucleus collision [17] or its exotic (extra-galactic) origin [82].

5.2 Current experiments at Tevatron and CERN SPS

Experiments at Fermilab ($p\overline{p}$ Tevatron at $\sqrt{s}$ = 1.8 TeV)

At Tevatron energy the situation is delicate because the expected energy threshold for Centauro production is roughly consistent with $p - \overline{p}$ collider energy, when assuming the Centauro formation in nucleon–nucleon collisions ($\sqrt{s}$ = 1.8 TeV is equivalent to about $1.7{\times}10^{14}$ eV in laboratory frame for nucleon-nucleon collisions). However, if Centauros were produced in nucleus-nucleus collisions the situation will be different, as the total interaction energy of the average cosmic-ray Centauro in "60 + 14" c.m. system is $\sqrt{s} \simeq$ 6.8 TeV.

The other question, mentioned already in the case of CERN SPS experiments, is the different kinematical range for cosmic ray experiments and accelerator ones. Cosmic ray experiments are primarily sensitive to energy flow, and generally detect particles from the fragmentation rapidity region whereas the accelerator studies are mainly focused on the central region of phase space in the c.m. system. It is illustrated in Figure 5.1.

In some Fermilab experiments the Centauro phenomenon is (or is going to be) searched in nucleon-nucleon collisions. These are:

Mini-Max (T-864)

This is a small experiment situated at the C0 interaction region of the Tevatron, with the primary goal to search for DCC in the forward region. It has been designed to measure the ratio of charged to neutral pions produced at $\eta \simeq 4.1$. The detector was designed as a telescope of multi-wire proportional chambers (MWPC's) together with scintillation counters along the beam pipe, and the lead converter inside the telescope. Charged particles can be observed in the chambers before and after the converter, and photon conversions in the chamber behind the converter. The electromagnetic calorimeter is placed behind the MWPC telescope. Mini-Max is able to observe both charged particles and photons in the region $3.3{<}\eta{<}4.5$ and is sensitive to low-p_T particles. The distribution of photons to charged particles ratio is expected to be different for the generic binomial and DCC particle production models (see section 4.3). The main problem of the experiment is the background from the accelerator beam pipe and the small acceptance for both γ's from π^0 (acceptance covers a circle of radius ~ 0.65 units in (η, ϕ) at $\eta = 4.1$). The combined ratios of the factorial moments, which result in experimentally robust variables (independent of acceptance and various efficiency factors), were used in analysis. A preliminary comparison of ratios of measured robust variables and those expected from various models showed that data are consistent with the generic production mechanism[107, 150]. The sensitivity to admixture of DCC mechanism is claimed to be at the 10-20% level.

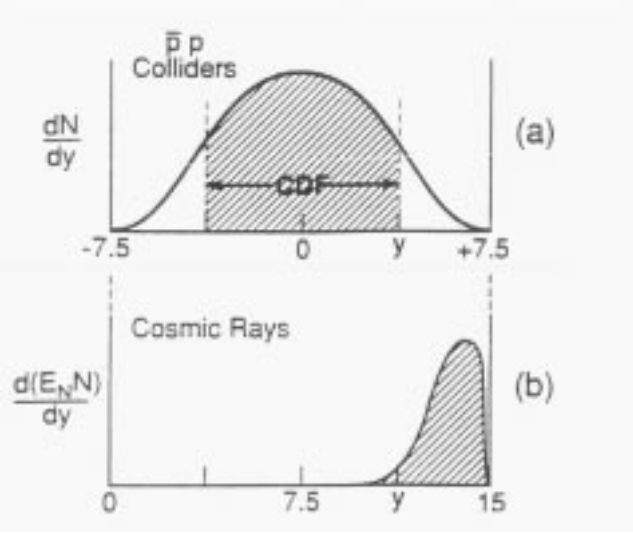

Figure 5.1: Kinematical range of rapidity for the Tevatron and cosmic-ray experiments [76]. Particle density vs. rapidity is shown in (a) for the Tevatron collider, with the range of sensitivity of the Fermilab Collider Detector. In (b) the same rapidity space for cosmic ray experiments is shown with energy flow, $d(E_N \cdot N)/dy$, vs. rapidity.

The C0 group has also designed the Zero Degree proposal for studying far forward physics. Unfortunately this proposal was not approved.

CDF

Also this experiment [151] reports preliminarily a negative search for Centauros in the central rapidity region. According to ref. [152] the CDF Collaboration has put an upper limit of 10 microbarns on the production of Centauros in $1.3<\eta<4.1$. Within each event particles were detected and identified as either hadronic requiring $E_T> 0.4$ GeV, or electromagnetic requiring $E_T \leq 0.2$ GeV, using calorimeter towers out to $|\eta|< 4.2$. The search for Centauro-like events was based primarily on their unique particle kinematics: particle multiplicities $N \sim 75$, $\langle p_T \rangle \sim 1.7$ GeV/c and $\langle \eta \rangle$ of hadrons centered around 2.2 with $\sigma_\eta \sim 0.7$ accordingly to phenomenological interpretation of Centauros as diffractive fireballs [32, 83]. In addition, looking for Centauro candidates with unusual hadronic to electromagnetic asymmetry, as predicted by DCC hypothesis, was done. This analysis, however, does not consider the possibility that Centauros decay to protons and neutrons what can be the additional reason of the negative result.

D0 Detector

The main purpose of D0 detector [153] is the study of high mass states, large p_T phenomena and the rapidity gap fraction. It basically consists of three elements: the central detector, the liquid argon-uranium calorimeter and the outer muon detector. It has charged particle tracking capability up to 3.2 units of pseudorapidity. The uranium-liquid argon calorimeters have full coverage for the psudorapidity range of $|\eta| <4.1$. The calorimeters are azimuthally symmetric and have electromagnetic and hadronic resolution of $15\%/\sqrt{E}$ and $50\%/\sqrt{E}$ respectively. The transverse segmentation of the calorimeter

towers is typically $\Delta\eta \times \Delta\phi = 0.1 \times 0.1$. Thus the detector is well suited to search for Centauro type events. The strategy of the search for Centauro events in the D0 detector depends on the interpretation of the event. Assuming the isotropic decay of a fireball with mass $\sim$ 180 GeV/c into baryons, a large deposit in the hadron calorimeter with no energy in the EM calorimeter is expected. Monte Carlo study shows that the detector is suitable for Centauro phenomenon investigation.

Fixed target experiments at CERN SPS

Some present CERN SPS experiments searched for Centauro–like phenomena in heavy ion collisions at energy 158 A GeV. Among them:

WA98

The WA98 [154] experiment emphasizes on high precision, simultaneous measurement of both hadrons and photons. The experimental setup consists of large acceptance hadron and photon spectrometers, detectors for charged particle and photon multiplicity measurements, and calorimeters for transverse and forward energy measurements. Among these detectors there are two which are well suited for the DCC search. One can measure charged particle multiplicities with a Silicon Pad Multiplicity Detector ($2.35<\eta<3.75$) and photons with a Photon Multiplicity Detector covering $3.0<\eta<4.2$. WA98 uses various methods of DCC analysis, such as:

- Global event characteristics, i.e. the total number of photons and charged particles over the entire phase space covered by the photon and charged particle detectors;
- Methods for DCC domains, when the available phase space is divided into several $\eta - \phi$ bins. Among them the wavelet analysis (multiresolution scanning the entire phase space, no averaging over events or $\eta - \phi$ space), various moments and their combinations, i.e. "robust observables" were calculated from the distribution of photons and charged particles in each bin.

To date they have observed no events with a large charge to neutral fluctuation from among 200K events, and reported no significant DCC signal. The preliminary analysis of the Pb+Pb data showed zero DCC candidates.

EMU16

It is a Magnetic-Interferometric Emulsion Chamber where it is possible to study isospin fluctuations (DCC) at small y $\leq$ 2.

Negative results of the Centauro search at collider energies (CERN and Fermilab) allows one to suspect that:

- either the investigated energy region is below the threshold for such events formation;
- either the methods of looking for Centauro events are not fully adequate because of some misunderstanding the experimental observation (different rapidity regions should be explored, different types of produced particles should be looked for etc.);
- or the primary particle of Centauro events is not a proton but nucleus or even some exotic substance such as a quark glob, as suggested by Bjorken and McLerran [82]. If Centauro fireballs are created in nucleus–nucleus collisions, as it is suggested in [17, 18] then in the future collider experiments, at RHIC and LHC, the appropriate conditions for formation of these objects can be expected.

5.3 Future experiments at RHIC and LHC

Relativistic Heavy Ion Collider (RHIC) at Brookhaven has just started. In the nearest future the collisions of relativistic heavy ions (i.e. Au-Au) with a center of mass energy of 200 A GeV are expected to be investigated. Few years later (in 2006) it is planned to start the Large Hadron Collider (LHC) at CERN, with the Pb+Pb beams, carrying the center of mass energy of about 5.5 A TeV. Majority of the future experiments has a wide program with the main purpose to find the quark–gluon plasma by looking at many different observables. Among them some exotic signatures related to Centauro phenomena are planned to be used in the following experiments at RHIC:

PHOBOS

PHOBOS detector [1] consists of two parts. The first one is a multiplicity detector covering almost the entire pseudorapidity range of the produced particles, and measuring total charged multiplicity only, $dN/d\eta$. The second one is a two-arm spectrometer at mid-rapidity. The PHOBOS configuration is that it will give fairly subtle measurements in the midrapidity ($0 < \eta < 2$) and low p_T region. It will be able to look for DCC, produced in the central rapidity region, by signatures such as the anomalies (unusual fluctuations) in the pseudorapidity distribution of charged particles. (No direct comparison between the electromagnetic and hadronic component will be possible.)

STAR

STAR [1] (Solenoidal Tracker at RHIC) consists of high resolution tracking detectors, trigger detectors, and partial coverage of electromagnetic calorimetry inside a 0.5 T solenoid. The measurements will be carried out at midrapidity, over a large pseudorapidity range ($|\eta|<4$) with full azimuthal coverage ($|\Delta(\phi)| = 2\pi$). The tracking detectors are a silicon vertex tracker covering $|\eta|<1.7$, and a forward radial-drift TPC covering $2.5<|\eta|<4$. In addition to the tracking detectors, the electromagnetic calorimeter will measure the transverse energy of events, and trigger on and measure high transverse momentum photons. The STAR detector system will simultaneously measure many experimental observables to study signatures of the QGP phase transition as well as the space-time evolution of the collision process.

A highly granular photon multiplicity detector is being planned for the STAR, which in combination with charged particle detectors and forward TPC, will be quite adequate for DCC search, in event-by-event mode. Here one would be able to select on the low p_T particles, characteristic of DCC pions, and to study π^{+-} spectra at low p_T.

PHENIX

The physics goals of PHENIX [1] (Pioneering High Energy Interaction eXperiment) are to measure as many potential signatures of the QGP as possible. PHENIX will measure lepton pairs, photons and hadrons, being sensitive to very small cross section processes, as the production of the $J/\psi, \psi'$ and high p_T spectra. DCC search in PHENIX will be possible by correlating signals from charged particle detectors and photons from electromagnetic calorimeter. A silicon multiplicity-vertex detector covers $|\eta| < 2.7$ around midrapidity.

BRAHMS

Small experiment [1] with a forward and midrapidity hadron spectrometer. BRAHMS experiment is considering to add a photon arm to look for DCC.

Among the experiments planned for LHC there was **FELIX** (Forward ELastic and

Inelastic eXperiment) [155]. It was a proposal for a full-acceptance detector and experimental program for the LHC dedicated to study QCD in all its aspects, hard and soft, perturbative and non-perturbative, particularly to investigate also exotic phenomena. Unfortunately it was rejected.

The other one is **CASTOR** [11, 136].
It is a dedicated detector for Centauro and strangelet search in the very forward rapidity region, in nucleus-nucleus collisions. It will be operated as the part of the ALICE experiment [156]. For more details see the next chapter.

Generally, different strategies of looking for Centauro related phenomena are proposed by different experiments, dependently on the preferred model. The present and future experiments prefer mostly the DCC mechanism, where the large imbalance in the production of charged to neutral pions could be the result of the approximate restoration of the chiral symmetry. Sophisticated analysis methods are being developed to disentagle DCC events out of the large background of events with conventionally produced particles.

Table 5.1: Centauro search in accelerators.

Accel.	*Exper.*	*Reaction*	*Region*	*Remarks*
		PAST EXPERIMENTS		
SPS CERN collider	UA1	$p-\overline{p}$ $\sqrt{s}=630$ GeV	central $\lvert\eta\rvert \leq 3$	no Centauros too low energy and
	UA5	$p-\overline{p}$ $\sqrt{s}=546$ GeV $\sqrt{s}=900$ GeV ($E_{lab}=431$ TeV)	central	central region
		CURRENT EXPERIMENTS		
SPS CERN fixed target	WA98	heavy ions (Pb+Pb) 158 A GeV	multip. det. in central reg. $2.8<\eta<3.75$ common reg.	no DCC by measurement of photons and charged
	NA49			possible DCC search
	EMU16		y <2	possible DCC search
TEVATRON FERMILAB collider	T-864 Mini-Max	$p-\overline{p}$ $\sqrt{s}=1.8$ TeV ($E_{lab}\simeq 1700$ TeV)	$\eta \simeq 4.1$	no Centauros via DCC
	CDF		$\theta >30$ mrad $\lvert\eta\rvert<4.2$	no Cent. fb. no DCC (not considered Centauro decay into nucleons)
	D0		$\lvert\eta\rvert<4.1$	Centauro search in calorim. possible

Table 5.2: Centauro search in accelerators, continuation.

Accel.	*Exper.*	*Reaction*	*Region*	*Remarks*
		FUTURE EXPERIMENTS		
RHIC FNAL collider	P899 rejected	heavy-ions (Au+Au) $\sqrt{s}$ =200 A GeV	zero degree at C0 $0 < \theta <$ several mrad y$\sim$ 9	Centauros and DCC search
	PHOBOS		spectrometer: $0<\eta<2$ mid-rap. and low p_T multipl.detectors: $-5.4 < \eta < +5.4$	DCC via anomalous structures in charged particle η distr.
	STAR		central $\|y\| < 2$	DCC via electr./charged energy ratio, π^{+-} spectra at low p_T
	PHENIX		silicon mult. det. $\|\eta\| < 2.7$	DCC via fluct. in isospin $\pi^0/(\pi^+ + \pi^-)$
	BRAHMS		midrap. and fragm. region $\|\eta\| < 4$	adding a photon arm to look for DCC is considered
LHC CERN collider	FELIX rejected	heavy-ions Pb+Pb $\sqrt{s}$ = 5.75 TeV/n	full accept.	
	CASTOR		$5.6< \eta < 7.2$ forward rap.	Centauro and strangelet search

Chapter 6

CASTOR: a detector for Centauro And STrange Object Research

The main part of the ALICE [156] heavy ion experiment at CERN LHC will be fully instrumented for hadron and photon identification only in limited angular region around midrapidity, covering the pseudorapidity interval $\mid \eta \mid \leq 1$. It constitutes only a small part of the available phase space which, at the beam energy of 2.75 A TeV for Pb ions at LHC, extends to $\mid \eta \mid = 8.7$. Therefore, in addition to the main detector system some smaller detectors covering more forward rapidity region are also foreseen. These are:

- Muon detector [157] which will be installed on one side and will cover the pseudorapidity interval $2.5 \leq \eta \leq 4.0$;
- A pre–shower photon multiplicity detector [158] which will also be installed on one side and will cover the pseudorapidity interval $2.3 \leq \eta \leq 3.3$;
- Small–aperture zero degree calorimeters [159], located far downstream in the machine tunnel (neutron calorimeter at a distance of about 116 m and proton calorimeter at about 115.5 m from interaction point) which will provide fast information about the centrality of the collisions;
- A specialized detector system CASTOR [11, 136].

Already at the early stages of the preparation of the ALICE proposal we pointed out that the interesting physics beyond midrapidity [160] should be the additional subject of ALICE investigations. From these considerations evolved the idea of the CASTOR detector. CASTOR is dedicated to study the novel phenomena expected to appear in the high baryochemical potential environment produced in Pb+Pb collisions at LHC energies, in particular the formation of Deconfined Quark Matter (DQM), which could exist e.g. in the core of neutron stars, with characteristics different from those expected in the much higher temperature baryon–free region around midrapidity. Its signatures could be Centauro species and strongly penetrating objects. CASTOR will cover the very forward rapidity region ($\sim 5.6 < \eta < 7.2$) and it was originally proposed to consist of a silicon charged particle multiplicity detector, a silicon photon multiplicity detector, and a quartz fibre tungsten calorimeter with electromagnetic and hadronic sections. The scheme of the apparatus is shown in Figure 6.1.

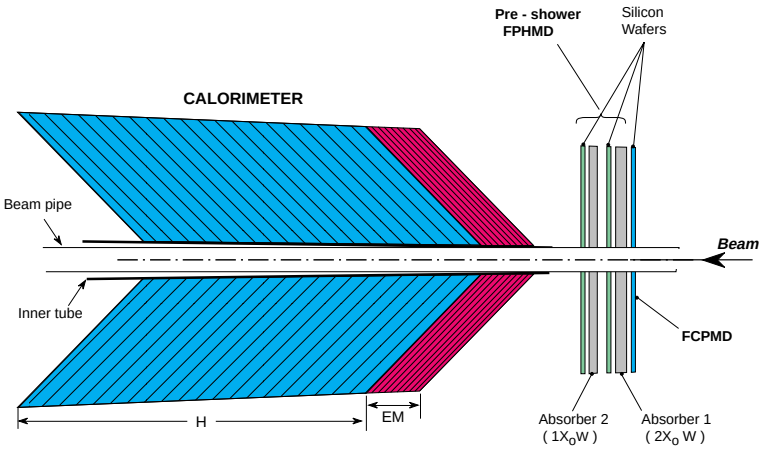

Figure 6.1: Scheme of the CASTOR detector.

The LHC, with an energy equivalent to $\sim 10^{17}$ eV for a moving proton impinging on one at rest, will be the first accelerator to effectively probe the highest cosmic energy domain. From Figure 1.2 it is seen that CASTOR is located at the region of maximum baryon number, high energy flow and low multiplicity, similarly as majority of cosmic–ray experiments.

The basic experimental aim of CASTOR is to identify events with characteristics similar to those of the exotic cosmic–ray events, in an event-by-event mode. We will look for:

- extreme imbalance between the hadronic and photonic components, both in terms of the particle multiplicity and the energy content of the event,
- non-uniform (in azimuthal angle ϕ) deposition of a large amount of energy,
- highly penetrating objects, far beyond the range of normal hadrons,
- abnormal shapes and structures seen in the transition cascade curves in the calorimeter.

The project is motivated by the experimental evidence of exotic cosmic–ray events on the one side and by theoretical expectations on the other hand [18, 161]. To design the detector we based on experimental results from cosmic-ray experiments. The model [17, 18] described in detail in subsection 4.4.2 was used to simulate the detector system performance.

6.1 The design of the CASTOR calorimeter

At the first stage of project realization the building of only the calorimeter is planned. Here will be considered the basic version of the calorimeter. Some further refinements of

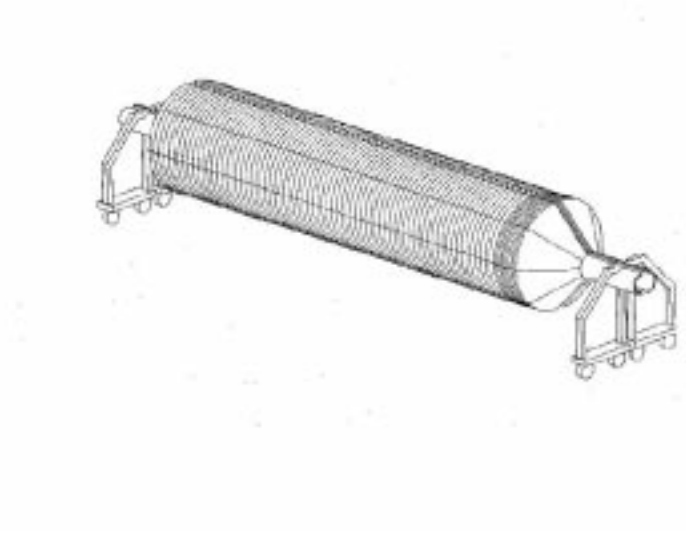

Figure 6.2: The view of the CASTOR calorimeter.

this design are being considered, but these are not expected to alter its response in an essential way. The general view of the CASTOR calorimeter is shown in Figure 6.2.

The calorimeter will be made of layers of active medium sandwiched between tungsten absorber plates. The active medium consists of planes of silica fibres and the signal will be the Cherenkov light produced as they are traversed by charged particles from the shower. The fibres are inclined at 45 degrees relative to the incoming particles to maximize light output. The calorimeter is azimuthally divided into 8 octants. Each octant is longitudinally segmented into 80 layers, the first 8 ($\simeq$ 14.7 X_0) comprising the electromagnetic section and the remaining 72 ($\simeq 9.47\lambda_I$) the hadronic section. The light output from groups of 4 consecutive active layers is proposed to be coupled into the same light guide, giving a total of 20 readout channels along each octant. Such a calorimeter works as a "shower core" detector, sampling essentially only the part of the shower which lies within a narrow cone around the direction of the particle. Thus the energy of a hadronic shower can be reliably measured also very close to the calorimeter's edge. The transverse width of the hadron shower is about 7 mm (at 200 GeV). The calorimeter will be located at a distance of $\sim$ 1740 cm from the beam interaction point. The detailed specifications of the basic version of the calorimeter are given in Table 6.1.

6.2 Probes and observables of LHC Centauros and Strangelets

According to our model, described in subsection 4.4.2, Centauros are formed in central collisions of ultrarelativistic nuclei. Thus the future collider experiments with heavy–ion beams seem to be appropriate to look for them. Some predictions concerning Centauros which could be produced at RHIC have been given in [17]. The kinematical conditions accessible at RHIC will be very close to these at which cosmic ray Centauros are produced. Almost the same value of energy per nucleon ($\sqrt{s}^{RHIC}$ = 200 A GeV in comparison with

Table 6.1: CASTOR calorimeter specifications

	Electromagnetic	*Hadronic*
Material	Tungsten + Quartz Fibre	Tungsten + Quartz Fibre
Dimensions	$\langle R_{in} \rangle = 26$ mm, $\langle R_{out} \rangle = 129$ mm	$\langle R_{in} \rangle = 27$ mm, $\langle R_{out} \rangle = 134$ mm
Absorber Plates	Thickness = 5 mm	Thickness = 10 mm
at 45^0	Eff. thickness = 7.07 mm	Eff. thickness = 14.1 mm
No. layers	8	72
Eff. length	56.6 mm $\simeq 14.7$ $X_0 \simeq 0.53\lambda_I$	1018.1 mm $\simeq 9.47\lambda_I$
Quartz Fibre	~ 0.45 mm	~ 0.45 mm
No. of QF planes	2 per sampling	4 per sampling
Sampling	$\simeq 1.84 X_0$	$\simeq 0.13\lambda_I$
Reading	Coupling of 4 samplings	Coupling of 4 samplings
No. Readings	2	18
No. Channels	$2 \times 8 = 16$	$18 \times 8 = 144$
QF/W vol.	10%	10%

$\sqrt{s}^{CENT}_{cos.ray} = 233$ A GeV) allows one in easy way to predict the typical features of Centauros expected to be produced at RHIC. In particular, the assumption that transverse momentum of the fireball decay products will be the same for cosmic ray and RHIC Centauros seems to be very reasonable. At the LHC the situation will be different, although the crucial conditions for Centauro events production seem to be well fulfilled. The energy accessible in Pb+Pb central collisions at the LHC ($\sqrt{s}^{LHC} \simeq 5.5$ A TeV, i.e. $\sqrt{s_{TOT}}^{LHC} \simeq$ 1150 TeV) will be much higher than the threshold energy for Centauro species production. At the LHC a region of vanishing baryon density is expected at midrapidity and the pronounced baryon–rich region with maximum baryon density at rapidity between 5–7 (see Figure 1.2). Thus the *existence of baryon rich environment*, which is the essential requirement of our model for Centauro species production, is also expected. The baryon rich environment is expected to be placed at LHC in the forward rapidity region, what is consistent with the observation of cosmic ray Centauros in the projectile fragmentation range (see Table 4.1).

6.2.1 Rate of Centauros in CASTOR

The important point is how many Centauros can be produced and detected in CASTOR. The evaluation of the possible rate of Centauros N_{Cent} can be obtained from the formula:

$$N_{Cent} \simeq N^{centr}_{coll} \times P^{prod}_{Cent} \times P^{decay}_{Cent} \tag{6.1}$$

where N_{coll}^{centr} is the number of central Pb+Pb collisions during one year of ALICE run, P_{Cent}^{prod} is a probability of producing Centauro event in such collision, and P_{Cent}^{decay} is a probability of Centauro fireball decay before the CASTOR detection system.

In our calculations we assumed that observation of distinct Centauro characteristics in the calorimeter needs a decay of the fireball at a distance shorter than 1 m from the interaction point. Then

$$P_{Cent}^{decay} = 1 - exp(-1m/(c\tau_0\gamma)) \tag{6.2}$$

Assuming the Centauro fireball gamma factor $\gamma \simeq 300$ and its lifetime $\tau_0 = 10^{-9}$ s one obtains probability of Centauro decay at the path shorter than 1 m greater than 1%. In opposite case it could be possible to observe a very big amount of energy released somewhere in the calorimeter and concentrated within very narrow angular cone. Assuming further $N_{coll}^{centr} \simeq 10^7$ per ALICE running year, and very conservatively that Centauros are produced only in 10^{-2} of all central collisions it can be expected that at least ~ 1000 Centauro events will be produced and detected in CASTOR during one year.

6.2.2 Average characteristics estimates

The main features of Centauros and strangelets produced at the LHC can be evaluated by extrapolating the characteristics of these objects registered in cosmic ray energy range or by doing analytical calculations based on the model. More detailed characteristics and the distributions of the characteristic quantities can be predicted by using Monte Carlo methods (see the next chapter).

In particular, keeping in mind that shapes of the angular and energy fraction spectra of Centauro secondaries are consistent with isotropic emission of particles from a fireball, we expect a Gaussian–type pseudorapidity distribution for decay products of "LHC" Centauros. The center of the distribution, being the function of both the nuclear stopping power Δy_{stop} and a rapidity shift caused by transverse momentum of emitted particles Δy_{PT}, is generally expected to be placed close to the maximum of the baryon number distribution, i.e.

$$\langle y \rangle_{Cent}^{LHC} \simeq y_{beam} - \Delta y_{stop} - \Delta y_{PT} \simeq 8.7 - 2.0 - 0.9 \simeq 5.8 \tag{6.3}$$

The first rough evaluation of the optimal position and size of the CASTOR detector and the estimation of its geometrical acceptance [136, 162] were done in this way.

Evaluation of other characteristic quantities, as for example the types and multiplicities of produced particles needs, however, some additional assumptions. In [162] we estimated the expected multiplicities of kaons $N_{K^+ + K^0}$, non-strange baryons N_h, the total number of nuclear active particles N_n, and the baryon number of a strangelet A_{str} emitted from a decay of Centauro fireball produced in central Pb+Pb collisions at LHC energies. Two different, extreme scenarios were considered:

1. *Lower limit of energy density (and temperature).*

In the most conservative case it can be assumed that the transverse momentum of decay products of LHC Centauro fireball is the same as for cosmic–ray Centauros, i.e. $\langle p_T \rangle \sim$ 1.7 GeV/c. Then the average Centauro fireball mass can be estimated from the relation:

$$\langle M_{fb} \rangle = \langle N_n \rangle \langle E_n \rangle \tag{6.4}$$

where $\langle N_n \rangle$ is the mean number of nuclear active particles emitted from the Centauro fireball and $\langle E_n \rangle$ is the mean particle energy in the fireball rest system. We assumed that $\langle N_n \rangle$ equals to the number of participating projectile nucleons $\langle N_p \rangle$, i.e. it is in the range of 150-207 for central Pb+Pb collisions and

$$\langle E_n \rangle = \sqrt{((4/\pi)p_T)^2 + M_N^2} \simeq 2.4\,\mathrm{GeV} \tag{6.5}$$

where M_N is the nucleon mass.

The volume V_{fb} of the fireball and the number of participating nucleons N_p can be evaluated from simple geometrical considerations. For the volume $V_{fb} \sim 117$ fm^3, corresponding to a central collision with the number of participating nucleons $N_p \sim 150$ (b $\leq$ 5 fm) [17], these assumptions lead to $M_{fb} \simeq 350$ GeV and to energy density of LHC quark matter fireball

$$\varepsilon_{fb} = M_{fb}/V_{fb} \simeq 3\,\mathrm{GeV/fm^3} \tag{6.6}$$

which is close to that reached in cosmic ray Centauro events. Using the phase curve given by eq. (4.15) with the reasonable strangeness equilibration factor ($\gamma_s \sim 0.4$) one can find that such energy density corresponds to the temperature T $\sim$ 130 MeV and to the quarkchemical potential $\mu_q \sim 590$ MeV, and the average characteristics of LHC Centauros could be close to these observed in cosmic ray experiments. In particular, the maximal number of emitted K^+ and K^0 for T = 130 MeV and the volume corresponding to the numbers of participating nucleons in the range of $N_p \sim 150$ - 207, is estimated to be $N_{K^+ + K^0} \sim$ 16–20 (from equations (4.23) and (4.24)). The maximal baryon number of a strangelet will be reached when in the process of strangeness distillation all s–quarks will be absorbed in the strangelet, and then $A_{str} \simeq 16$ - 20. Consequently the number of emitted non-strange baryons

$$N_h \simeq N_n - N_{K^+ + K^0} \simeq 134 - 187. \tag{6.7}$$

In general, assumption of constancy of $\langle p_T \rangle$ allows one to expect that the values of characteristic quantities (N_h, M_{fb}, ε, T, μ) for Centauros possibly produced at RHIC (Au+Au) and at LHC (Pb+Pb) should be similar one to the other. These values should not also be very different from these found for cosmic ray Centauros.

2. *Upper limit of energy density (and temperature).*

Assumption of the same $\langle p_T \rangle$ of decay products of cosmic ray and RHIC Centauros seems to be reasonable because $\sqrt{s}_{NN}^{RHIC} \simeq \sqrt{s_{NN}}^{cos.ray}$. However, it could be no longer valid for LHC because $\sqrt{s}_{NN}^{LHC} \gg \sqrt{s}_{NN}^{cos.ray}$. We can expect $\varepsilon_{Cent}^{LHC} \gg \varepsilon_{Cent}^{RHIC} > \varepsilon_{Cent}^{cos.ray}$. J. Schukraft quoted in [163] the values of $\varepsilon_{LHC} \sim$ 8–27 GeV/fm^3 (averaged over different papers) as expected at Pb+Pb central collisions. K. Geiger [164] claimed even 31(17) GeV/fm^3 as upper limit of energy density, averaged over the whole central volume, at Au+Au (S+S) central collisions. In such a case the assumption of constancy of the mean transverse momentum can be unjustified. In connection with it, much higher values of temperature and quarkchemical potential can be reached. It would probably allow to reach the region of the *ideal QGP*, however, it is not easy to predict the quantitative features of Centauros at these conditions. In [11, 136, 162] we attempted to estimate the ranges of characteristic

Table 6.2: Estimates of multiplicities of kaons $N_{K^+ + K^0}$, non-strange baryons N_h and total number of nuclear active particles N_n from a Centauro fireball produced in central Pb+Pb collisions with the number of projectile participating nucleons $N_p \geq 150$ ($b <$ 5 fm).

Assumptions	$p_T = 1.7$ GeV/c $\Rightarrow$ $\varepsilon = 3$ GeV/fm^3, T $\sim$ 130 MeV $\mu_q \sim 600$ MeV		$\varepsilon \sim 8$ - 27 GeV/fm^3 $\Rightarrow$ T $\sim$ 190 MeV $\mu_q \sim$ 600-1000 MeV	
	$N_p = 150$	$N_p = 207$	$N_p = 150$	$N_p = 207$
$A_{str}^{max} = N_{K^+ + K^0}$	16	20	55	68
N_h	134	187	95	139
N_n	150	207	150	207

quantities and indicated the most typical signatures of "LHC" Centauros. Generally, much higher numbers of produced strange quarks ($\rho_{\overline{s}} \gg 0.14$ fm^{-3}, e.g. $\rho_{\overline{s}} \simeq 0.5$ fm^{-3} for T = 190 MeV), and hence higher multiplicities of produced kaons and bigger strangelets can be expected. At a temperature T $\sim$ 190 MeV the number of emitted kaons could be $N_{K^+ + K^0} \sim$ 55-68, the number of non-strange baryons $N_h \sim$ 95-139, and strangelets with baryon numbers as large as $A_{str} \sim$ 55-68 could be formed.

These expectations are summarized in Table 6.2. In Table 6.3 there are compared some average characteristic quantities of Centauros and Strangelets produced in cosmic rays and expected at the LHC.

6.2.3 Expected signatures

From the above considerations it is clear that " LHC" Centauros should be characterized by signatures dramatically different from other "normal" events. The most typical signatures will be the following:

1. *Abnormal photonic to hadronic ratio.*

   It is the main well–known signature of Centauros. We expect that both:

   - hadronic to photonic energy ratio E_h/E_γ,
   - hadron to photon multiplicity ratio N_h/N_γ

   should be much bigger than in " normal " hadronic interactions.

2. *Very low total multiplicity .*
   The total multiplicity of "LHC" Centauro decay products, $N_{tot} \leq 207$, is expected to be extremely small in comparison with enormous total multiplicity of particles

Table 6.3: Average characteristics of Centauro events and Strangelets produced in cosmic rays and at the LHC [11].

Centauro	*Cosmic Rays*	*LHC*
Interaction	"$Fe + N$"	$Pb + Pb$
$\sqrt{s}$	$\geq$ 6.76 TeV	5.5 A TeV
Fireball mass	$\geq$ 180 GeV	$\sim$ 500 GeV
y_{proj}	≥ 11	8.67
γ	$\geq 10^4$	$\simeq 300$
η_{cent}	9.9	$\sim$ 5-7
$\langle p_T \rangle$	1.75 GeV	1.75 GeV (*)
$Life - time$	10^{-9} s	10^{-9} s (*)
Decay prob.	10% (x $\geq$ 10 km)	1% (x $\leq$ 1 m)
Strangeness	14	60-80
$f_s(S/A)$	$\simeq 0.2$	$\sim$ 0.1-0.4
Z/A	$\simeq 0.4$	$\sim$ 0.3-0.45
Event rate	$\geq$ 1 %	$\simeq$ 1000/ALICE-year
"*Strangelet*"	*Cosmic Rays*	*LHC*
Mass	$\simeq$ 7-15 GeV	10-80 GeV
Z	≤ 0	≤ 0
f_s	$\simeq 1$	$\simeq 1$
η_{str}	η_{Cent} + 1.2	η_{Cent} + 1.2

(*) assumed

predicted to be produced in "usual" events in Pb+Pb central collisions at LHC energies [163].

3. *Very specific picture of time development connected with abnormal particle composition.*
   The following products of time evolution of the "LHC" Centauro (at projectile fragmentation rapidity) could in principle be observed:

   - **Particles $\mathbf{K}^+$ and $\mathbf{K}^o$;**
     K^+ and K^0 are expected to be the firstly emitted particles from the long–lived Centauro fireball. Regardless of the long lifetime ($\tau_0 \simeq 10^{-9}$ s) of the fireball these pre–equilibrium particles will be emitted within very short time interval ($\Delta\tau \simeq 10^{-22}$ s) and could be observed in detectors much earlier than other decay products of Centauro [1].
     The total number of emitted K^+ and K^0 can be maximally equal to the number of $s\overline{s}$ pairs created in the volume V_{fb} of the Centauro fireball and according to our earlier estimates (see previous section) several tens kaons could be produced.
   - **Strange quark matter metastable object with small Z/A ratio**;
     This state is formed after the pre–equilibrium emission of kaons. Then the fireball is a mixture of u, d and s quarks and experimentally it can be identified by its Z/A ratio less than that of the ordinary nuclear matter. The change of Z/A ratio, because of kaon emission can be calculated from formulas (4.25) and (4.26). Assuming $(Z/A)_i \simeq 0.5$ and the temperature in the range $\sim$ 130–190 MeV we evaluate $(Z/A)_f \simeq 0.45 - 0.3$. This slightly strange quark–matter fireball decays after a relatively long time $\tau_0 \sim 10^{-9}$ s. Taking into account consequences of the collider kinematics, which decreases the lab–frame decay lengths, and assuming $\gamma \sim 200 - 300$, the object will decay after traveling the path of the order $\sim$ 60–90 m.
   - **Non–strange baryons and highly penetrating strangelet(s)**.
     They should be observed at the last stage of the "Centauro" evolution as the result of the decay of strange quark matter state after the process of strangeness separation. Assuming that all strange quarks are absorbed in the strangelet and $\frac{N_s}{A_{str}} \sim 1$, we can expect the formation of small strangelets characterized by the baryon numbers of several tens (see the previous section). In principle, the formation of one bigger or several smaller strange droplets could be possible. The number of emitted non–strange baryons depends on the size of the strangelet and was estimated to be in the range $\sim$ 70–190.

The events of such type may be easily observed in detectors with particle identification, such as silicon detectors, TPC, etc. (the most important is to distinguish between kaons, baryons and pions). What regards strangelets, if our hypothesis that cosmic–ray long–flying component is a result of passing of strangelets through the apparatus is true, we could look for them using the deep forward calorimeters (we expect $< y >_{str}^{LHC} \sim 6-7$).

[1] They are emitted practically at the point of interaction; $l = c\gamma\Delta\tau = c \cdot coshy \cdot \Delta\tau \simeq (0.6-0.9)10^{-11} cm$, when assuming $\gamma = coshy = 200 - 300$.

Penetrating through calorimeters they could produce (via their weak decays or by interactions with absorber nuclei) succesive maxima seen in their transition curves. Observation of anomalous transition curves needs sufficiently deep calorimeters (above 120 cascade units) with granularity good enough for watching individual cascade development, and detection layers placed every 2–3 cascade units. One could consider also the idea of using simple and unexpensive CR–39 plastic detectors which could look for both the high Z quark matter fireballs and for accompanying strangelets (which are expected to have, however, rather small Z). According to [143] the minimum detectable value of Z/β is ~ 6 for CR–39.

The important questions, concerning the sensitivity of the CASTOR detector for these signatures and the influence of the background on the distinction of the signals, have been answered by means of the Centauro and Strangelets generators described in the next chapter.

Chapter 7

Centauro and/or Strangelet Simulations

7.1 Generator for Centauros

The Monte Carlo generator of Centauro events is based on our phenomenological model [17, 18] and it was described in detail in [165]. The model is formulated in terms of impact parameter b of the ion collisions, two thermodynamical parameters, baryochemical potential μ_b and temperature T, and the nuclear stopping power Δy_{stop}. The generator calculates the Centauro fireball parameters and produces a full event configuration according to the fireball evolution scenario.

According to the model the Centauro events occur in the projectile fragmentation region when the projectile nucleus penetrating through the target nucleus transforms its kinetic energy into heat and forms hot quark matter (Centauro fireball) with high baryochemical potential. At the initial stage the fireball contains only u, d quarks and gluons. The high baryochemical potential suppresses the fragmentation of gluons into $u\overline{u}$ and $d\overline{d}$ pairs due to Pauli blocking. Therefore gluons quickly fragment into $s\overline{s}$ pairs. The produced glob of deconfined quark matter is characterized by temperature T and baryochemical potential μ_b. Its energy density ε and other thermodynamical quantities, such as baryon/quark number density n_q are calculated from equations (4.15) and (4.17) respectively. The number of quarks N_q in the Centauro fireball is defined from collision geometry as $N_q = 3N_b$. Baryon number of the fireball, N_b, was calculated from the relation:

$$N_b = 0.9 V_{ovr}(A_1/V_1) \tag{7.1}$$

The factor 0.9 stands for the central part of the overlapping region V_{ovr} of colliding nuclei with the atomic numbers A_1 and A_2. Hence one can obtain the volume V_{fb} as well as the mass M_{fb} of the fireball

$$V_{fb} = N_q/n_q,\ M_{fb} = \varepsilon V_{fb} \tag{7.2}$$

At the second stage of the Centauro fireball evolution a partial chemical equilibrium is achieved by coupling $\overline{s}$-quarks with u and d quarks and emission of K^+ and K^0 mesons, what decreases the temperature and entropy. The number of $s\overline{s}$ pairs inside the fireball and hence the number of emitted kaons is calculated from equations (4.23) and (4.24).

$$N_s = N_{K^+ + K^0} = n_s V_{fb} \tag{7.3}$$

After emission of $2N_{\overline{s}}$ quarks with kaons, the mass of remaining strange quark matter (SQM) fireball is defined by the average quark energy and the number of quarks in the Centauro and SQM fireball:

$$M_{SQM} = M_{fb}(1 - 2N_{\overline{s}}/n_q) \tag{7.4}$$

This anti–strangeness emission is described as an isotropic decay of the Centauro fireball into $N_{\overline{s}}$ kaons and the SQM fireball with mass M_{SQM}. At the final stage of the evolution the SQM fireball decays into baryons and strangelets.

7.2 Simulations of Centauro events

As it was shown in [165] the generator reproduces the main features of Centauro cosmic ray events. Simulations of Centauro events formed in Pb+Pb central collisions at $\sqrt{s}$ = 5.5 A TeV have been firstly performed in [165] and there were shown the results obtained with the following model parameters:

- impact parameter b = 0, 5, 8 fm;
- temperature T = 130, 190, 250 MeV;
- baryochemical potential μ_b = 1.5, 1.8, 3.0 GeV;
- nuclear stopping power $\Delta y_{n.s.}$ = 2.0, 2.5, 3.0;
- strong coupling constant α_s = 0.3;
- strangeness equilibration factor γ_s = 0.4.

New simulations, in an extended range of parameters were done more recently [166, 167]. Different sets, each consisting of 10000 events, were generated. The very central collisions with $0<b<1$ fm were studied. Simulations were done for the temperature T = 130, 200, 250 and 300 MeV and baryochemical potential μ_b = 1, 1.8 and 3 GeV. The question is, of course, if such values of temperatures and baryochemical potential can be reached at the LHC in the fragmentation region. Unfortunately, theoretical predictions concern only the central region and it is claimed that energy densities up to about $\sim$ 30 GeV/fm^3 will be there possible [163, 164]. As at midrapidity a small baryochemical potential value is expected, such energy densities could correspond to the temperature of about $\sim$ 400 MeV (for $\mu_b \simeq 0$). We can also expect that the baryochemical potential reached in the fragmentation region, in central Pb+Pb collisions at LHC, can be higher than that observed in cosmic ray Centauros, as they are produced in collisions of smaller nuclei and at lower energies, i.e. $\mu_b >$ 1.8 GeV.

The nuclear stopping power parameter values were put $\Delta y_{n.s.}$ = 1.5, 1.0, 0.5. Keeping in mind the high values of the temperature, and in consequence very high transverse momenta of particles emitted from the fireball, such values of Δy_{stop} lead to the effective stopping bigger than the assumed Δy_{stop} value, at least about one rapidity unit. It gives the position of the maximum of the pseudorapidity distribution of baryons in accordance with that predicted by HIJING/VENUS generators. The strong coupling constant α_s was taken as 0.3.

The characteristics of simulated Centauro events are apparently different from those obtained from "usual" (e.g. HIJING) generators. In particular, Centauro events are characterized by almost total absence of a photonic component among secondary particles. The majority of secondary particles are baryons. Some kaons emitted from the primary fireball decay into neutral pions which in turn give photons, but the neutral pion production is suppressed here strongly. The next surprising feature is a multiplicity of Centauro events which is much smaller than the one predicted by "conventional" generators for nucleus-nucleus collisions at that energy. In ref. [162] the expected average multiplicities of kaons, non-strange baryons and the total number of nuclear active particles emitted from a decay of Centauro fireball, produced in central Pb+Pb collisions at LHC energies, were estimated in analytical way (see subsection 6.2.2). The results of the present simulations are illustrated in Fig. 7.1 which shows the average multiplicities of different kinds of particles produced by Centauro mechanism, contained within the geometrical acceptance of the CASTOR, in comparison with the HIJING predictions. The average multiplicities for three sets of events, characterized by T = 300, 130, 300 MeV and μ_b = 1.8, 1.8, 3.0 GeV are shown as the examples.

Secondary particles in the Centauro events have larger mean transverse momenta in comparison with ordinary hadronic interactions. In usual events the average transverse momentum of produced particles $\langle p_T \rangle$ = 0.44 GeV/c, as predicted by HIJING, which is several times smaller than that of Centauro events. Fig. 7.2 shows distributions of transverse momenta of strangelets (upper picture) and other Centauro decay products (lower picture) for three different temperatures T = 130, 200 and 300 MeV.

The position and shape of rapidity(pseudorapidity) distributions of decay products of the Centauro fireball depend on thermodynamical variables (μ_b and T) and mainly on the nuclear stopping power $\Delta y_{n.s}$. Thus the detection probability of Centauro events in the CASTOR detector is also the funcion of these variables. Fig. 7.3 shows the probability of the production of a strangelet (full line) and other particles (dashed line) from the Centauro fireball decay, as a function of pseudorapidity η. The region of geometrical acceptance of CASTOR is indicated. Four sets of events with different values of parameters were chosen as examples. It is seen that a strangelet, as it should be expected from cosmic ray observations, always flies in more forward direction that other particles. The difference is of the order of one pseudorapidity unit. As a consequence, the simultaneous detection of a strangelet and other Centauro decay products will be sometimes excluded. The big chance for detection of both species simultaneously is when temperature, quarkchemical potential and nuclear stopping power values are close to T $\sim$ 250 MeV, $\mu_b \sim 3$ GeV and $\Delta y_{stop} \sim 1.5$.

The question of acceptance has been investigated, in analytical way, in [162] and later, by simulations, in [165, 166, 167]. For the reasonable values of parameters more than 50% of energy (or of the number of produced particles) of an event falls into the detector. The maximal degree of containment of Centauro decay products is close to ~ 0.74.

7.3 Exotic objects in deep calorimeters

Basing on our model of strangelet formation in the quark-matter (Centauro) fireball, we expect that at the LHC kinematical conditions the production of a variety of strangelets,

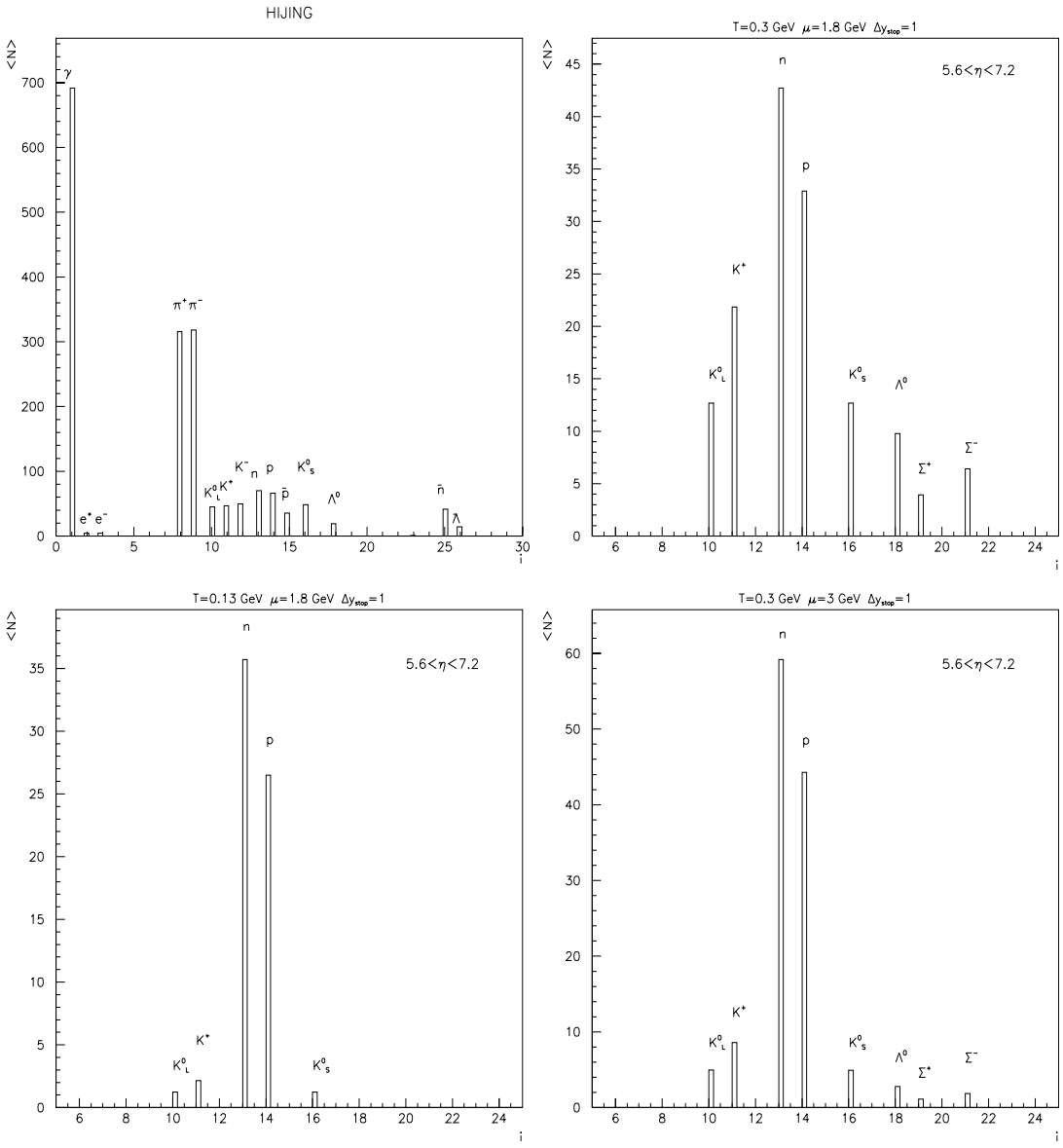

Figure 7.1: Average multiplicities of particles produced in "usual" (HIJING) event and by Centauro mechanism. Only particles within CASTOR acceptance are shown.

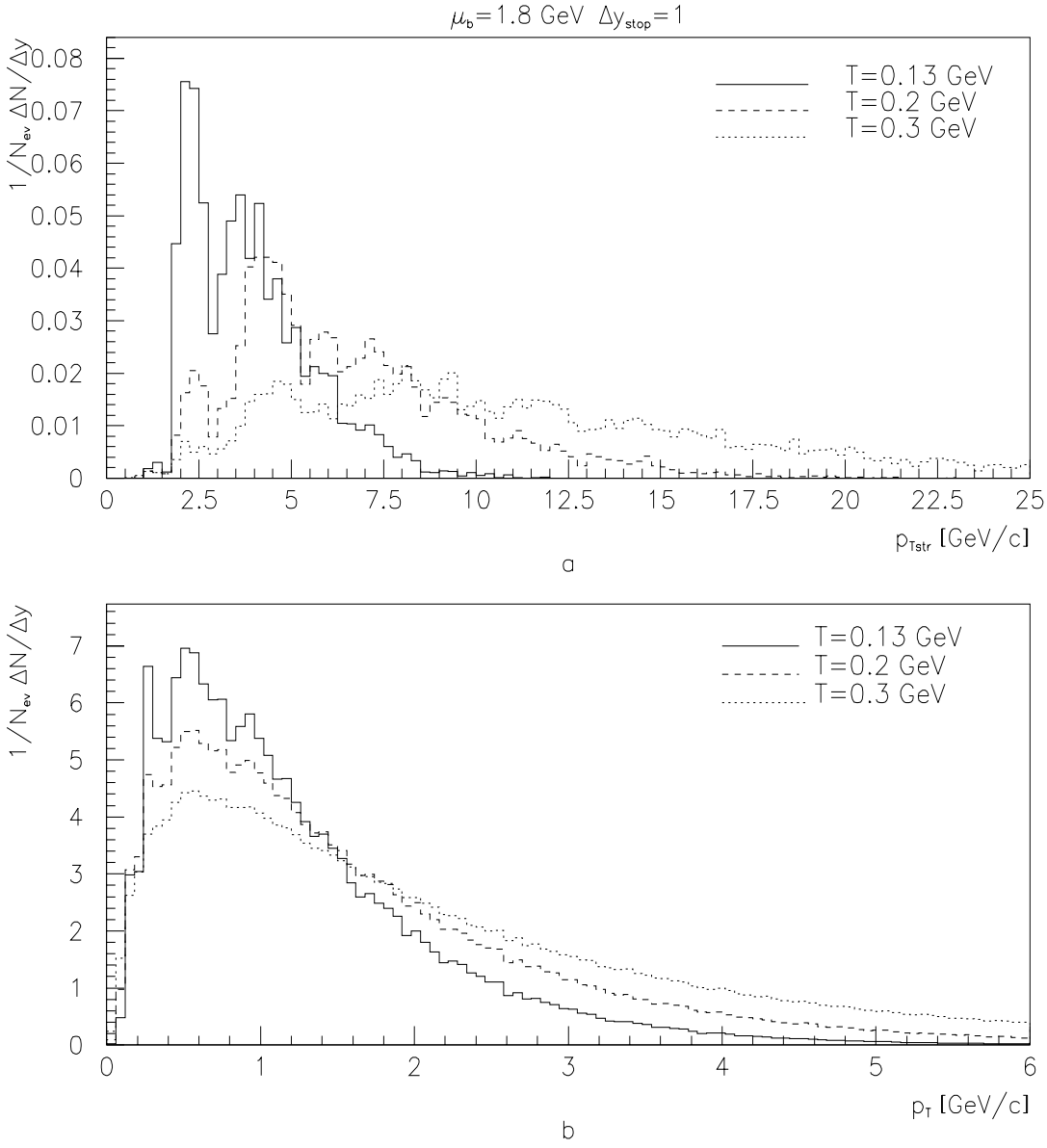

Figure 7.2: Transverse momentum distributions of (a) strangelets and (b) hadrons from Centauro decay.

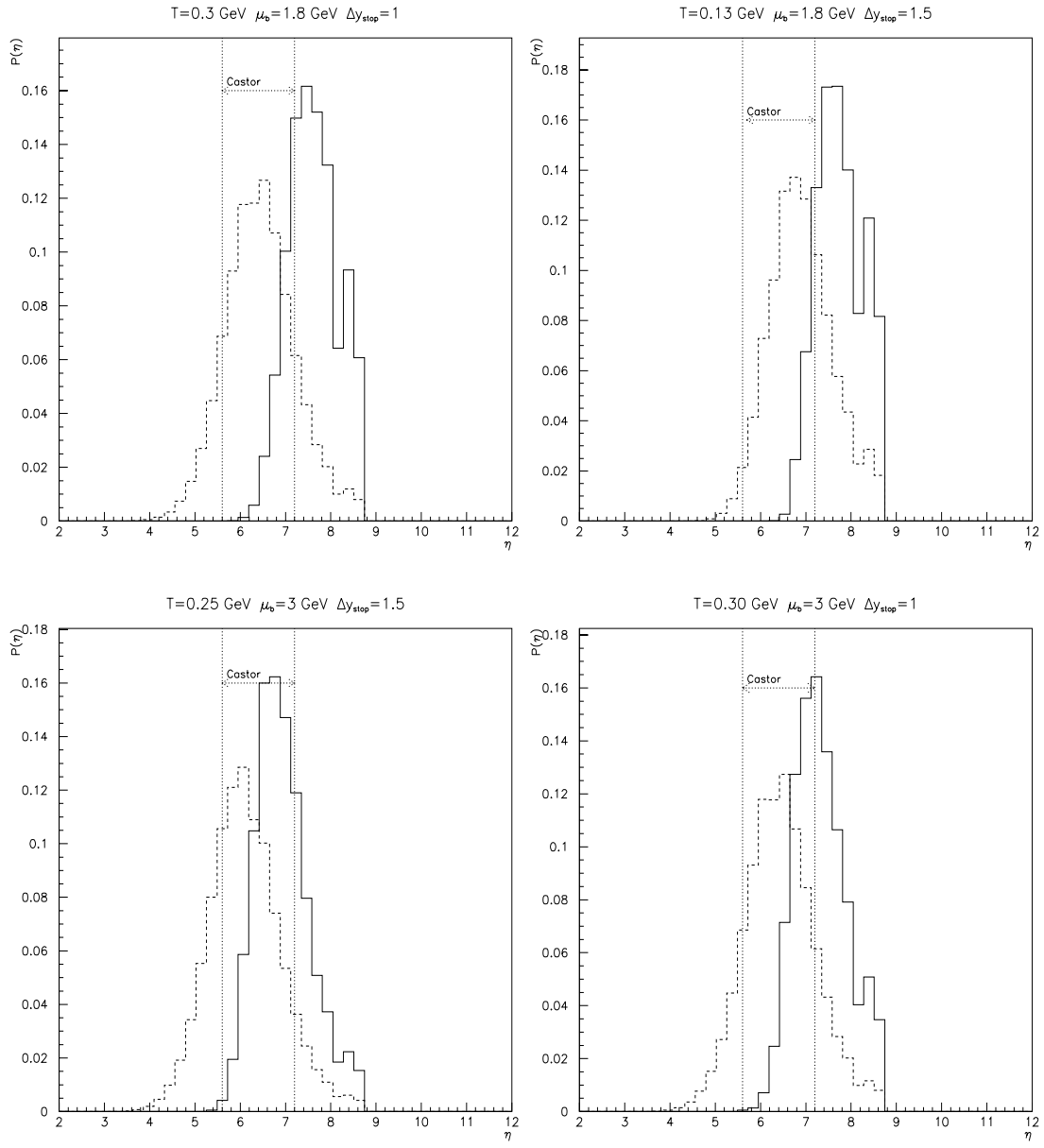

Figure 7.3: Probability of a strangelet (full line) and other particles (dashed line) production from the decay of Centauro fireball as a function of pseudorapidity. The region of the geometrical CASTOR acceptance is indicated with dotted lines.

characterized by a wide spectrum of the baryon numbers ($A_{str} \sim$ several tens for temperature $T \sim$ 130-190 MeV and quark chemical potential $\mu_q \sim$ 600-1000 MeV) should be possible (see Table 6.2). The important question is what signals will be produced by such exotic objects during their passage through the deep calorimeters, and if these signals can be distinguished from those produced by conventional events. It should be mentioned, however, that properties of CASTOR–type calorimeters differ from those of the deep emulsion chambers used in cosmic ray experiments. The latter have very fine lateral resolution ($\sim 100\mu m$), allowing for the observation of the development of individual cascades through the whole calorimeter depth. In contrast, in the CASTOR-type calorimeter, the signal produced by a strangelet will be detected simultaneously with those generated by other particles entering the same calorimeter octant. Thus, the additional question is the intensity and the shape of a possible background and our ability to extract an "exotic" signal from it. This question is of course connected with the origin of the background. In our simulations we estimated the background by means of the HIJING generator, assuming that a part of energy going into conventional particle production equals a difference between the total energy available in the phase space region (and being $\sim$ 150 TeV within the CASTOR acceptance) and energy taken by a Centauro fireball and/or a strangelet.

We investigated two possible "exotic" scenarios. In the first one we have assumed that strangelets were born anywise among other conventionally produced particles [19, 168] (see subsection 7.3.1). In the second case we considered strangelets produced as remnants of the Centauro fireball explosion, according to the mechanism proposed in [18] (see subsection 7.3.2). In this case the signal will be the sum of a strangelet transition curve and the one produced by nucleons coming from the isotropic decay of the Centauro fireball. This case has been preliminarily investigated in [19] and recently more detailed simulations have been done [167] by GEANT 3.21.

7.3.1 Strangelets in the CASTOR calorimeter

The scenario, in which strangelets are born together with other conventionally produced particles will be here described. We investigated this question in [19, 168], comparing the strangelet signal with the background estimated by means of the HIJING generator and considering both short-lived and stable strangelets.

Short-lived strangelets

We named short-lived strangelets the unstable objects which can decay via strong interactions ($\tau_0 \leq 10^{-20}$ s) or the metastable ones decaying via weak nucleonic decays (see subsection 4.4.2). Generally, however, the lifetimes of small metastable strangelets are not predicted precisely at present [118, 146] and they are still a matter of debate. If their lifetimes are shorter than $\sim 10^{-10}$ s they could decay before reaching the CASTOR calorimeter and give the same picture as unstable strangelets. In the opposite case the situation is analogous to the case of "stable" strangelets, considered later. The complete decay of a strangelet via strong processes or its fission into a daughter strangelet and an arbitrary number of hadrons is possible. A daughter strangelet will be shifted to a higher strangeness factor f_s. After surviving a strong and possibly also weak nucleonic decay it can reach the region of a very high strangeness factor ($f_s \geq 2.2$) where it is expected to become a long-lived (stable) object [115]. The algoritm of our calculations was the same

as used previously for cosmic ray events (see subsection 4.4.2). We have assumed, for simplicity, that a strangelet decays only via neutron emission. We have neglected other less probable processes (such as strong pion , proton or hyperon emission). In addition, it is important to note that the shape of resulting transition curves depends only very weakly on the nature of the evaporated hadrons. Both nucleon and hyperon bundles passing the calorimeter will give similar long-range cascades.

Unstable strangelets decay very fast, practically at the point of their formation, thus the considered picture resolves into the simple case of a bundle of neutrons entering the calorimeter.

As it has been shown in [19] the scenario in which an unstable or metastable strangelet via strong or weak decays produces a strongly collimated bundle of neutrons, successfully describes the long-range many–maxima cascades observed in the cosmic ray experiments. The successive maxima, seen in the structure of a transition curve, could be the result of interactions of such neutrons in the apparatus.

The general conclusion concerning the signals produced in the CASTOR calorimeter by short-lived strangelets, formed in Pb+Pb interactions at the LHC is the same as in the study of the cosmic-ray strangelets. Bundles of collimated neutrons can give in the CASTOR calorimeter the unconventional many-maxima signal. Its longitudinal structure and extent depend, of course, on the strangelet energy and on the number of evaporated neutrons N_n. Fig. 7.4 shows three examples of transition curves produced by bundles of 7 and 12 neutrons of energy $E_n \approx 1.2$ TeV and 20 neutrons of energy $E_n \approx 1$ TeV, evaporated by a short-lived strangelet with baryon number $A_{str} = 40$. They are compared with the possible background (full line histogram) estimated by HIJING, assuming that the rest of the available energy (i.e. not carried by the strangelet) is going into conventional particle production. For the comparison particles produced in one central Pb+Pb collision were taken. As their number is large (~ 1700 in the calorimeter acceptance region) we can expect negligible event-by-event fluctuations in the shape of the background cascade curve.

We used in this and also in subsequent figures both linear and logarithmic vertical scale. In the figures with the logarithmic scale the vertical axis starts at about 1000. This helps to illustrate the significance of the strangelet signal in the very deep part of the calorimeter where the conventional hadronic signal is negligible.

We find that a bundle of several neutrons ($N_n > 7$) possessing sufficiently high energies ($E_n > 1$ TeV) produces in the calorimeter a signal which can be distinguished from the conventional event signal. The strangelet signal is higher, has longer longitudinal extent and reveals a many-maxima structure in contrast to the rather smooth background.

Long-lived strangelets

We named long-lived strangelets the "stable" objects capable to reach and pass through the apparatus without decay, i.e. having a lifetime $\tau_0 \geq 10^{-8}$ s to traverse the CASTOR calorimeter. Similarly, as in the case of cosmic ray strangelets, the simplified picture [19] of the interaction of a stable strangelet in the calorimeter obsorber was assumed. Penetrating through the calorimeter a strangelet collides with tungsten nuclei. The mean interaction path of strangelets in the apparatus absorber can be calculated from equation (4.28). In each act of collision the spectator part of a strangelet survives and continues its passage

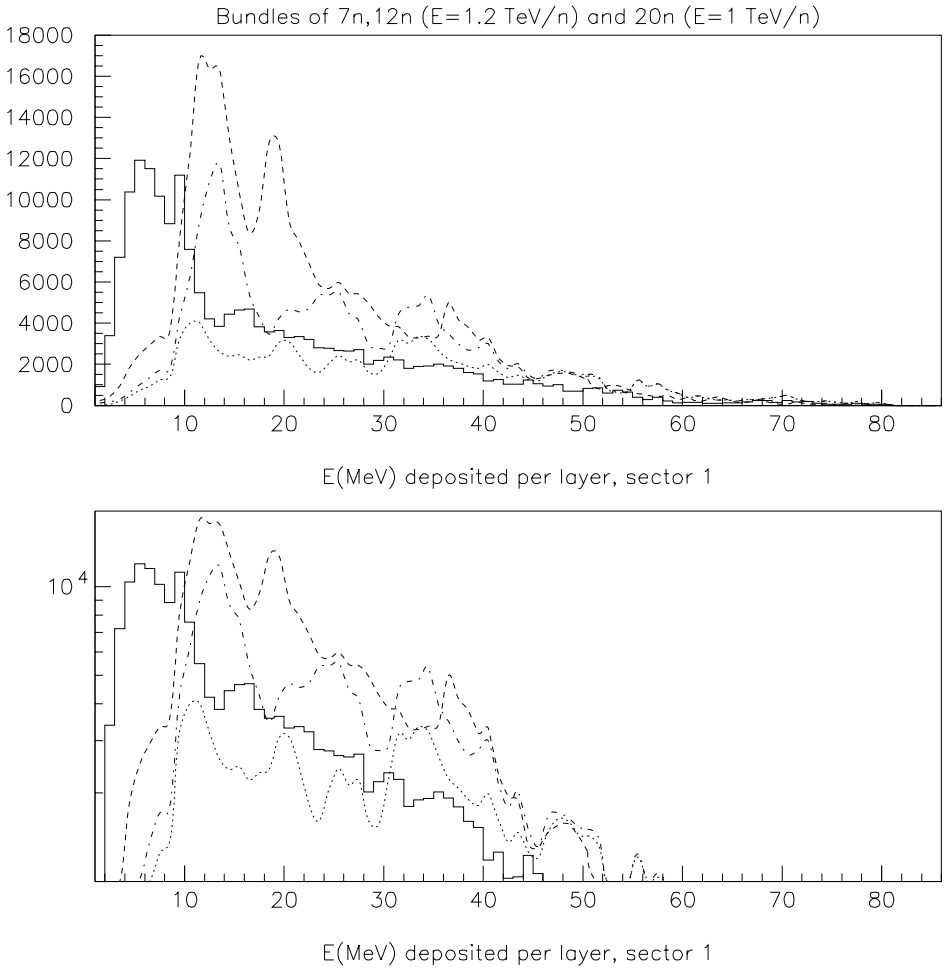

Figure 7.4: Transition curves produced by bundles of 7 (dotted-dashed curve) and 10 (dotted curve) neutrons of energy $E_n \approx 1.2$ TeV and 20 (dashed curve) neutrons of energy $E_n \approx 1$ TeV evaporated by a short-lived strangelet of $A_{str} = 40$. Full line histogram shows the HIJING estimated background. Energy deposit (MeV) in the calorimeter layers, in the octant containing a strangelet, is shown.

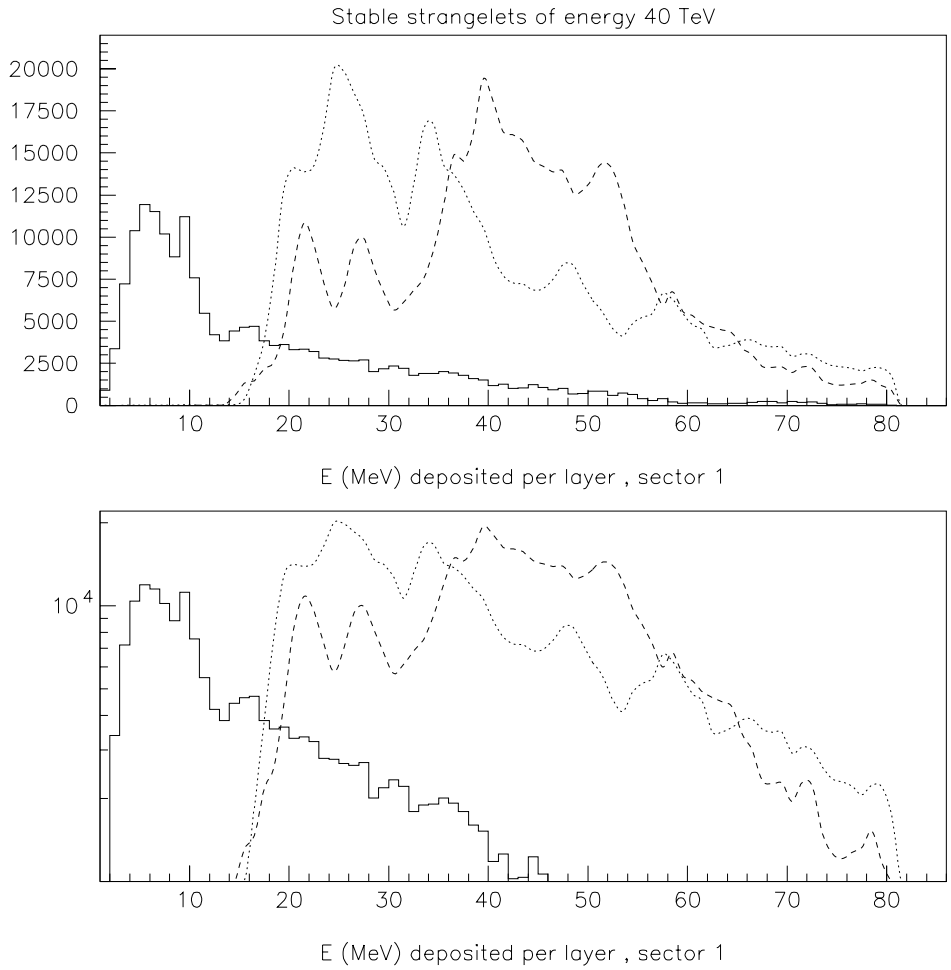

Figure 7.5: Transition curves of stable strangelets with energy $E_{str} = 40$ TeV, baryon number $A_{str} = 40$, quark chemical potential $\mu_q = 600$ MeV (dashed curve) and $\mu_q = 1000$ MeV (dotted curve). Energy deposit (MeV) in the calorimeter layers, in the octant containing a strangelet, is shown. Full line histograms in Figs. 7.5–7.10 show the HIJING estimated background.

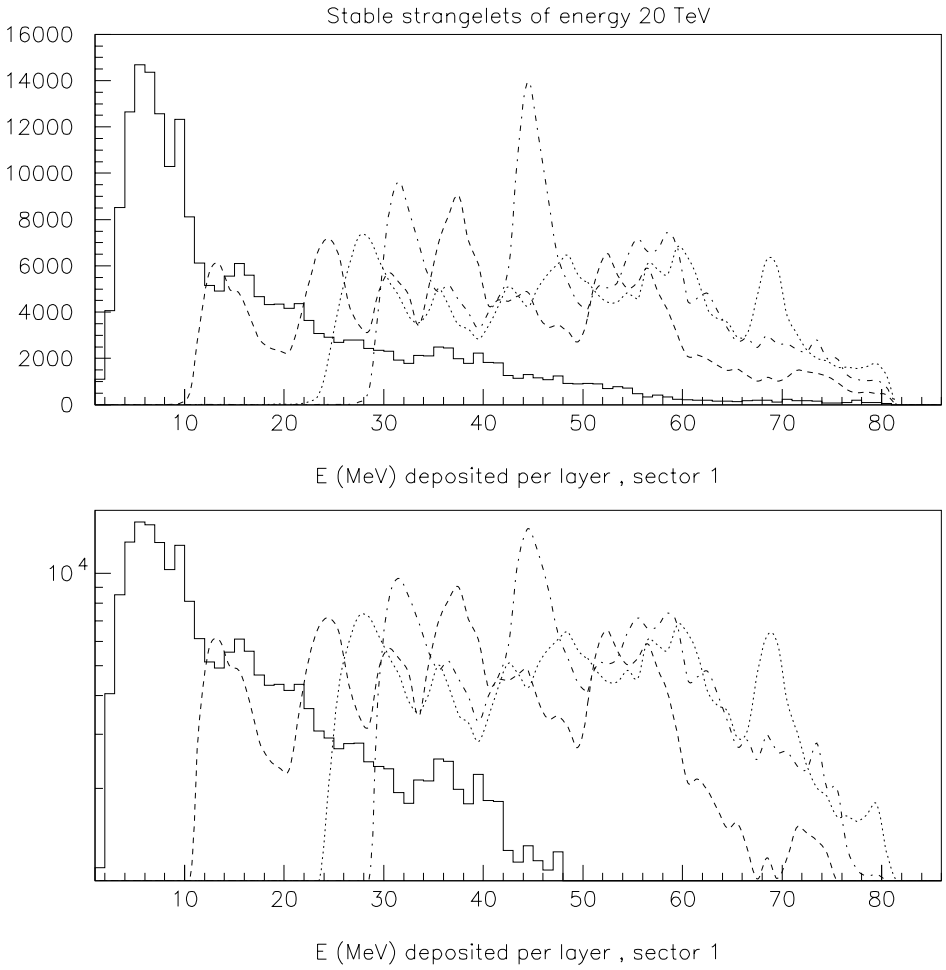

Figure 7.6: Transition curves of stable strangelets with E_{str} = 20 TeV, A_{str} = 20, μ_q = 600 MeV (two simulations: dashed and dotted curves) and μ_q = 1000 MeV (dotted-dashed curve). Energy deposit (MeV) in the calorimeter layers, in the octant containing a strangelet, is shown.

through the calorimeter and the wounded part is destroyed. Particles generated at the consecutive collision points interact with tungsten nuclei in usual way, resulting in the electromagnetic - nuclear cascade which develops in the calorimeter.

We have simulated the penetration of stable strangelets through the calorimeter, assuming $\alpha_s = 0.3$ and several different sets of the initial strangelet parameters:

- quark chemical potential values: μ_q = 300, 600, 1000 MeV;
- strangelet baryon numbers: A_{str} = 15, 20, 40;
- total strangelet energy: $E_{str} \approx$ 8 - 40 TeV (or 400 - 1000 A GeV).

Strangelets characterized by such values of the parameters could be produced at LHC energies [136, 165, 167] according to the picture proposed in [18] when a mechanism of strangeness distillation from the strange quark-matter fireball is invoked. The total energy of particles entering the CASTOR calorimeter for one central Pb+Pb event (generated by HIJING) is about 150 TeV. Thus, the assumed values of strangelet energy mean that a strangelet takes $\sim$ (5 - 30)% of the total energy accessible within the CASTOR acceptance. It is a reasonable value, as it is consistent with the cosmic ray data [36], where the strongly penetrating cascades carry a similar fraction of the visible energy of the events.

Examples of transition curves produced in the CASTOR calorimeter by different stable strangelets are presented in Figs. 7.5, 7.6, 7.7, 7.8, 7.9.

Here are mainly shown strangelets with $\mu_q = 600$ MeV, as such value of quark chemical potential has been estimated from cosmic ray Centauros. The curves are limited to one calorimeter octant containing a strangelet. The strangelet cascade profiles are compared with those of the conventional background, produced by particles generated by HIJING (full line histogram), after subtraction of energy carried by the strangelet.

It has been concluded that:

1. Stable strangelets can produce in the calorimeter long range many-maxima cascades.
2. The strangelet signal is manifestly different from that produced by background from a conventional event, i.e.:
   - higher (in the deep (hadronic) part of the calorimeter),
   - less attenuated,
   - farther extended longitudinally (some strangelets give a strong signal even at the very end of the calorimeter, i.e. after penetration of more than 80 cm of tungsten absorber (60 calorimeter layers), where the signal from a conventional event is practically negligible),
   - has a different shape (reveals many-maxima structure in contrast to the smooth background).
3. The penetrating power of the signal increases with the value of:
   - quark chemical potential μ_q (strangelet cross sections decrease with increasing μ_q),
   - strangelet baryon number A_{str},

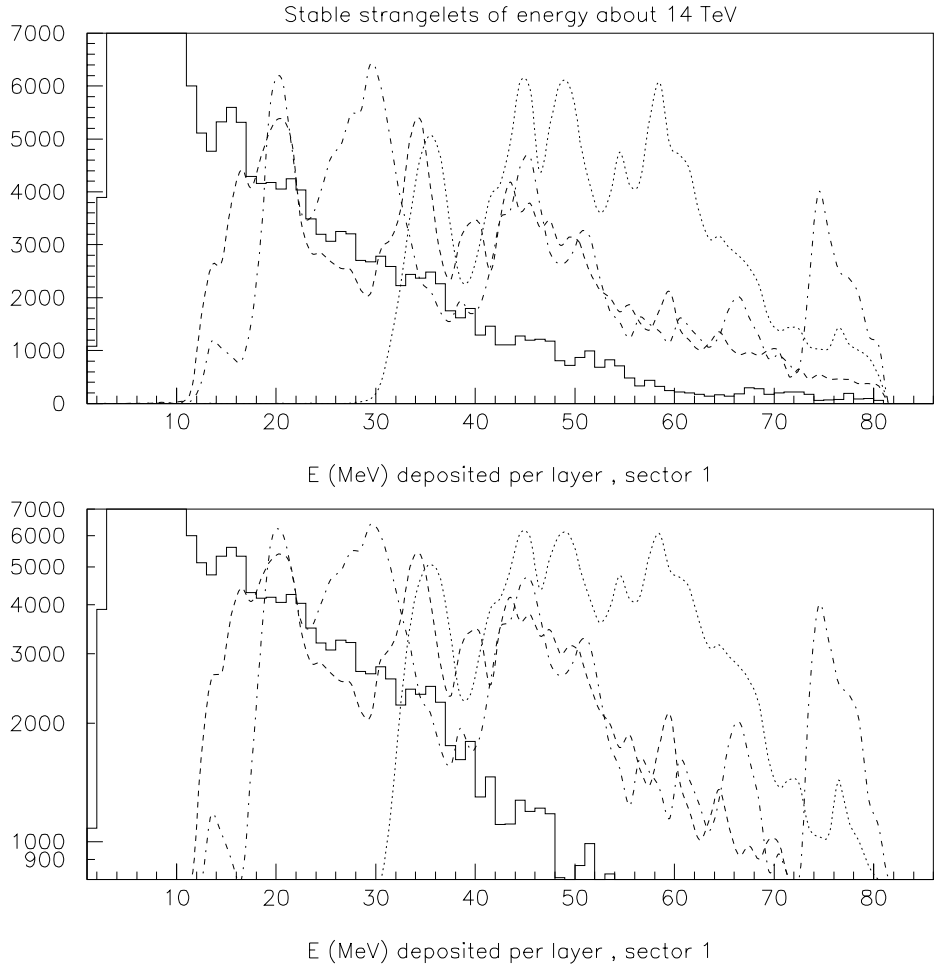

Figure 7.7: Transition curves of stable strangelets with E_{str} = 14-15 TeV. Dashed curve: $A_{str} = 20$, $E_{str} \approx 700$ A GeV, $\mu_q = 600$ MeV; Dotted curve: $A_{str} = 20$, $E_{str} \approx 700$ A GeV, $\mu_q = 1000$ MeV; Dashed-dotted: $A_{str} = 15$, $E_{str} \approx 1000$ A GeV, $\mu_q = 600$ MeV. Energy deposit (MeV) in the calorimeter layers, in the octant containing a strangelet, is shown.

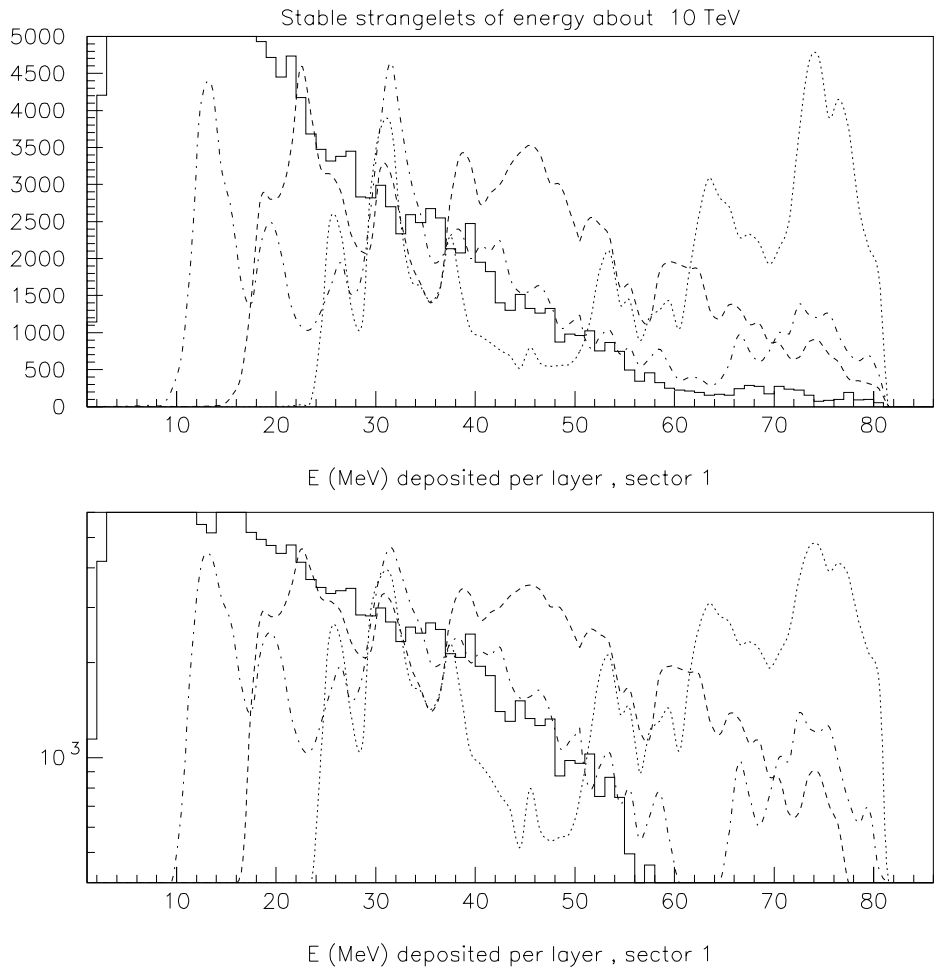

Figure 7.8: Transition curves of stable strangelets with $E_{str} \approx 10$ TeV. Dashed curve: $A_{str} = 20$, $E_{str} \approx 500$ A GeV, $\mu_q = 600$ MeV; Dotted curve: $A_{str} = 20$, $E_{str} \approx 500$ A GeV, $\mu_q = 1000$ MeV; Dashed-dotted curve: $A_{str} = 15$, $E_{str} \approx 700$ A GeV, $\mu_q = 600$ MeV. Energy deposit (MeV) in the calorimeter layers, in the octant containing a strangelet, is shown.

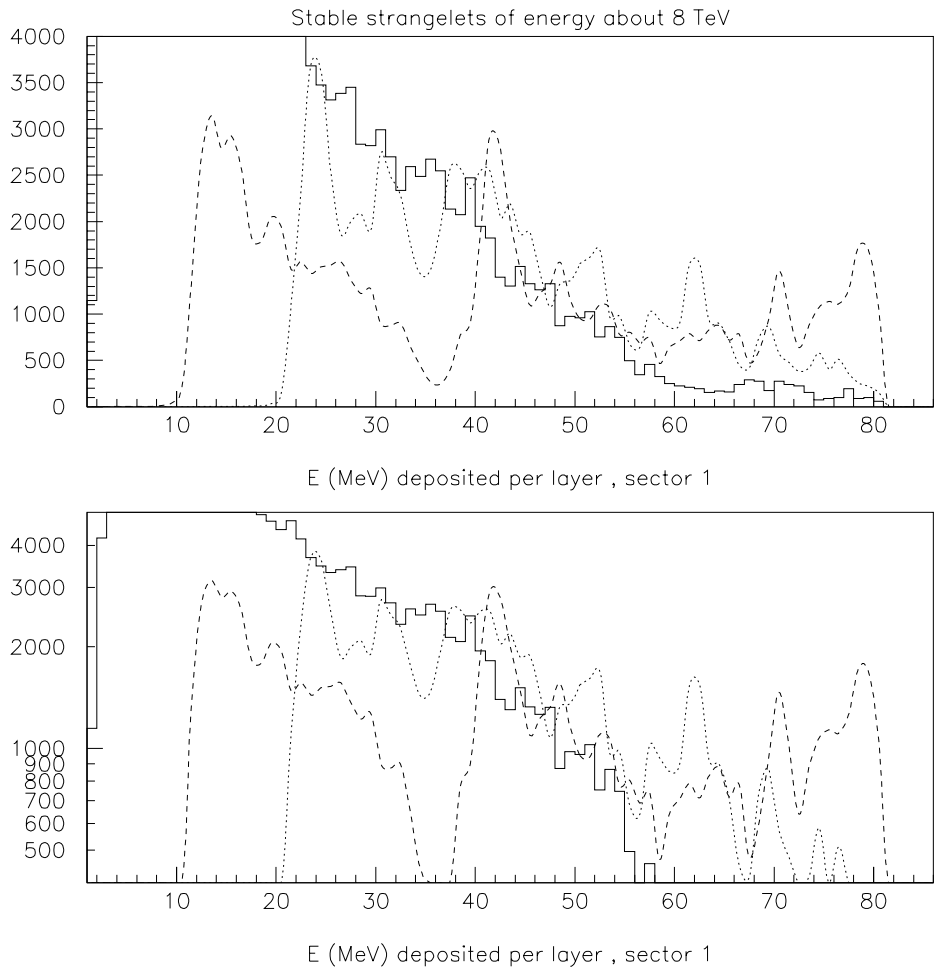

Figure 7.9: Transition curves of stable strangelets with $E_{str} \approx 8$ TeV. Dashed curve: A_{str} = 20, $E_{str} \approx 400$ A GeV, $\mu_q = 1000$ MeV; Dotted curve: $A_{str} = 15$, $E_{str} \approx 500$ A GeV, $\mu_q = 600$ MeV. Energy deposit (MeV) in the calorimeter layers, in the octant containing a strangelet, is shown.

- strangelet energy (however, sometimes even low energy strangelets with $E_{str} \sim$ 400 - 500 A GeV reveal a strongly penetrating power and produce, very deeply in the calorimeter, a much higher signal than that predicted by HIJING, see Fig. 7.9).

4. The longitudinal structure of transition curves depends mainly on the strangelet baryon number A_{str} (a many-maxima structure is more pronounced for smaller A_{str}).

The appearance of the many-maxima structure is the consequence of successive collisions of the strangelet with nuclei of the calorimeter material. At each act of collision some part of the strangelet energy is transformed into energy of the secondary particles which in the process of usual interactions initiate nuclear cascades in the calorimeter. Thus the distance between consecutive humps depends both on the value of the mean interaction path of the strangelet in the tungsten absorber λ_{s-W} (hence on μ_q and A_{str}) and on the values of the mean interaction paths of usual particles.

From these simulations it is seen that the deep calorimeter is an appropriate tool for strangelet detection, independently of the strangelet lifetime.

- *Stable strangelets* are expected to produce spectacular long range signals.

- The transition curves generated by *unstable strangelets* have shorter longitudinal extent than those obtained for stable strangelets but in this case also the strangelet signal differs significantly from the one generated by conventional events. If $N_n \sim 7$ - 20 nucleons being a strangelet decay products carry an amount of energy greater than $\sim$ 10 - 20 TeV, the strangelet signal should be easily separated from the background of accompanying conventional particle production.

- The calorimeter will also be able to detect the possible *strangelet evolution* when the strong nucleon emission process transforms a short-lived strangelet into a stable object. Fig. 7.10 shows the transition curve of a short-lived strangelet ($A_{str} = 23$, $E_{str} = 23$ TeV) which after evaporation of 7 neutrons, in the strong decay process, becomes a long-lived object.

The probability of strangelet detection in a calorimeter depends both on the strangelet properties and the calorimeter parameters. Generally, such factors as large depth, small longitudinal sampling length and fine granularity (division into radial as well as azimuthal sectors) improve the sensitivity to strangelet detection. A deep calorimeter can be sensitive to the detection of strangelets for a wide spectrum of their parameters. For the considered design, stable strangelets with total energy $E_{str} > 10$ TeV, or energy per baryon number $E_{str} \geq 500$ A GeV and baryon number $A_{str} \geq 15$, can be easily identified. Sometimes even less energetic strangelets, because of favourable fluctuations, can produce very deep in the calorimeter a characteristic signal allowing their identification, see Fig 7.9.

The results presented here have been obtained assuming that a strangelet enters the calorimeter at the centre of the sector. In this case leakage of the strangelet signal to neighbouring azimuthal sectors is negligible. Less favourable situations, when strangelets enter the calorimeter close to the sector edge or the border between two sectors were also checked. As it should be expected for a calorimeter where the transverse spread of hadronic cascades is reduced to about 7 mm, the most significant part of the energy is

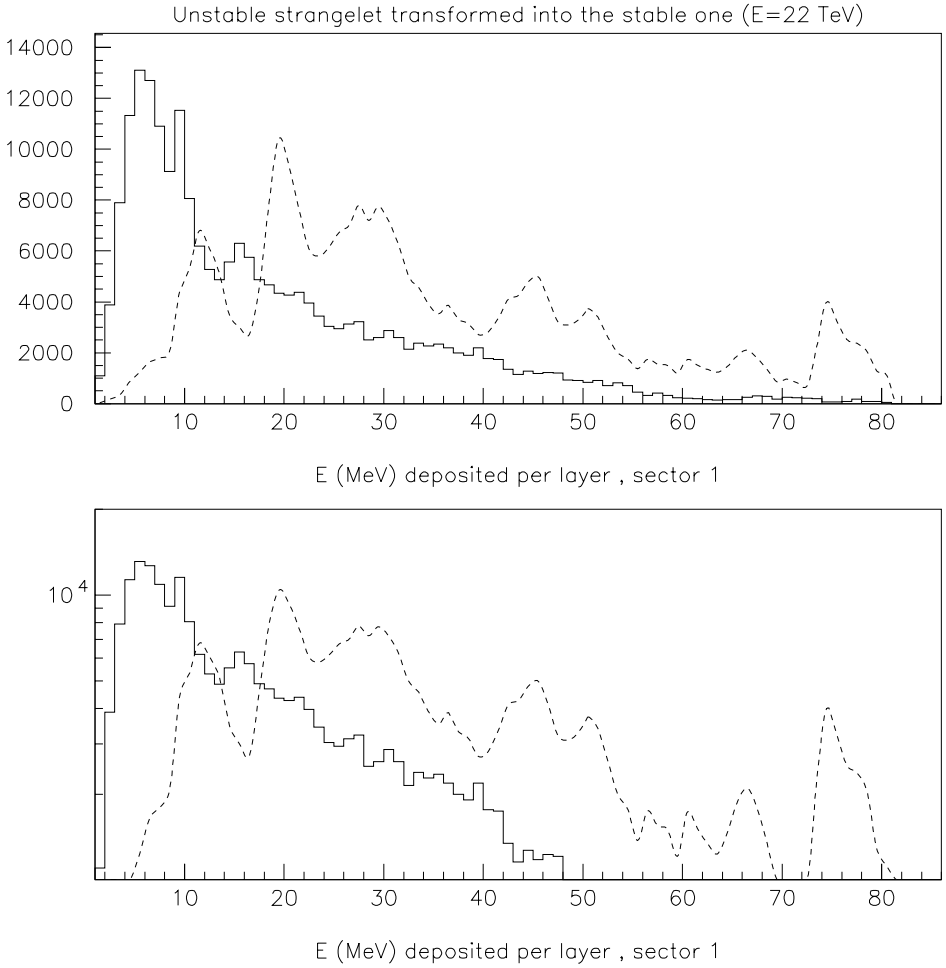

Figure 7.10: Unstable strangelet ($A_{str} = 22$, $E_{str} \approx 22$ TeV) transformed into a stable one after evaporation of 7 neutrons. Energy deposit (MeV) in the calorimeter layers, in the octant containing a strangelet, is shown.

deposited in the sector hit by the strangelet and only a small part of it leaks to adjoining sectors. This question is described in detail in [168].

In order to identify any unusually penetrating component we should observe the development, intensity (energy content) and propagation of hadronic cascades as a function of calorimeter depth. To meet this requirement, the calorimeter must be sampled along its length, with appropriate sampling steps. The simulations presented here have been done for the sampling and reading planes placed every 5 mm ($\sim 1.94X_0$ of effective thickness) in the electromagnetic part and every 10 mm ($\sim 3.88X_0$ of effective thickness) in the hadronic part of the calorimeter. Such sampling is similar to that in the cosmic ray emulsion chambers where the many-maxima long range cascades have been observed and it seems to be also suitable for observation of the many-maxima character of the transition curves produced by strangelets formed at the LHC. It has been also checked that making absorber plates thinner leads only to a small increase of the light output. An important question is how a many-maxima structure changes with the increase of the reading unit thickness, which is an option under consideration. It is illustrated in Fig. 7.11 where transition curves produced by a typical stable strangelet (A_{str} = 20, E_{str} = 20 TeV, μ_q = 600 MeV) are shown. Fig. 7.11 a shows the signals produced by the strangelet and the HIJING background, separately. Figs. 7.11 b and 7.11 c show the summed signal in the "strangelet" sector in comparison with the average output from the other sectors. Fig. 7.11 a and 7.11 b illustrate the standard sampling and reading step as described above. Fig. 7.11 c is the same transition curve obtained for readings of the summed signal from consecutive groups of 4 layers (i.e. every $\sim 16X_0$). As it can be expected, with decreasing the number of reading steps, the strangelet signal becomes smoother. The many-maxima structure becomes rather a wave-like structure but it is still visibly different from the still smoother background.

7.3.2 "Mixed" events in the CASTOR calorimeter

Further questions concern the shape of transition curves produced in the calorimeter by:

- strangelets coming from the Centauro fireball explosion and registered in the apparatus simultaneously with other Centauro decay products,
- Centauro fireball decay products without accompanying strangelets emission (or such case when a strangelet escapes the detection in the calorimeter).

To investigate this topic several exotic events generated previously by means of the Centauro code (see previous subsection) were chosen and passed through the CASTOR calorimeter, by using GEANT 3.21. For spectacular illustration of signals expected to be produced in the calorimeter, the events characterized by various initial parameters (μ_b, T, $\Delta y_{n.s.}$) were chosen as the examples. We restricted the choice to the events in which a strangelet does not escape the detection and it is registered in the apparatus together with other particles coming from the Centauro fireball. Both stable and unstable strangelets characterized by various energies, mass numbers and quarkchemical potentials were included to our studies. For each event we simulated separately the following transition curves:

- produced by the Centauro fireball decay products,

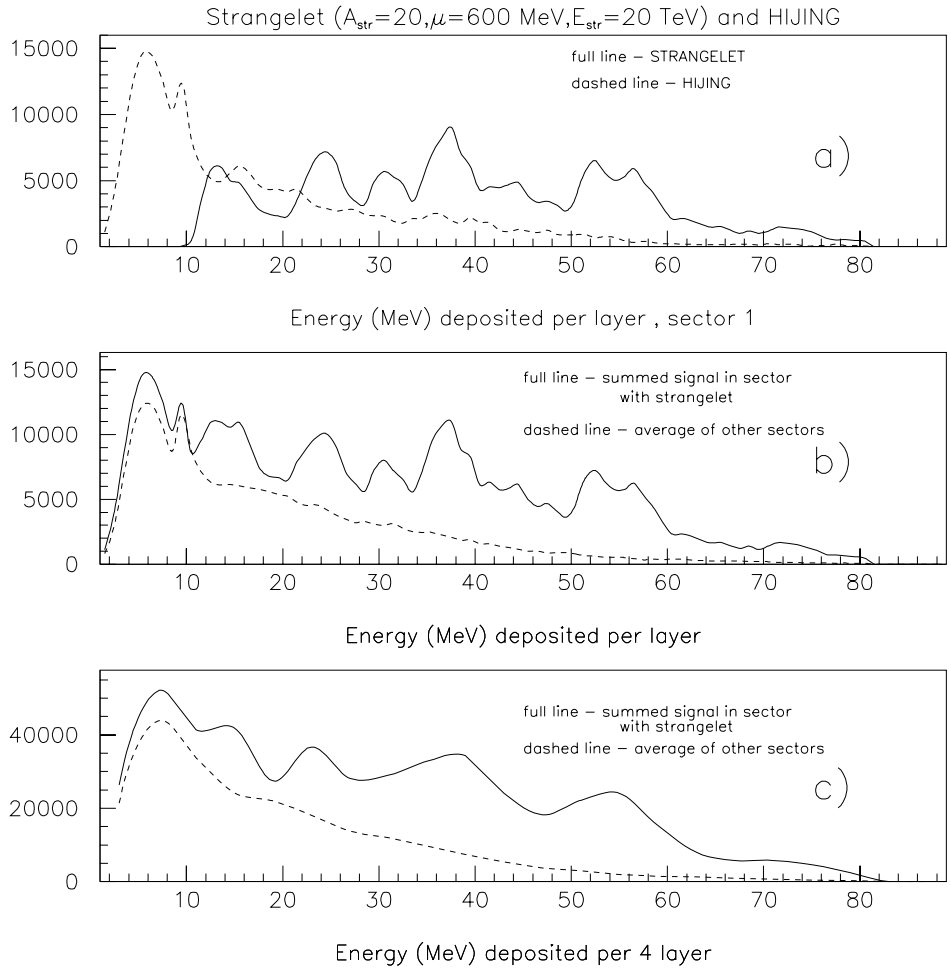

Figure 7.11: a) Transition curves produced by a stable strangelet (A_{str}= 20, E_{str} = 20 TeV, μ_q = 600 MeV) and by the HIJING background separately; b) Summed signal in the "strangelet" sector in comparison with the average of other sectors assuming readings of every layer, i.e. every 5 mm in electromagnetic and 10 mm in hadronic sectors; c) same as (b), but readings of the summed signal from consecutive groups of 4 layers.

- by the accompanying strangelet,
- and by background of conventionally produced particles, possibly accompanying the Centauro event (estimated by HIJING).

All these three contributions separately and also their sum, constituting the so–called "mixed" event, were compared with the "usual" transition curve, produced by HIJING. We have analysed Centauro events characterized by different values of parameters: temperature ($T = 250$, 300 MeV), quarkchemical potential ($\mu_q = 600$, 1000 MeV) and nuclear stopping power ($\Delta y_{stop} = 0.5$, 1.0, 1.5 what corresponds to the effective stopping in the range of about $\sim$ 1.5 - 3.0 pseudorapidity units). For investigated samples the total summed energy of Centauro and strangelet, covered by the calorimeter was in the range of 76-158 TeV, in comparison with $\sim$ 150 TeV predicted by HIJING for a central event. In some events strangelets with baryonic numbers $A_{str} \simeq$ 20-40 and energies $E_{str} \simeq$ 8-20 TeV were formed, what corresponds to the energy per baryon $E/A_{str} \simeq$ 0.3-1.0 TeV.

Examples of resulting transition curves are presented in Figs. 7.12, 7.13, and 7.14. Energy deposit in the consecutive calorimeter layers, in the sector containing a strangelet, is shown.

Separate contributions from: Centauro fireball decay products, a strangelet, the HIJING central event and a background from conventionally (HIJING) produced particles are plotted in Figs. 7.12, and 7.13.

The Centauro event with unstable strangelet produced among its secondaries is shown in Fig. 7.12. Figs. 7.13 and 7.14 illustrate the signals, expected in the calorimeter, assuming that stable strangelets are formed during the Centauro fireball decay.

This analysis indicates that Centauro events (as well accompanied and not accompanied by a strangelet) can be easily distinguishable from "usual" events. Centauro transition curves in the calorimeter are expected to have apparently different shape and longer extent from those produced by "normal" events. A Centauro produced signal has a maximum at about 14th calorimeter layer with the average $\langle N_{Cent} \rangle \simeq 25$. HIJING event produces the maximum of the signal at $\sim$ 8th calorimeter layer, with the average at $\langle N_{HIJ} \rangle \simeq 19$ layer. Generally, Centauro produced signal is stronger in the deeper (hadronic) part of the calorimeter, in opposite to the HIJING generated one, which is peaked in the electromagnetic section of the calorimeter.

Strangelet transition curves have been analysed in details in the previous subsection, with the general conclusion that they are apparently different from those produced by "normal" events and that strangelets produced among other conventional particles should give easily distinguished signal. Here are shown signals, being the sum of Centauro, strangelet and background contributions. These transition curves are again very different from conventionally produced ones. They have much longer extent (they are strongly pronounced in the deep hadronic part of the calorimeter) and many-maxima structure. Their shape depends, of course, on the strangelet and Centauro parameters. The important quantity is the Centauro and strangelet energy falling into the calorimeter acceptance. Generally, higher energy of the exotic species bears smaller conventional background and in consequence gives more pronounced signal. The Centauro fireball energy depends mainly on the value of nuclear stopping power. The plot no 2 of Fig. 7.14 is the example of the event in which the Centauro fireball energy, covered by the calorimeter equals to 158 TeV, exceeding the HIJING predicted value ($\sim$ 150 TeV). It results in zero conventional

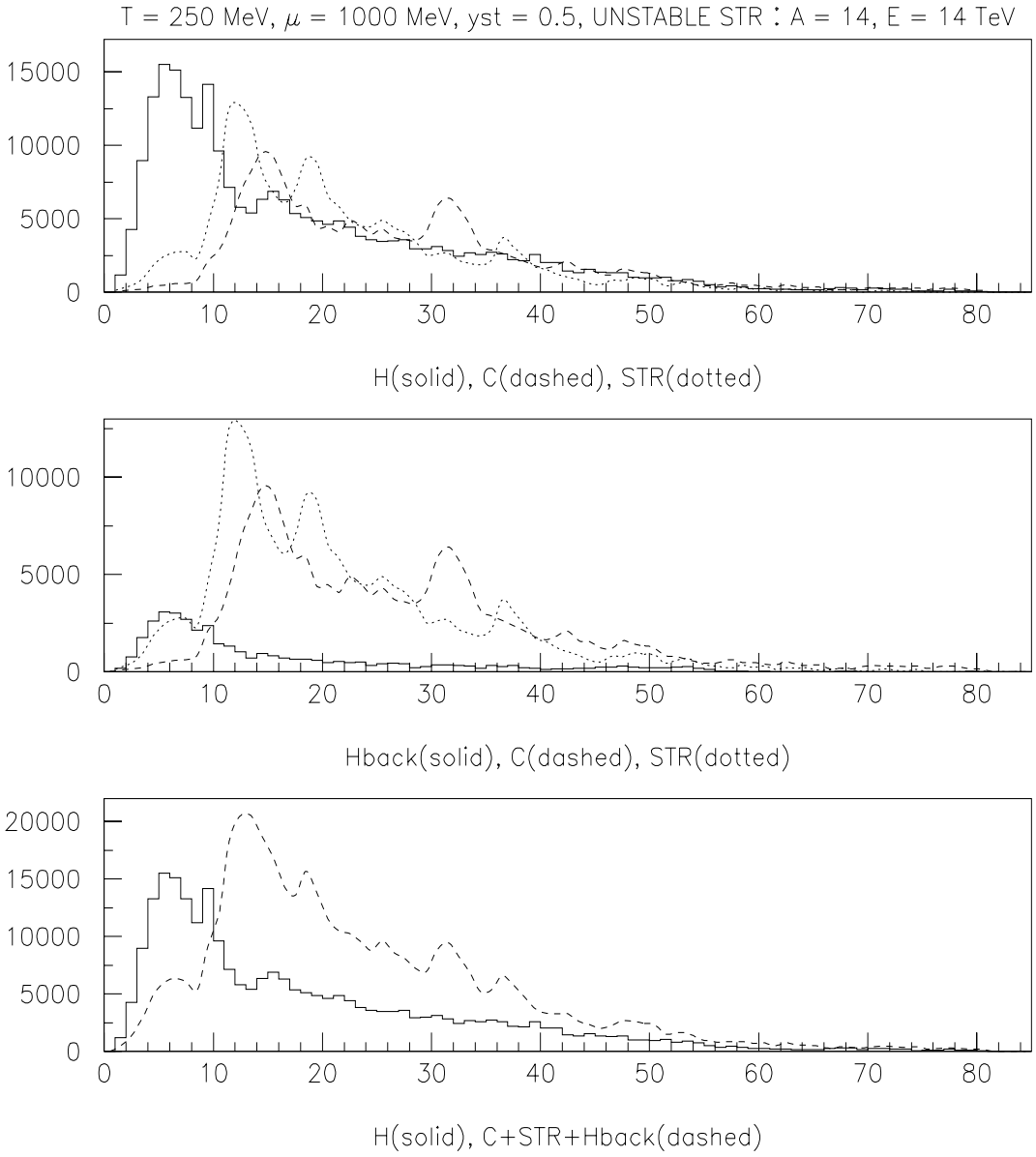

Figure 7.12: Transition curves produced by Centauro event "C"(T = 250 MeV, $\mu_q = 1000$ MeV) with an ustable strangelet "STR"($A_{str} = 14$, $E_{str} = 14$ TeV), in comparison with HIJING "H". Energy deposit (MeV) in the calorimeter layers, in the octant containing a strangelet, is shown.

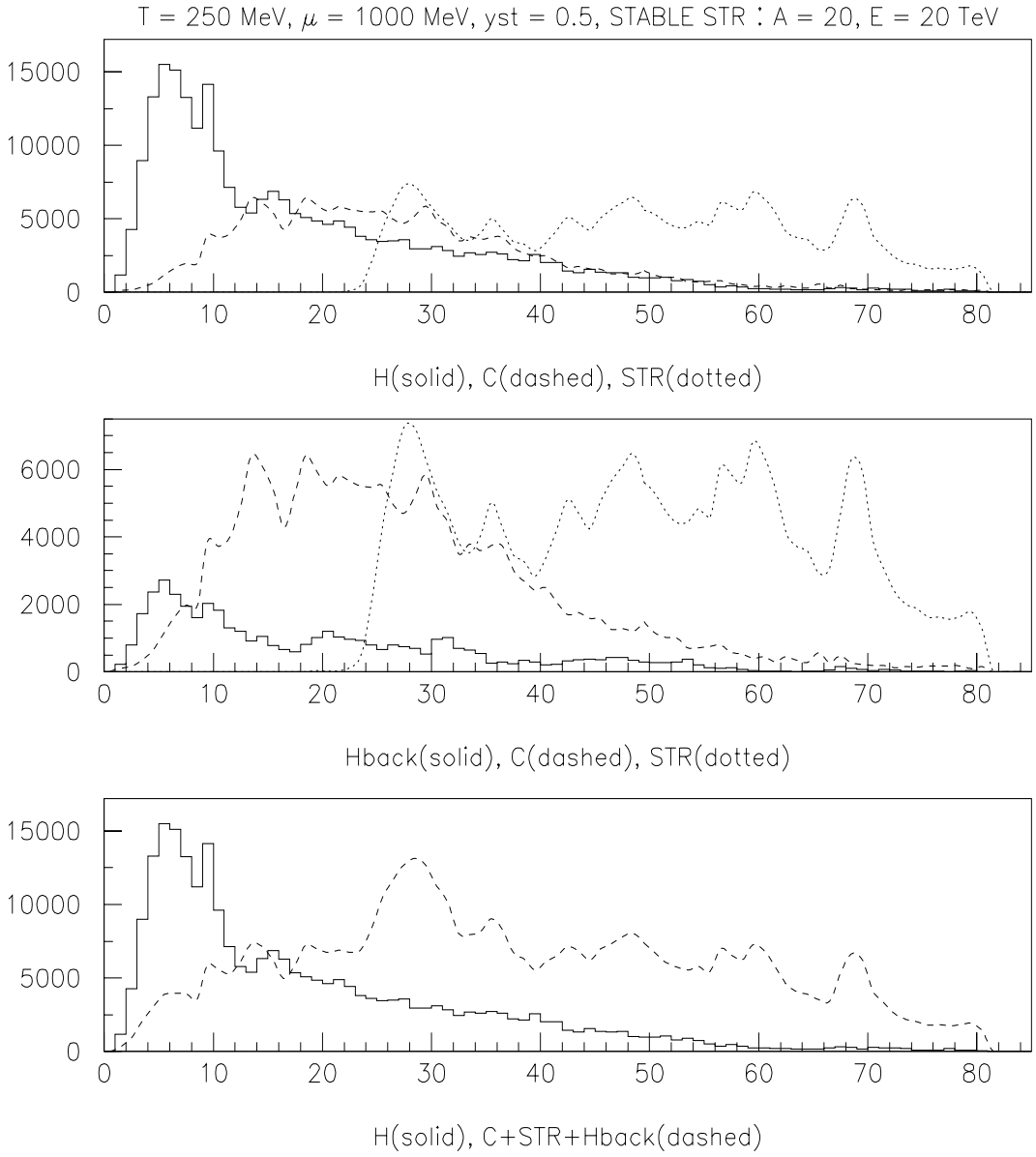

Figure 7.13: Transition curves produced by Centauro event "C" (T = 250 MeV, μ_q = 1000 MeV) with a stable strangelet "STR"($A_{str} = 20$, $E_{str} = 20$ TeV), in comparison with HIJING "H". Energy deposit (MeV) in the calorimeter layers, in the octant containing a strangelet, is shown.

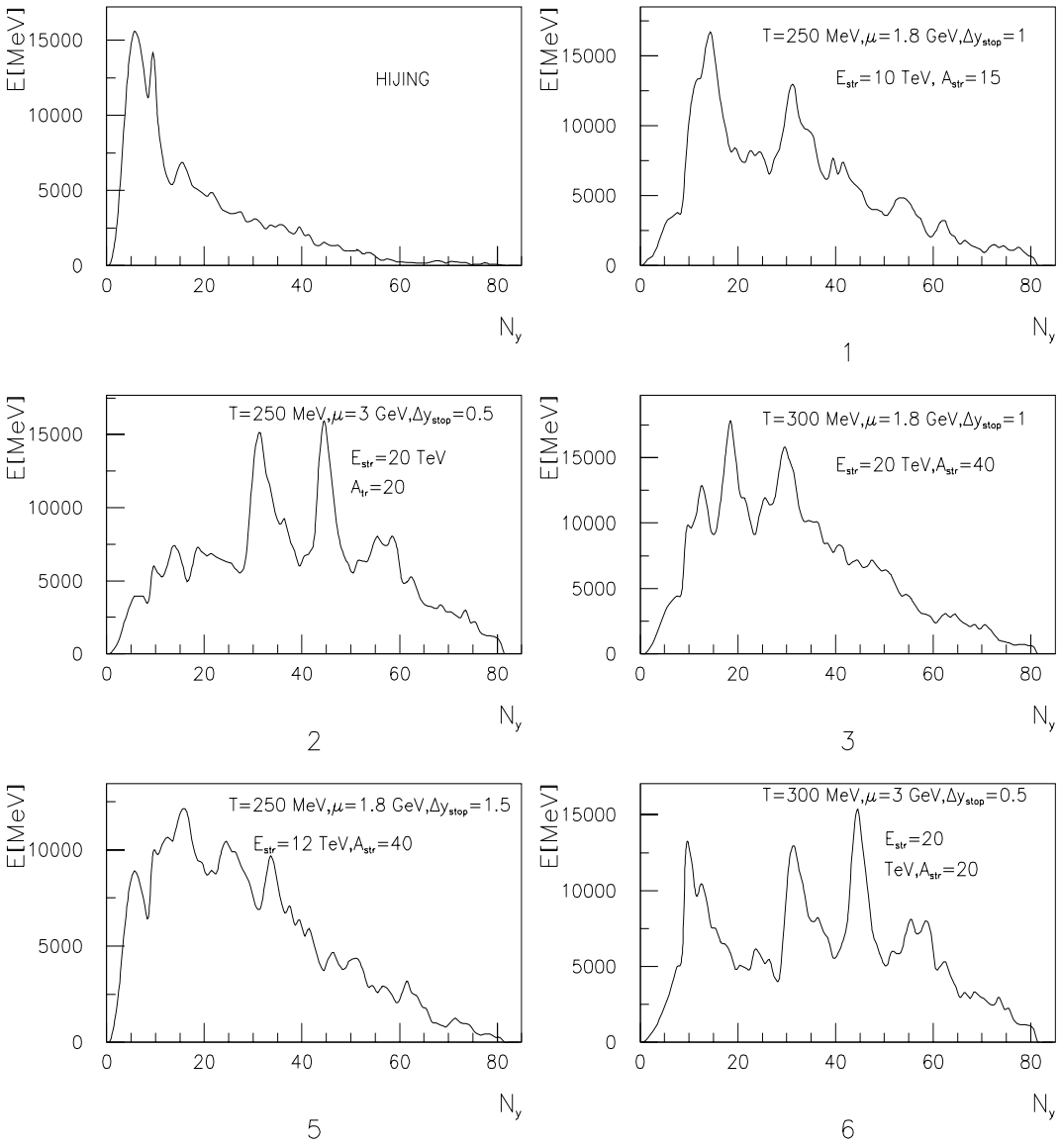

Figure 7.14: Examples of resulting transition curves being the sum of Centauro, strangelet and background contributions, and in comparison the HIJING event. Energy deposit (MeV) in the calorimeter layers, in the octant containing a strangelet, is shown.

background and hence the summed transition curve is very different from the HIJING predicted one. On the contrary, the event illustrated in the plot no 5 of Fig. 7.14 in which the Centauro fireball energy equals to 79.5 TeV, carries only about one half of the energy allowed by HIJING in that kinematical region. The remaining energy could go into the conventional particle production. This fact in connection with the small strangelet energy causes the expected signals to be weaker than others presented in Figs. 7.14. But also such events have apparently different characteristics than the "normal" ones and should be easily picked up in the process of analysis of the shape and extent of transition curves in the calorimeter.

Chapter 8

Summary

In this work the experimental data from cosmic ray mountain experiments have been reviewed. In spite of many experimental uncertainties and some doubts, it can be concluded that they give a compelling evidence of unusual events which are hardly explained by means of "conventional" models. Among many theoretical attempts to understand these anomalies the more attractive ones are the scenarios with the QGP. In particular, the picture assuming the production of a strange quark matter fireball in nucleus–nucleus collisions seems to be the most convincing. At the last stage of the fireball evolution the Centauro–type events and strangelets can be formed. The model allows to explain simultaneously many different anomalies, such as the existence of hadron–rich events, a strongly penetrating component, mini–clusters etc. In addition, such picture is consistent with up to now negative results of Centauro search in accelerator experiments and allows to expect their appearance in future, in heavy ion interactions at RHIC and LHC colliders. The CASTOR, a subsystem of the ALICE detector is proposed to study the baryon–rich environment formed in Pb+Pb collisions at LHC energies, and to search for exotic events, such as Centauros and strangelets.

Acknowledgments

I would like to thank all of my collegues with whom whenever I worked or discussed the topics concerning the cosmic ray exotic phenomena. In particular, many thanks prof. Z. Włodarczyk for our common study of a strangelet question and dr A. Angelis for common work in designing the CASTOR detector, his great help on the field of computer calculations and his software being the basis of the codes simulating the passage of the exotic objects through the deep calorimeter. Thank you both of them for the comments and figures included to the paper. I am especially grateful prof. J. Bartke for helpfull discussions and very carefull and patient reading of the raw version of the manuscript, plenty important remarks and corrections. This work was partly supported by Polish State Committee for Scientific Research grant No. 2P03B 011 18 and SPUB-M/CERN/P03/DZ1/99.

Bibliography

[1] J. W. Harris, Lectures at Lake Louise Winter Institute on Quantum Chromodynamics, 1998, Lake Louise, Alberta, Canada, Proc. ed. by A. Astbury et al., Singapore, World Scientific, 1999, p. 99 and preprint YRHI-98-13, 1998.

[2] H. Białkowska, Acta Physica Polonica **B28** (1997) 2793.

[3] Proc. of the Twelfth International Conference on Ultra- Relativistic Nucleus-Nucleus Collisions- Quark Matter'96, Nucl. Phys. **A 610** (1996).

[4] Proc. of the Thirteenth International Conference on Ultra-Relativistic Nucleus-Nucleus Collisions-Quark Matter'97, Nucl. Phys. **A638** (1998).

[5] Proc. of the Fourteenth International Conference on Ultra-Relativistic Nucleus-Nucleus Collisions - Quark Matter'99, Nucl. Phys. **A661** (1999).

[6] http://www.cern.ch/CERN/Anouncements/2000/NewStateMatter.

[7] M. Tamada, talks given at the Intern. Conf. on High Energy Physics, Tampere (Finland), 1999 and the Intern. Symposium Chacaltaya–Pamir, Łódź (Poland), 1999; Inst. Cosmic Ray Research, University Tokyo, Report ICRR-454-99-12.

[8] A. Ohsawa and Chacaltaya Emulsion Chamber Collaboration, Nucl. Phys. B (Proc.Suppl.) **74A** (1999) 3;
A. Ohsawa and Chacaltaya Emulsion Chamber Collaboration, Proc. 26th ICRC, Salt Lake City (USA), 1999.

[9] C. Aguirre et al., Phys. Rev. **D62** (2000) 032003.

[10] U. Das Gupta et al., Phys. Rev. **D45** (1992) 1459;
MACRO Coll., 23th ICRC, Calgary, 1993, Canada, ed. by R. B. Hicks et al., World Scientific, Singapore, 1994, Vol. 2, p. 97;
JACEE Collaboration., Astrophys. J. **349** (1990) L25;
M. Ichimura et al., Phys. Rev. **D48** (1993) 1949.

[11] A. L. S. Angelis et al., XXVIII Intern. Symp. on Multiparticle Dynamics, 1998, Delphi (Greece), ed. N. G. Antoniou et al., World Scientific, 1998, p. 134 and hep-ex/9901038.

[12] V. A. Aseikin et al., Proc. 14th ICRC, Munich, 1975, Vol. 7, p. 2462;
V. I. Yakovlev, S. I. Nikolsky, V. P. Pavluchenko, Proc. 15th ICRC, Plovdiv, 1977, Vol. 7, p. 115;

V. I. Yakovlev et al., Proc. 16th ICRC, Kyoto (Japan), Vol. 6 (1979), p. 59;
I. M. Dremin et al., Proc. 20th ICRC, Moscow, Vol. 6, 1987, p. 360;
E. V. Bazarov et al., Proc. 17th ICRC, Paris 1981, Vol. 5, p. 32;
V. I. Yakovlev, Proc. of the VIIth Intern. Symp. on VHECRI, Ann Arbor (1992) , ed. L. Jones, 1993, p. 154.

[13] J. M. Dremin et al., Voprosy atomnoy nauki i tekhniki, seria: Tekhnika fizicheskovo eksperimenta, Vypusk 4(25), p. 3, 1985; ISSN-0207-0480 (in Russian).

[14] G. Altarelli et al., Z. Phys. **C45** (1989) 109;
A. B. Kurepin, ALICE/95-47, Internal Note/PHY 1995; A. B. Kurepin, ALICE/93-03, Internal Note/PHY 1993.

[15] J. Berges and K. Rajagopal, e-preprint hep-ph/9804233 (1998);
R. Rapp, T. Schaefer, E. V. Shuryak and M. Velovsky, e-preprint hep-ph/9711396 (1997);
M. Alford, K. Rajagopal and F. Wilczek, e-preprint hep-ph/9711395 (1997).

[16] F. Weber, J. Phys.G: Nucl. Part. Phys. **25** (1999) R195 (topical review).

[17] A. D. Panagiotou et al., Z. Phys. **A333** (1989) 335;
A. D. Panagiotou et al., Phys. Rev. **D45** (1992) 3134.

[18] M. N. Asprouli, A. D. Panagiotou and E. Gładysz-Dziaduś, Astroparticle Phys. **2** (1994) 167;
E. Gładysz-Dziaduś and A. D. Panagiotou, Intern. Symp. on Strangeness and Quark Matter, Krete (1994), World Scientific, Singapore, 1995, ed's G. Vassiliadis et al., p. 265.

[19] E. Gładysz-Dziaduś and Z. Włodarczyk, ALICE/97-17, Internal Note/CAS, 1997 [1];
E. Gładysz-Dziaduś and Z. Włodarczyk, J. Phys. G: Nucl. Part. Phys. **23** (1997) 2057.

[20] S. Hasegawa, Proc. VIII Intern. Symp. on VHECRI, Tokyo, 1994, ed. by Local Organising Commitee, p. 115.

[21] Japan-Brasil Coll., Proc. 13th ICRC, Denver (Canada), 1973, Vol. 4, p. 2671.

[22] S. L. C. Barroso et al., contr. to 25th ICRC, Durban (1997) and Chacaltaya Cosmic-Ray Collaboration., ICRR-Report-390-97-13A.

[23] C. M. G. Lattes, Y. Fujimoto and S. Hasegawa, Phys. Rep. **65** (1980) 151;
S. Hasegawa, Brasil-Japan Coll., talk at FNAL CDF seminar (ICRR Report 151-87-5(1987)).

[24] S. L. C. Barroso et al., Proc. VIII Intern. Symposium on VHECRI, Tokyo, 1994, ed. by Local Organising Commitee, p. 166.

[25] M. Tamada, Il Nuovo Cimento **41B** (1977) 245.

[1] for ALICE Internal Notes look at the web; http://www.cern.ch/ALICE/documents.html

[26] J. A. Chinellato et al., Brasil-Japan Collaboration, Proc. 5th Intern. Symp. VHECRI, Łódż (Poland), 1988, ed. by University of Łódź Publishers, Łódź 1988, p. 309.

[27] J. Bellandi et al., Proc. Workshop Cos. Ray Interactions High Energy Results, La Paz (Rio de Janeiro), 1982, ed. by C. M. G. Lattes, p. 42 and 102.

[28] Y. Funayama, Proc. of Intern. Symp. on Cos. Rays and Particle Physics, 1984, Tokyo, ed. by A. Ohsawa and T. Yuda, p. 335.

[29] S. Hasegawa, Chacaltaya Collaboration, VIth Intern. Symp. on VHECRI, Tarbes (France), 1990, ed. by J. N. Capdevielle and P. Gabinski, p. 227.

[30] Brasil-Japan Collaboration, Proc. 21th ICRC, Adelaide, 1990, Vol. 8, p. 259 and 263.

[31] S. Hasegawa and M. Tamada, Nucl. Phys., **B474** (1996) 141.

[32] C. E. Navia et al., Phys. Rev. **D50** (1994) 5732.

[33] A. Borisov et al., Pamir and Chacaltaya Coll., Phys. Lett. **B190** (1987) 226.

[34] Pamir Collaboration and Chacaltaya Collaboration, Proc. 20th ICRC, Moscow (1987), Vol. 5, p. 334.

[35] L. T. Baradzei et al., Pamir Collaboration, FIAN Preprint 208, Moscow, 1989.

[36] Z. Buja, E. Gładysz, S. Mikocki, M. Szarska, L. Zawiejski, Proc. 17th ICRC, Paris (1981), Vol. 11, p. 104.

[37] Z. Buja, E. Gładysz, S. Mikocki, M. Szarska, L. Zawiejski, Pamir Coll. Workshop, Cedzyna (Poland), 1980, ed. by University of Łódź, 1980, p. 73.

[38] S. G. Bayburina et al., Nucl. Phys. **B191** (1981) 1.

[39] A. A. Bielyayev, I. P. Ivanienko et al., "Electromagnetic Cascades in Cosmic Rays of Ultra-High Energy", Moscow, 1980 (in Russian).

[40] V. I. Yakovlev, Proc. Intern. Seminar on Cosmic Ray Cascades, Sofia, 1980, p. 111.

[41] H. Kumano, Proc. 20th ICRC, Moscow (1987), Vol. 5, p. 387.

[42] H. Bielawska et al., Il Nuovo Cimento **2C** (1989) 763;
M. Tamada and A. Tomaszewski, Proc. 5th Intern. Symp. VHECRI, Łódź (Poland), 1988, ed. by University of Łódź Publishers, Łódź 1988, p. 330.

[43] A. Borisov et al., Pamir Collaboration, Proc. 20th ICRC, Moscow, (1987), Vol. 5, p. 351.

[44] S. Yamashita, Journ. Phys. Soc. of Japan, **54** (1985) 529.

[45] N. Amato et al., J. Phys. G: Nucl. Part. Phys. **20** (1994) 141.

[46] J. A. Chinellato et al., Proc. 20th ICRC, Moscow (1987), Vol. 5, p. 363;
S. Yamashita et al., Proc. 20th ICRC, Moscow (1987), Vol. 5, p. 367.

[47] Pamir Collaboration, Pamir Coll. Workshop, Cedzyna (Poland), 1980, p. 94;
Pamir Coll., Proc. 17th ICRC, Paris (1981), Vol. 5, p. 291.

[48] Japan-USSR Joint Em. Chamber Exp., Proc. 19th ICRC, La Jolla (1985), Vol. 6, p. 332.

[49] A. S. Borisov et al., Proc. 20th ICRC, Moscow (1987), Vol. 5, p. 383.

[50] S. Hasegawa, Proc. Intern. Symp. on Cos. Rays and Particle Physics, 1984, Tokyo, ed. by A. Ohsawa and T. Yuda, p. 718.

[51] A. S. Borisov et al., Proc. Intern. Symp. on Cosmic Rays and Particle Physics, Tokyo, 1984, ed. by A. Ohsawa and T. Yuda, p. 248 and Proc. Workshop Cosmic Ray Inter. High Energy Results, La Paz (Rio de Janeiro), 1982, p. 445.

[52] J. A. Chinellato et al., Brasil-Japan Coll., AIP Conf. Proc. No. 85 (1981) 500;
S. Hasegawa et al., Proc. Intern. Symp. on Cos. Rays and Particle Physics, 1984, Tokyo, ed. by A. Ohsawa and T. Yuda, p. 319.

[53] L. T. Baradzei, Nucl. Phys. **B370** (1992) 365.

[54] T. Arisawa et al., Nucl. Phys. **B424** (1994) 241.

[55] L. T. Baradzei et al., Proc. Workshop Cos. Ray Inter. High Energy Results, La Paz (Rio de Janeiro), 1982, p. 449.

[56] M. Tamada and K. Yokoi, Bulletin of Science and Engineering Research Lab. Waseda Univ. No. 113 (1986) p. 21.

[57] Chacaltaya and Pamir Collaboration, ICRR-report-295-93-7 (1993), p. 9 (contribution to 23th ICRC, Calgary, 1993).

[58] V. Kopenkin and Y. Fujimoto, Il Nuovo Cimento **19** (1996) 1017.

[59] S. Hasegawa, Proc. Intern. Symp. on Cos. Rays and Particle Physics, 1984, Tokyo, ed. by A. Ohsawa and T. Yuda, p. 62;
M. Tamada, Proc. Intern. Symp. on Cos. Rays and Particle Physics, 1984, Tokyo, ed. by A. Ohsawa and T. Yuda, p. 352.

[60] S. Hasegawa, ICR-report-197-89-14.

[61] M. Tamada and Y. Funayama, Report of Sci. and Eng. Res. Lab., Waseda University No. 85-5, 1985;
Y. Funayama and M. Tamada, Report of Sci. and Eng. Res. Lab., Waseda University No. 85-6, 1985.

[62] H. Bielawska et al., Proc. Intern. Symposium on Cos. Ray Particle Physics, Tokyo, 1984, ed. by A. Ohsawa and T. Yuda, p. 374.

[63] Chacaltaya and Pamir Collaboration, Proc. 22th ICRC, Dublin (Ireland), 1991, Vol. 4, p. 101.

[64] J. N. Capdevielle and S. A. Slavatinsky, Nucl. Phys. B (Proc.Suppl.) **75A** (1999) 12.

[65] M. Tamada, Nucl. Phys. Proc. Suppl. **97** (2001) p. 146 and p. 150 (contribution to XIth ISVHECRI, Campinas (Brasil), 2000).

[66] A. S. Borisov et al., Pamir Collaboration., Proc. of Intern. Symp. on Cos. Rays and Particle Physics, 1984, Tokyo, ed. by A. Ohsawa and T. Yuda, p. 3.

[67] M. Tamada and V. V. Kopenkin, Nucl. Phys. **B494** (1997) 3;
M. Tamada and V. V. Kopenkin, Nucl. Phys. (Proc. Suppl.) **B52** (1997) 222.

[68] M. Tamada and A. Ohsawa, Proc. 26th ICRC, 1999, Salt Lake City (USA), 1999, Vol. 7, p. 11;
M. Tamada and A. Ohsawa, Nucl. Phys. **B581** (2000) 73.

[69] V. S. Hlytchieva et al., IVth Intern. Symp. on VHECRI, Tarbes (France), 1990, ed. by J. N. Capdevielle and P. Gabinski, Tarbes, 1990, p. 184.

[70] S. B. Shaulov, Heavy Ion Physics **4** (1996) 403.

[71] E. Gładysz, Ph.D. Thesis, Institute of Nuclear Physics, Kraków 1980.

[72] M. Akashi et al., Proc. 15th ICRC., Plovdiv (1977) , Vol.7, p. 184.

[73] J. R. Ren et al., Phys. Rev. **D38** (1988) 1417.

[74] T. H. Burnett et al., Jacee Collaboration, Proc. 20th ICRC, Moscow 1987, Vol. 5, p. 185.

[75] J. D. Bjorken, K. L. Kowalski and C. C Taylor SLAC-PUB-6109 (1993);
J. D. Bjorken, Acta Physica Polonica **B28** (1997) 2773.

[76] L. W. Jones, Proc. VIIIth Intern. Symp. on VHECRI, Tokyo, 1994, ed. by Local Organizing Committee, p. 312.

[77] H. Wilczynski, Raport INP Krakow 1718/PH, Krakow, 1996;
H. Wilczynski, contribution to 10th Symposium on VHECRI, Gran Sasso (Italy), 1998.

[78] B. S. Acharaya et al., Proc. 16th ICRC, Kyoto **6** (1979) 289;
A. M. Dunaevskii et al., Proc. 16th ICRC, Kyoto **7** (1979) 154;
M. Shibata, Proc. 16th ICRC, Kyoto **7** (1979) 176;
T. G. Levina et al., Proc. 16th ICRC, Kyoto **7** (1979) 148;
B. S. Acharya et al., Il Nuovo Cimento Lett., 31 (1981) 149;
R. W. Ellsworth et al., Phys. Rev., **D23** (1981) 771;
R. A. Mukhamedshin, Proc. 17th ICRC, Paris **5** (1981) 343;
Pamir Collaboration, Proc. 20th ICRC, Moscow, 1987, Vol. 5, p. 334, 351 and 383;
S. Yamashita, A. Ohsawa and J. A. Chinellato, Proc. Intern. Symp. Cosmic Rays and Particle Physics, Tokyo, 1984, ed. by A. Ohsawa and T. Yuda (Institute for Cosmic Ray Research, Tokyo, 1984), p. 30.

[79] B. S. Acharya and M. V. S. Rao, J. Phys. G: Nucl. Part. Phys., **17** (1991) 759.

[80] B. Mc Cusker, Proc. of the XVI ICRC, Kyoto (Japan), 1979, ed. by Miyake.

[81] P. B. Price et al., Proc. Nat. Acad. Sci. USA 77 (1980) 44.

[82] J. D. Bjorken and L. D. McLerran, Phys. Rev. **D20** (1979) 2353.

[83] K. Goulianos, Proc. 7th Symposium. on Very High Energy Cosmic Ray Interactions (ISVHECRI), Ann Arbor MI (USA), 1992, ed. by L. W. Jones, 1993, p. 244 and RU92/E-39;
K. Goulianos, Comments Nucl. Part. Phys. **17** (1987) 195.

[84] K. Kang and A. White, Phys. Rev. **D42** (1990) 835;
A. R. White, Proc. 8th Intern.Symp. on VHECRI, Tokyo, 1994, ed. by Local Organising Commitee, p. 468.

[85] C. R. A. Augusto et al., Proc. 8th Intern. Symp. on VHECRI, Tokyo (1994) ed. by Local Organising Commitee, p. 396.

[86] G. Wilk and Z. Włodarczyk, J. Phys. **G22** (1996) L105;
G.Wilk and Z. Włodarczyk, Heavy Ion Physics **4** (1996) 395;
M. Rybczyński, Z. Włodarczyk and G.Wilk, e-preprint hep-ph/0009164 (2000), to be published in Il Nuovo Cimento.

[87] I.V. Andreev, Sov. Physica JETP Lett., **33** (1981) 367.

[88] C.S. Lam and S.Y. Lo, Phys. Rev. Lett. **52** (1984) 1184;
C.S. Lam and S.Y. Lo, Phys. Rev. **D33** (1986) 1336;
C.S. Lam and S. Y. Lo, Intern. Journ. of Modern Phys. **A1** (1986) 451.

[89] C. Greiner, C. Gong and B. Müller, Phys. Lett. **B316** (1993) 226.

[90] S. Pratt and V. Zelevinsky, Phys. Rev. Lett. **72** (1994) 816;
S. Pratt, Phys. Rev. **C50** (1994) 469.

[91] A. A. Anselm, M. G. Ryskin, Phys. Lett. **B266** (1991) 482.

[92] J. P. Blaizot and A. Krzywicki, Phys. Rev. **D46** (1992) 246.

[93] M. Martinis, V. Mikata-Martinis, A. Svarc and J. Crnugelj, Phys. Rev. **D51** (1995) 2482.

[94] K. Rajagopal and F. Wilczek, Nucl. Phys. **B399** (1993) 395;
K. Rajagopal and F. Wilczek, Nucl. Phys. **404** (1993) 577;
K. Rajagopal, e-preprint hep-ph/9703258 (1997), CALT-68-2104.

[95] S. Gavin, Nucl. Phys. **A590** (1995) 163c.

[96] Z. Huang and X. N. Wang, nucl-th/9312005, 1993.

[97] G. Wilk and Z. Włodarczyk, Nucl. Phys. (Proc. Suppl.) **B52** (1997) 215.

[98] C. E. Navia et al., Phys. Rev. **D55** (1997) 5834.

[99] P. Carruthers, E. M. Friedländer and R. M. Weiner, Preprint LA-UR-86-1447;
P. Carruthers, E. M. Friedländer, C. C. Shih and R. M. Weiner, Phys. Lett. **B222** (1989) 487.

[100] J. Bartke, E. Gładysz-Dziaduś and P. Stefański, Proc. 20th Intern. Symposium on Multiparticle Dynamics, p. 530, Gut Holmecke 1990, Singapore: World Scientific 1991;
J. Bartke, E. Gładysz-Dziaduś and P. Stefański, NA35 Coll., poster E44, Quark Matter'91 Conference, Gatlinburg (USA), 1991;
J. Bartke, E. Gładysz-Dziaduś and P. Stefański, Proc. 6th Intern. Symposium on Very High Energy Cosmic Ray Interactions (ISVHECRI), ed. by J. N. Capdevielle and P. Gabinski, Tarbes, France 1990, p. 207;
J. Bartke, E. Gładysz-Dziaduś and P. Stefański, Proc. CAMP Workshop, Marburg 1990, p. 198, Singapore: World Scientific 1991. J. Bartke, E. Gładysz-Dziaduś and P. Stefański, Nucl. Phys. **A545** (1992) 321c;
NA35 Collaboration, J. Bachler et al., Z. Phys. **C56** (1992) 347.

[101] R. C. Hwa, Phys. Lett. **B201** (1987) 165;
R. C. Hwa, Z. Phys.C-Particles and Fields **38** (1988) 277;
R. C. Hwa, Int. J. Mod. Phys. **A4** (1989) 481.

[102] P. Carruthers, H. Eggers, I. Sarcević, Phys. Rev. **C44** (1991) 1629;
H. Eggers et al., Phys. Rev. **D44** (1991) 1975;
G. N. Fowler, E. M. Friedländer, M. R. Weiner, Phys. Lett. **B104** (1981) 239.

[103] J. Bartke, E. Gładysz-Dziaduś and P. Stefański: poster E42 at Quark Matter'91 Conference, Gatlinburg (USA), 1991.

[104] J. Bjorken, SLAC-PUB-6488 (1994).

[105] C. R. A. Augusto et al.," DCC signature on γ- hadron families seen through robust observables", unpublished.

[106] C. R. A. Augusto et al., Nucl. Phys. B (Proc.Suppl.)**75A** (1999) 206;
C. R. A. Augusto et al., Phys. Rev. **D59** (1999) 54.

[107] T. C. Brooks et al., Phys. Rev. **D55** (1997) 5667.

[108] E. Gładysz-Dziaduś, Modern Phys. Lett. **A4** (1989) 2553;
E. Gładysz-Dziaduś, Raport No 1432/PH, Institute of Nuclear Physics, Kraków, 1988.

[109] G. Wilk and Z. Włodarczyk, J. Phys. G: Nucl. Part. Phys. **19** (1993) 761.

[110] E. Witten, Phys. Rev. **D30** (1984) 272.

[111] M. S. Desai and G. L. Shaw, AIP Conf. Proc. No. 340 (1995) 53;
A. Dar, A. de Rújula and U. Heinz, CERN-TH/99-324; e-preprint hep-ph/9910471;
W. Busza et al., e-preprint hep-ph/9910333, 1999;
A. Kent, DAMTP-2000-12 and e-preprint hep-ph/0009130, 2000;
J. Madsen, e-preprint hep-ph/0008217, 2000, submitted to Phys. Rev. Lett.

[112] F. Fahri and R. L. Jafee, Phys. Rev. **D30** (1984) 2379.

[113] M. S. Berger and R. L. Jaffe, Phys. Rev. **C35** (1987) 213.

[114] S. Chin and A. Kerman, Phys. Rev. Lett. **43** (1979) 1292.

[115] J. Schaffner-Bielich et al., Phys. Rev. **C55** (1997) 3038.

[116] E. Gilson and R. Jaffe, Phys. Rev. Lett. **71** (1993) 332.

[117] J. Madsen, Phys. Rev. **D50** (1994) 3328.

[118] C. Greiner, P. Koch and H. Stoöcker, Phys. Rev. Lett. **58** (1987) 1825;
C. Greiner, D. H. Rischke, H. Stöcker and P. Koch, Phys. Rev. **D38** (1988) 2797;
C. Greiner and H. Stöcker, Phys. Rev. **D44** (1991) 3517.

[119] J. Madsen, "*Physics and Astrophysics of Strange Quark Matter*", in "*Hadrons in Dense Matter and Hadrosynthesis*", Cape Town (1998), Lecture Notes in Physics, Springer, eds. J. Cleymans et al., p. 162 and e-preprint astro-ph/9809032 (1998).

[120] C. Greiner and J. Schaffner-Bielich, "*Physics of Strange Matter*" in "*Heavy Elements and Related New Phenomena*", ed. R. K. Gupta and W. Greiner, (Singapore: World Scientific); preprint LBNL-41324 and nucl-th/9801062 (1998).

[121] T. K. Hemmick et al., Phys. Rev. **D41** (1990) 2074.

[122] C. Alcock and A. Olinto, Ann. Rev.Nucl. Part. Sci. **38** (1988) 161.

[123] V. M. Aushev et al., Izvestia RAS, ser. phys. V. 61, No. 3 (1997) 486;
V. A. Antonova et al., Nucl. Phys. B (Proc. Suppl.) **75 A** (1999) 333 (Proc.Suppl.).

[124] M. Rybczyński, Z. Włodarczyk and G.Wilk, e-preprint hep-ph/0005217 (2000), to be published in Nucl. Phys. B (Proc. Suppl.).

[125] X. D. Li et al., Phys. Rev. Lett. **83** (1999) 3776 and references therein.

[126] T. Saito, Y. Hatano, Y. Fukada and H. Oda, Phys. Rev. Lett. **65** (1990) 2094.

[127] P. B. Price et al., Phys. Rev. **D18** (1978) 1382.

[128] M. Ichimura et al., Il Nuovo Cimento **A106** (1993) 843.

[129] E864 Collaboration, T. A. Armstrong et al., nucl-ex/0010017 (2000);
Z. Xu for E864 Coll., J. Phys. G: Nucl. Part. Phys. **25** (1999) 403;
G. van Buren for E864 Coll., J. Phys. G: Nucl. Part. Phys. **25** (1999) 411;
M. K. Munkoz for E864 Coll., J. Phys. G: Nucl. Part. Phys. **25** (1999) 417;
E814 Collaboration, J. Barrette et al., Phys. Lett. **B252** (1990) 550;
E858 Collaboration, M. Aoki et al., Phys. Rev. Lett. **69** (1992) 2345;
E878 Collaboration, D. Beavis et al., Phys. Rev. Lett. **75** (1995) 3078;
E886 Collaboration, A. Rusek et al., Phys. Rev., **C54** (1996) R15.

[130] NA52 Collaboration (NEWMASS), G. Ambrosini et al., J. Phys. G: Nucl. Part. Phys. **23** (1997) 2135.

[131] R. Klingenberg, J. Phys. G: Nucl. Part. Phys. **25** (1999) R273.

[132] O. Miyamura et al., Proc. 24th ICRC, Rome (1995), Vol. 1, p. 890.

[133] J. N. Capdevielle et al., Proc. 24th ICRC, Rome (1995), Vol. 1, p. 910 and Il Nuovo Cimento **C19** (1996) 623.

[134] A. Baltz et al., Phys. Lett. **B325** (1994) 7.

[135] P. Braun-Munzinger and J. Stachel, J. Phys. G: Nucl. Part. Phys. **21** (1995) L17.

[136] A. L. S. Angelis et al., Nucl. Phys. B (Proc. Suppl.) **75A** (1999) 203;
A. Angelis et al., CASTOR draft proposal, ALICE/97-07, Internal Note/CAS.

[137] O. P. Theodoratou and A. D. Panagiotou, e-preprint hep-ph/9908210; Astroparticle Phys. **13** (2000) 173.

[138] B. Müller, Preprint DUKE-TH-92-36, e-preprint hep-th/9211010;
B. Müller, NATO ASI Series, (Il Ciocco, 1992) ed. by H. Gutbrod and J. Rafelski, Series B: Physics Vol. 303 (1992) 11;
J. W. Harris, and B. Müller, Ann. Rev. Nucl. Part. Sci. **46** (1996) 71, and preprint DUKE-TH-96-105 and e-preprint hep-ph/9602235.

[139] M. N. Asprouli and A. D. Panagiotou, Phys. Rev. **D51** (1995) 1086.

[140] B. Petersson, Proc. ECFA Large Hadron Collider Workshop, Aachen, Germany, 1990, ed. by G. Jarlskog and D. Rein (CERN Report No. 90-10, Geneva, Switzerland, 1990), Vol. II.

[141] S. Gottlieb et al., Phys. Rev. **D35** (1987) 3972.

[142] J. Ellis, J. I. Kapusta and K. A. Olive, Phys. Lett. **B273** (1991) 123.

[143] K. Kinoshita and P. B. Price, Phys. Rev. **D24** (1981) 1707;
Barwick et al. , Phys. Rev. **D28** (1983) 2338;
S. Nakamura et al., Phys. Lett. **B263** (1991) 529;
P. B. Price, Phys. Rev. **D47** (1993) 5194.

[144] A. R. Bodmer, Phys. Rev. **D4** (1971) 1601.

[145] T. S. Biro and J. Zimányi, Nucl. Phys. **A395** (1983) 525;
J. Zimányi, P. Lévai, B. Lukács and A. Rácz, NATO ASI series, ed. by H. Gutbrod and J. Rafelski (Il Ciocco, 1992), Series B: Physics Vol. 303 (1992) 243.

[146] J. Madsen, Intern. Symposium on Strangeness and Quark Matter, Krete(1994), World Scientific, ed's G. Vassiliadis et al., p. 191.

[147] H. J. Crawford, M. S. Desai and G. L. Shaw, Phys. Rev. **D45** (1992) 857.

[148] G. Arnison et al., UA1 Collaboration, Phys. Lett. **122B** (1983) 189.

[149] K. Alpgard et al., UA5 Collaboration, Phys. Lett. **115B** (1982) 71;
G. J. Alner et al., UA5 Collaboration, preprint CERN-EP/86-127, 1986.

[150] J. Streets, for Mini-Max Coll., hep-ex/9608012, 1996.

[151] P. L. Melese for CDF Collaboration, Proc. 11th Topical Workshop on $\overline{p}p$ Collider Physics, PBARP96, Padova (Italy), ed. by D. Bisello, G. Busetto and L. Stanco, Singapore: World Scientific, University of Padova 1997, p. 360.

[152] L. W. Jones, XXVIII Intern. Symp. on Multiparticle Dynamics, Delphi, Greece, 1998, ed. N. A. Antoniou et al., World Scientific, 1998, p. 501.

[153] M. V. S. Rao for the D0 Coll., Proc. of the VIII Intern, Symp. on VHECRI, Tokyo, 1994, ed. by Local Organising Commitee, p. 299;
S. Abachi et al., Phys. Rev. Lett. **72** (1994) 2332.

[154] T. K. Nayak for WA98 Collaboration, invited talk at the QM'97, Tsukuba, Japan, 1997, Nucl. Phys. **A638** (1998) 249c and hep-ex/9802019, 1998;
M. M. Aggarwal et al., Phys. Lett. **B420** (1998) 169 and hep-ex/9710015.

[155] FELIX, Letter of Intent, CERN/LHCC 97-45, 1997.

[156] The ALICE Technical proposal, CERN/LHCC/95-71, LHCC/P3, 1995.

[157] The ALICE forward muon spectrometer, CERN/LHCC 96-32; ALICE TDR5 CERN/LHCC 99-12.

[158] Y. P. Viyogi, Internal Note ALICE/PMD 98-52; ALICE TDR6 CERN/LHCC 99-32.

[159] G. Dellacasa et al., Zero Degree Calorimeter ZDC, ALICE TDR 3, CERN/LHCC 99-5, 1999.

[160] J. Bartke, E. Gładysz-Dziaduś, M. Kowalski and A. D. Panagiotou, ALICE Internal Note, PHYS/93-12.

[161] E. Gładysz-Dziaduś and A. D. Panagiotou, ALICE/95-18, Internal Note/PHY (1995).

[162] E. Gładysz-Dziaduś and A. D. Panagiotou, ALICE/97-16, Internal Note/CAS (1997).

[163] J. Schukraft, preprint CERN-PPE/94-139, August 1994.

[164] K. Geiger, Phys. Rev. **D46** (1992) 4965 and 4986.

[165] E. Gładysz-Dziaduś et al., Proc. Third Intern.Conf. on Physics and Astrophysics of Quark-Gluon Plasma, Jaipur 1997, eds. Bikas C. Sinha et al., Narosa Publishing House, New Delhi, 1998, p. 554;
E. Gładysz-Dziaduś et al., ALICE/97-06, Internal Note/PHY (1997).

[166] M. Sowa, Master Degree Thesis, Institute of Nuclear Physics, Kraków (Poland), 2000.

[167] E. Gładysz-Dziaduś, ALICE-INT-2001-21, Internal Note (2001) .

[168] A. L. S. Angelis, J.Bartke, E. Gładysz-Dziaduś and Z. Włodarczyk, EPJdirect C9, 1-18(1999), DOI 10.1007/s1010599c0009 (or C9, 1-18(2000), DOI 10.1007/s1010500c0009); Report No. 1800/PH, Institute of Nuclear Physics, Krakow, 1998;
ALICE Internal Note, CAS/98-38, 1988.